CONDUCTION BASED COMPACT THERMAL MODELING FOR THERMAL ANALYSIS OF ELECTRONIC COMPONENTS

A THESIS SUBMITTED TO
THE GRADUATE SCHOOL OF NATURAL AND APPLIED SCIENCES
OF
MIDDLE EAST TECHNICAL UNIVERSITY

BY

MUSTAFA OCAK

IN PARTIAL FULFILLMENT OF THE REQUIREMENTS
FOR
THE DEGREE OF MASTER OF SCIENCE
IN
MECHANICAL ENGINEERING

JUNE 2010

Approval of the thesis:

CONDUCTION BASED COMPACT THERMAL MODELING FOR THERMAL ANALYSIS OF ELECTRONIC COMPONENTS

submitted by **MUSTAFA OCAK** in partial fulfilment of the requirements for the degree of **Master of Science in Mechanical Engineering Department, Middle East Technical University** by,

Prof. Dr. Canan Özgen _____
Dean, Graduate School of **Natural and Applied Sciences**

Prof. Dr. Süha Oral _____
Head of Department, **Mechanical Engineering**

Asst. Prof. Dr. Cüneyt Sert _____
Supervisor, **Mechanical Engineering Dept., METU**

Examining Committee Members:

Prof. Dr. Haluk Aksel _____
Mechanical Engineering Dept., METU

Asst. Prof. Dr. Cüneyt Sert _____
Mechanical Engineering Dept., METU

Asst. Prof. Dr. İlker Tarı _____
Mechanical Engineering Dept., METU

Asst. Prof. Dr. Tuba Okutucu Özyurt _____
Mechanical Engineering Dept., METU

Emre Öztürk, M.Sc. _____
General Manager, ANOVA

Date: 10.06.2010

I hereby declare that all information in this document has been obtained and presented in accordance with academic rules and ethical conduct. I also declare that, as required by these rules and conduct, I have fully cited and referenced all material and results that are not original to this work.

Name, Last Name : Mustafa OCAK

Signature :

ABSTRACT

CONDUCTION BASED COMPACT THERMAL MODELING FOR THERMAL ANALYSIS OF ELECTRONIC COMPONENTS

Ocak, Mustafa
M.Sc., Department of Mechanical Engineering
Supervisor: Asst. Prof. Dr. Cüneyt Sert

June 2010, 140 pages

Conduction based compact thermal modeling of DC/DC converters, which are electronic components commonly used in military applications, are investigated. Three carefully designed numerical case studies are carried out at component, board and system levels using ICEPAK software. Experiments are conducted to gather temperature data that can be used to study compact thermal models (CTMs) with different levels of simplification.

In the first (component level) problem a series of conduction based CTMs are generated and used to study the thermal behavior of a Thin-Shrink Small Outline Package (TSSOP) type DC/DC converter under free convection conditions. In the second (board level) case study, CTM alternatives are produced and investigated for module type DC/DC converter components using a printed circuit board (PCB) of an electro-optic system. In the last case study, performance of the CTM alternatives generated for the first case are assessed at the system level using them on a PCB placed inside a realistic avionic box.

Detailed comparison of accuracy of simulations obtained using CTMs with various levels of simplification is made based on experimentally obtained temperature data. Effects of grid size and quality, choice of turbulence modeling and space discretization schemes on numerical solutions are discussed in detail.

It is seen that simulations provide results that are in agreement with measurements when appropriate CTMs are used. It is also showed that remarkable reductions in modeling and simulation times can be achieved by the use of CTMs, especially in system level analysis.

Keywords: Conduction based Compact Thermal Modeling , DC/DC converters

ÖZ

ELEKTRONİK BİLEŞENLERİN ISIL ANALİZLERİ İÇİN İLETİM TEMELLİ BASİT ISIL MODELLEME YÖNTEMİ

Ocak, Mustafa
Yüksek Lisans, Makina Mühendisliği Bölümü
Tez Yöneticisi: Yrd. Doç. Dr. Cüneyt Sert

Haziran 2010, 140 sayfa

Bu çalışmada iletim temelli basit ısıl modelleme yöntemi, askeri tip elektronik sistemlerde sıklıkla kullanılan DC/DC çevirici elektronik bileşenler için incelenmiştir. Sırasıyla bileşen, kart ve sistem düzeyinde olmak üzere 3 sayısal çalışma, ICEPAK hesaplamalı akışkanlar dinamiği (HAD) yazılımı kullanılarak gerçekleştirilmiştir. Sayısal çalışmalar deneysel çalışmalardan elde edilen sıcaklık ölçüm değerleri ile desteklenmiştir.

Bileşen seviyesindeki ilk sayısal çalışmada, alternatif basit ısıl modeller (BİM) Thin-shrink small outline package (TSSOP) tipi DC/DC çevirici bir bileşenin doğal taşınım koşulları altında ısıl davranışının incelenmesi için türetilmiştir. Kart seviyesindeki ikinci çalışmada ise modül tipi DC/DC dönüştürücü bileşenler için BİM alternatifleri oluşturulmuş ve incelenmiştir. Çalışmada, üzerinde DC/DC dönüştürücü modüller bulunan ve bir elektro-optik sistemin parçası olan baskı devre kartı kullanılmıştır. Son çalışmada, birinci çalışmada türetilen BİM alternatiflerinin sistem düzeyindeki değerlendirilmesi yapılmıştır. Bu doğrultuda standart ölçülerdeki

bir hava elektroniği kutusu bir baskı devre kartıyla birlikte sayısal olarak modellenmiş ve analiz çalışmalarına dâhil edilmiştir.

BİM alternatifleri kullanılarak elde edilen sayısal çalışma sonuçları deneysel çalışmalardan elde edilen sıcaklık değerleri ışığında değerlendirilmiştir. Buna ek olarak, DC/DC çevirici bileşenlerin ısıl davranışlarının çözümlenmesi için BİMlerin kendi aralarındaki karşılaştırmaları yapılmıştır. Aynı zamanda farklı ağ yapılarının, türbülans modeli seçiminin, diskretizasyon şemalarının çözümlere olan etkisi de tartışılmıştır.

Sonuç olarak uygun iletim temelli BİM alternatiflerinin kullanıldığı durumlarda, deneysel sonuçların sayısal sonuçlarla örtüştüğü gözlenmiştir. Buna ek olarak BİM kullanımı ile modelleme ve çözüm sürelerinde, özellikle sistem düzeyi analiz çalışmalarında, kayda değer azalmaların sağlanabileceği değerlendirilmiştir.

Anahtar Kelimeler: İletim temelli basit ısıl modelleme, DC/DC çeviriciler

To My Family

ACKNOWLEDGMENTS

The author wishes to express his sincere appreciation to his supervisor Asst. Prof. Dr. Cüneyt SERT for the endless support, encouragement and patience during his research activities.

The author would like to thank ASELSAN, Inc. and his manager Mr. İhsan ÖZSOY, for his support and guidance in his study and let to use experimental facilities of mechanical/optical design department.

The author is thankful to his superior Dr. Ali M. ÇOLAKOĞLU for the encouragement and guidance. Without his unconditional support in guiding the author to study electronics cooling, this dissertation would never have come into existence.

The author owes special thanks to his colleagues Bülent HAVUR and Erkan ÖNAL for their assistance and contributions to experimental parts of the dissertation.

The authors would like to express his appreciation to his colleagues A. Berkan ERDOĞMUŞ, A. Levent AVŞAR and A. Cem GÖZÜKARA for their valuable support and understanding.

The author would like to extend his thanks to Mr. Emre ÖZTÜRK for his endless technical support and invaluable recommendations about computational fluid dynamics.

Lastly the author would like to express his endless gratitude to his family for their love, support and faith in him.

TABLE OF CONTENTS

LIST OF TABLES

LIST OF FIGURES

LIST OF SYMBOLS

Latin Symbols

a	: Absorption coefficient
C_p	: Specific heat
C_μ, C_2 , $C_{1\varepsilon}$	: Constants of turbulence models
d	: Distance from wall
f_x, f_y, f_z	: Source terms
g	: Gravitational acceleration
G_b	: Generation of turbulence kinetic energy due to buoyancy
G_k	: Generation of turbulence kinetic energy due to mean velocity gradients
h	: Enthalpy
I	: Radiation intensity
I	: Current
k	: Thermal conductivity or Turbulence kinetic energy
$k_{eff\text{-}isotropic}$	: Effective isotropic thermal conductivity
$k_{parallel}$	: In-plane thermal conductivity
k_{serial}	: Through-thickness thermal conductivity
k_t	: Turbulent thermal conductivity
ℓ	: Mixing length
L	: Length
m	: Mass
n	: Refractive index
p	: Pressure
P	: Power

P_D : Power dissipated

$P_{TPS54610}$: Power dissipation of *TPS54610* as heat

Pr : Prandtl number

$\vec{r}$: Position vector

R : Resistance (electrical)

R_{ca} : Resistance value between case and ambient

$R_{electric\ load}$: Resistance of electric load

R_{L1} : Resistance of L1

R_{jc} : Resistance value between junction and case

R_{xy} : Resistance value between x and y

Ra : Rayleigh number

s : Path length for Radiation transport equation

S : Mean rate of strain tensor for Zero equation turbulence model

$\vec{s}$: Direction vector

$\vec{s}'$: Scattering direction vector

S_h : Source term (volumetric)

T : Temperature

T_f : Fluid temperature

T_w : Wall temperature

T_∞ : Ambient temperature

$\overline{u}_i$: Mean velocity

u_i' : Instantaneous velocity components

u, v, w : Velocity components

V : Volume

V : Voltage

$\vec{V}$: Velocity vector

Y_M : Contribution of the fluctuating dilatation incompressible turbulence to the overall dissipation rate

$(a+\sigma_s)s$: Optical thickness of the medium

Greek Symbols

α : Thermal diffusivity

β : Expansion coefficient

υ : Kinematic viscosity

ε : Turbulence dissipation rate

η : Efficiency

$\eta_{TPS54610EVM}$: Efficiency of *TPS54610* evaluation module

θ_{bside} : Resistance value between side and board

θ_{cside} : Resistance value between case and side

θ_{jb} : Resistance value between junction and board

θ_{jc} : Resistance value between junction and case

θ_{jside} : Resistance value between junction and side

κ : Karman constant

λ : Bulk viscosity coefficient

ϕ : Scalar

μ : Dinamic viscosity

μ_t : Turbulent (eddy) viscosity

ρ : Density

σ : Stefan-Boltzman constant

σ_s : Scattering coefficient

τ : Viscous stress

ω : Turbulence specific dissipation rate

Φ : Phase function

Ω' : Solid angle

Subscripts

i	: Component in the array of features being lumped
eff	: Effective
in	: Input
out	: Output
x, y, z	: Spatial coordinate directions
o	: Operating Temperature
i,j, k	: Suffix notation for x, y and z directions
k	: Turbulence kinetic energy
ε	: Turbulence dissipation rate

CHAPTER 1

INTRODUCTION

Electronic components are indispensable technologies of today's world. They are widely used in both industrial and military applications. It is very important to have highly reliable electronic systems especially in military defence industry. However, every new brand electronic package consumes more electrical power and is exposed to higher temperatures, which increases the chances for failure. Therefore thermal management of electronic systems (keeping them within the operating temperature range) becomes increasingly important. Both performance and occupancy of electronic components can be increased with good thermal designs. Consequently, keeping electronic systems reliable and durable with thermal management is one of the key issues of today's electronic industry.

1.1 Advances in Electronics

Moore's Law (Figure 1.1) predicts that the transistor density on integrated circuits doubles every 18 months. This sharp increase in transistor count results in better performance but also causes increased heat generation.

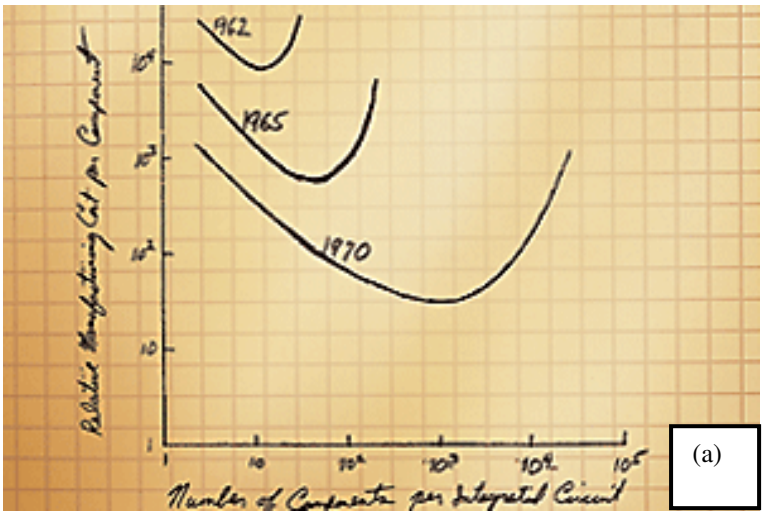

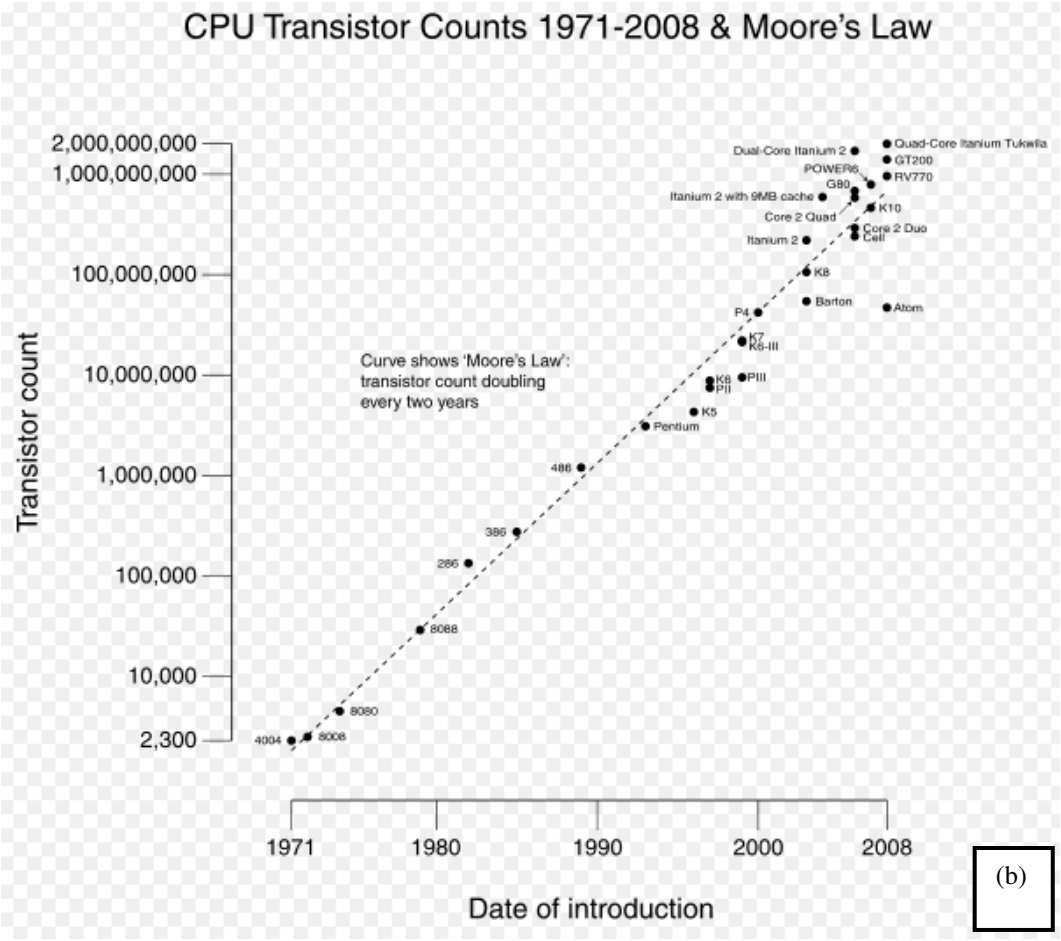

Figure 1.1 Moore's Law a) Original hand drawing [1], b) Updated version [2]

It is stated in the thermal design guidelines of Pentium 4 CPU that typical aluminium extruded heat sink may not be adequate to provide necessary cooling for the entire range of dissipated power [3]. Recent year trends of power consumption and related heat dissipation of is shown in Figure 1.2. With the increase in power dissipation, the need to cool local hotspots becomes extremely challenging in the thermal management of the microprocessors. So more advanced cooling techniques are necessary to keep the processor within the operational thermal specifications to avoid potential failures.

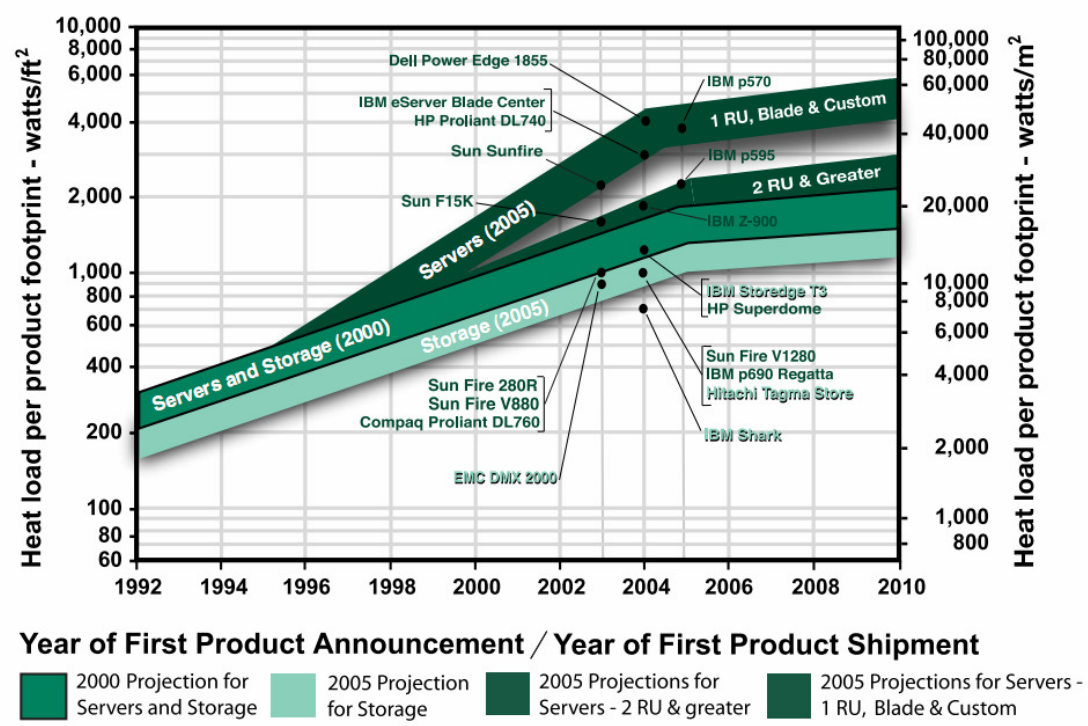

Figure 1.2 Electronics heat density trends chart from 1990 to 2010 [4]

Advanced cooling techniques have especially been used in defence industry to satisfy hard working specifications which are stipulated by military standards. Hence companies like Aeronautical Radio Inc. (ARINC) developed their own test standards and own cooling systems to obtain high quality and reliable electronic systems [5]. To develop such highly reliable electronics cooling systems, system and component manufacturers have started to include “thermal management of electronics” in earlier

parts of their design practices. They have realized that thermal management (or thermal modelling) is an important requirement in the development of low cost and durable electronic systems.

1.2 Thermal Modelling

Predicting surface temperatures of electronic components especially in complicated electronic systems has been a big concern for engineers since electronics became a part of today's world. Nowadays computational simulation tools provide solution opportunities for prediction of temperatures in electronics systems with thermal modelling. Thermal modelling can be defined as "A mathematical model that dynamically predicts the temperature of an object. The accuracy of the model is a function of its algorithm and the accuracy of the values used for the objects thermal capacitance, thermal resistance to its surroundings, and heat generated in or removed from the object" [6]. Today thermal modelling and corresponding simulations are seen as essential by manufacturers, because simulations can allow quick assessment and elimination of design alternatives of electronic devices. In addition to that it can also be used for design optimization and final electronic device selection.

Although computational simulation tools make thermal modelling convenient, it is still difficult to implement near-exact physical models (known as Detailed Thermal Models (DTM)) of electronic systems in thermal simulations. Wide range of length scales of near-exact physical models cause computational inefficiencies. To find a solution to this problem simplification efforts have been performed in the past years. Simplified models, known as compact thermal models (CTM), enable thermal simulations with less grid-intensive representations and provide good accuracy for temperatures at important points [7].

Another challenge has been the validation of thermal models with experimental studies. Many researchers performed experimental studies in the past for their

thermal models and some standardization organizations, such as JEDEC Solid State Technology Association, had tried to ensure test procedures. JEDEC provided a consistent framework for the use of modelling and validations methods and for reporting the results. Documents published by JEDEC had been provided guidance in the use of particular modelling approaches. Modular structure for thermal modelling suggested by JEDEC is shown in Figure 1.3.

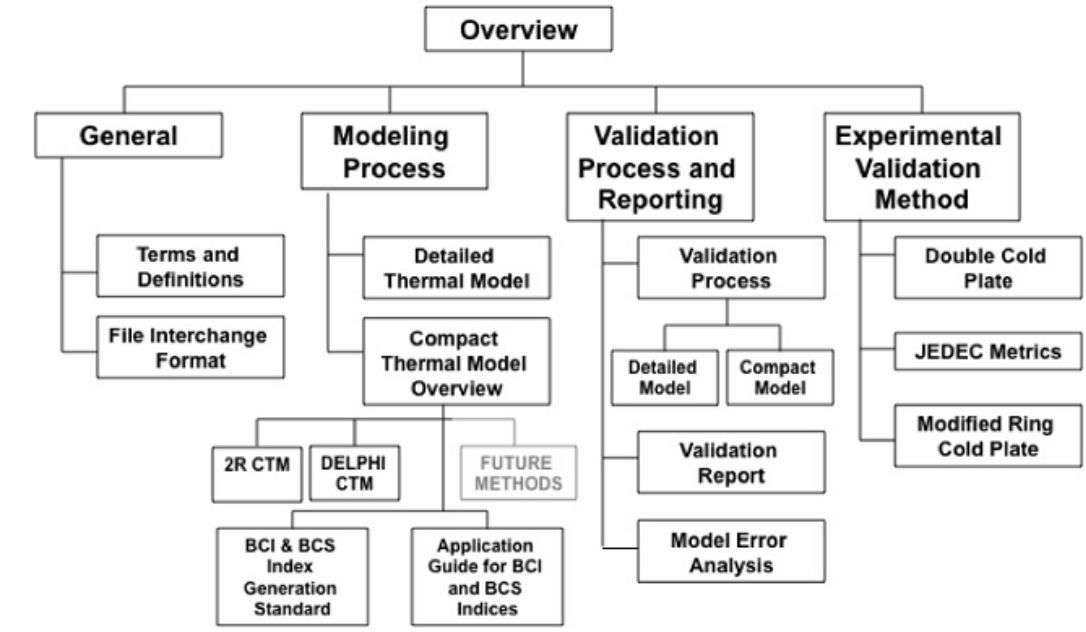

Figure 1.3 Modular structure for thermal modelling suggested by JEDEC [8]

As mentioned above, detail thermal models can be defined as near-exact physical models of electronic packages. DTMs are considered to be proper for component level thermal analysis, but not for system level studies simply due to computational restrictions. DTMs have been used not only to predict surface temperatures of components but also as base models to form compact thermal models (CTM) by CFD application engineers and researchers. Nowadays many of the CFD software used for electronic cooling applications provide opportunities to form DTM, but the user needs to supply quite a lot of information. For example for a standard Quad Flat electronic Package (QFP), as shown in Figure 1.4, material property and geometry

details of die, die paddle, die attach, mold compound, wire bonds and leads are required.

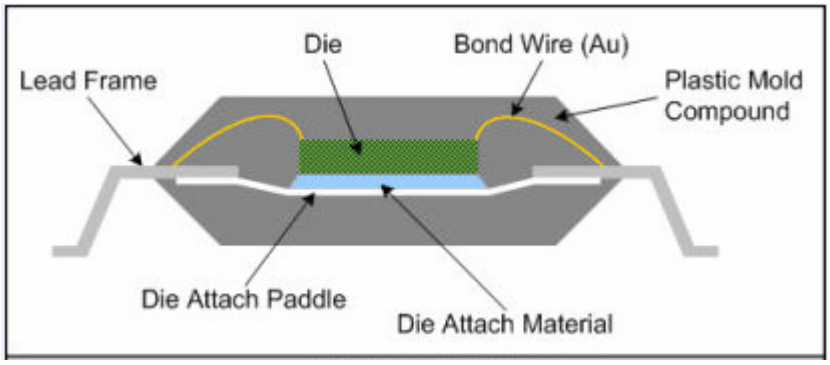

Figure 1.4 Cross section of a QFP

For an electronic package with Ball Grid Array (BGA) type connection the amount of required information is even more. As seen in Figure 1.5, additional details for solder balls, substrate material, substrate copper contents for each layer, thermal gap filler material and adhesive materials are required.

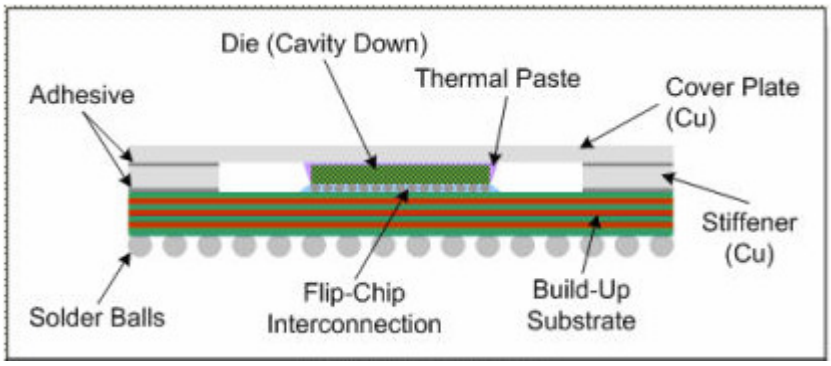

Figure 1.5 Cross section of a BGA

For component level CFD analysis detailed models have been used by component manufacturers, for whom obtaining the required detailed information is not an issue. However for an ordinary practicing thermal design engineer acquiring all this information is a challenging task. In addition to this high grid counts that results in

using DTMs in system level simulations force designers to work with compact models.

1.2.1 Compact Thermal Modeling (CTM)

JEDEC defines CTM as "a special class of simplified component models which satisfy the technical requirements of accuracy and software compatibility and also act as a viable means of exchanging the required data from supplier to customer in the world wide electronics industry" [9].

In earlier CTM studies, component manufacturers supplied the necessary models to system manufacturers. Later on researchers and application engineers had tried to create their own CTMs in their system level analyses. As a result of these practices many different CTM alternatives were generated without proper standardization. DELPHI project as explained below was an effort to fill this gap.

1.2.1.1 Standardization Studies of Compact Thermal Models

To standardize the CTM creation process DELPHI (DEvelopment of Libraries of PHysical models for an Integrated design environment) project had been performed by frontiers of electronic component manufacturers. DELPHI was a project supported by a grant from the Esprit III technology development program of the European Community during the years 1993 – 1996 (project no. 9197). Its aim was to refine both the numerical and validation aspects of the CTM methodology.

The CTM methodology was further developed with subsequent projects entitled SEED (Supplier Evaluation and Exploitation of DELPHI; Esprit III project no. 22797; 1997-1998) and PROFIT (Prediction of Temperature Gradients Influencing the Quality of Electronic Products; European Community IST Program, project no.

12529; 2000 – 2002). The reports and publications of all these projects are in the public domain [9].

Members of the DELPHI, SEED, and PROFIT projects have continued to be active in the JC15 committee to promote an awareness of developments in CTM methodology and to participate in standardization efforts [9].

The ultimate purpose of the DELPHI project was “to get component manufacturers to supply validated thermal models of their parts to end users by adopting the experimental techniques used to validate the detailed thermal conduction models of the parts, and the methods to generate compact models”. DELPHI project had brought some discrete definitions and constraints to common terms (like boundary condition independence, compact model, design, detailed model, double cold plate method, generic model, interface thermal resistance model, supplier, user, etc.) of compact thermal modelling concept. Later on JEDEC solid state technology association became a part of the effort and worked to facilitate the adoption of these methods by the electronics industry world-wide. JEDEC published a series of documents and suggested the modular structure shown in Figure 1.6 about standardization of compact thermal modelling [9].

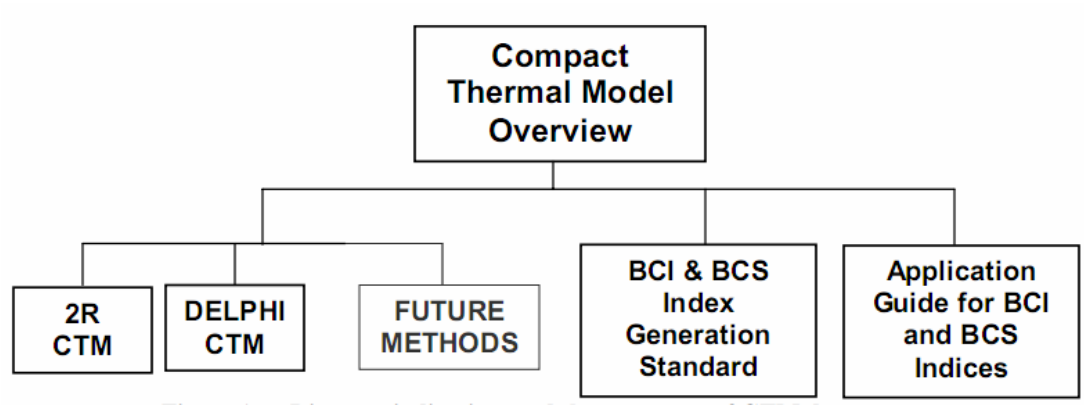

Figure 1.6 Modular structure of compact thermal modelling suggested by JEDEC [9]

JEDEC defines compact thermal models as “A CTM is a simplified component model intended to reproduce the thermal behaviour of a component in a wide variety of system-level simulations”, and add that “Its ultimate purpose is to allow a component-level thermal model generated at the component supplier to be efficiently inserted in a system level thermal simulation conducted within another organization” [9]. According to JEDEC CTMs should satisfy the criteria listed below.

- “It should be of limited complexity. In today’s technology, this equates to tens of nodes. It is conceivable that this number could increase over time with improvements in computer calculating power and the sophistication of CTM techniques.
- It should satisfy appropriate levels of Boundary Condition Independence (BCI). Absolute BCI is a property of a CTM whereby it calculates a chip temperature in all possible application environments, which is in perfect agreement with the results of a detailed model calculation. These environments, in essence, impose different boundary conditions on the component. It is a goal of the CTM standardization effort that CTMs should demonstrate a high level of BCI.
- It should be vendor-and software-neutral.
- A CTM generation technique should be adaptable to mainstream conduction codes for performing a package-level thermal analysis.
- The CTM should be capable of insertion into standard numerical codes for system-level (including board-level) analysis.
- It should be fully documented and nonproprietary.”

1.2.1.2 Types of Compact Thermal Models

Engineers mainly use two different methods to create their own CTMs; resistor (network) compact models and conduction compact models.

1.2.1.2.1 Resistor (Network) Compact Thermal Models

Resistor (network) modelling is the most popular modelling approach since thermal resistance concept was proposed by Siegel [10]. In this method electronic components are formed as a thermal resistance scheme to simulate the thermal behaviour of the component. This model is similar to an electrical network scheme which follows Ohm's law. As shown in Figure 1.7, electronic packages can be simplified to a network that represents heat transfer paths to the enclosure, through the enclosure, and from the enclosure to the outside ambient and etc.

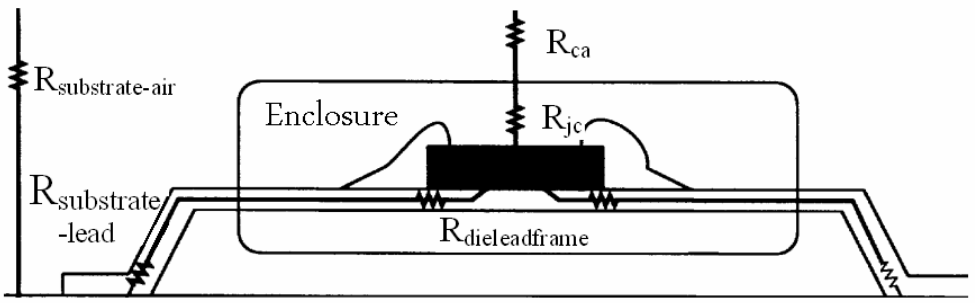

Figure 1.7 Typical resistor network scheme of an electronic component

The resistance value is computed by the following simple formula

$$R_{xy} = \frac{T_x - T_y}{P_D} \tag{1.1}$$

Where

R_{xy}: Resistance value between x and y

T_x : Temperature value of x

T_y : Temperature value of y

P_D : Power dissipated through x to y

Resistor compact models can be classified according to their connectivity. Two resistor, star and shunt models will be explained below. In addition to these DELPHI provides a more complex resistor model, called DELPHI compact model, created to be a boundary condition independent model [11].

Two Resistor Model

This is the simplest resistor scheme, containing only junction to board and junction to case resistances as shown in Figure 1.8. Two-resistor model is commonly employed, accuracy of it has always been questionable. It was not accepted as a boundary condition independent model by Dutta [12] and Joiner and Adams [13].

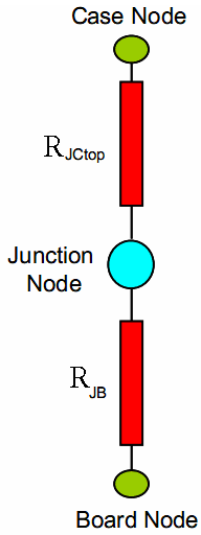

Figure 1.8 Two resistor model

Star Resistor Model

Compared to two-resistor model, star-resistor model contains additional resistances for package surfaces as seen in Figure 1.9. Junction-to-side resistance values are added to this model to simulate the effect of side faces on the heat transfer. Star resistor model is used in electronics cooling focused CFD softwares like Icepak and Flotherm.

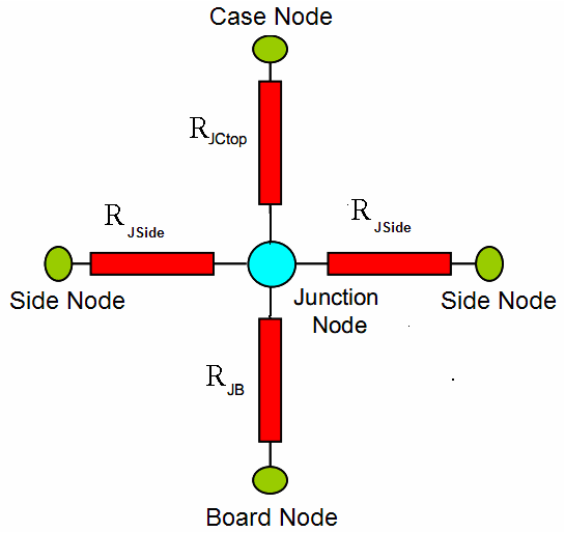

Figure 1.9 Star resistor model

Shunt Resistor Model

Shunt resistor model can be described as an improved version of Star resistor model. It enables heat transfer paths between top and bottom faces with side faces (Figure 1.10). But these resistor values are not easy to find in component manufacturer datasheets.

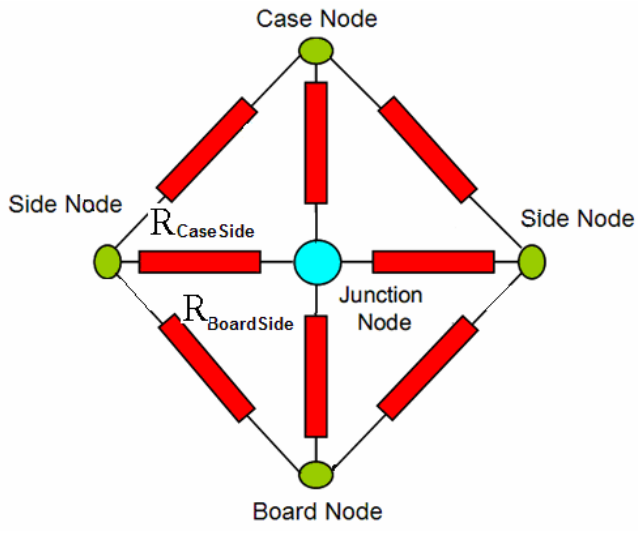

Figure 1.10 Shunt resistor model

1.2.1.2.2 Conduction (Based) Compact Thermal Models

Complex structures of DTMs such as outer leads, solder bumps and very thin parts/regions such as die attach and die paddle air gaps under the packages causes numerical grids with unacceptably high grid counts. In conduction based compact models (CCM) these complicated structures are properly simplified and if necessary lumped into simple prism-like volumes with averaged thermo-physical properties. Also thin parts and gaps are modelled as zero thickness two-dimensional objects, which have no real thickness in the computational grid, but they still can be used to simulate the thermal resistance created by the parts or gaps that they replace [14]. Zero thickness elements were compared with thick ones in that study and due to writers assertions "the use of zero thickness plate objects result in significant reduction in cell count when compared to an equivalent case using thick ones" [14]. Two samples of commonly implemented simplifications in CCMs are shown in Figure 1.11.

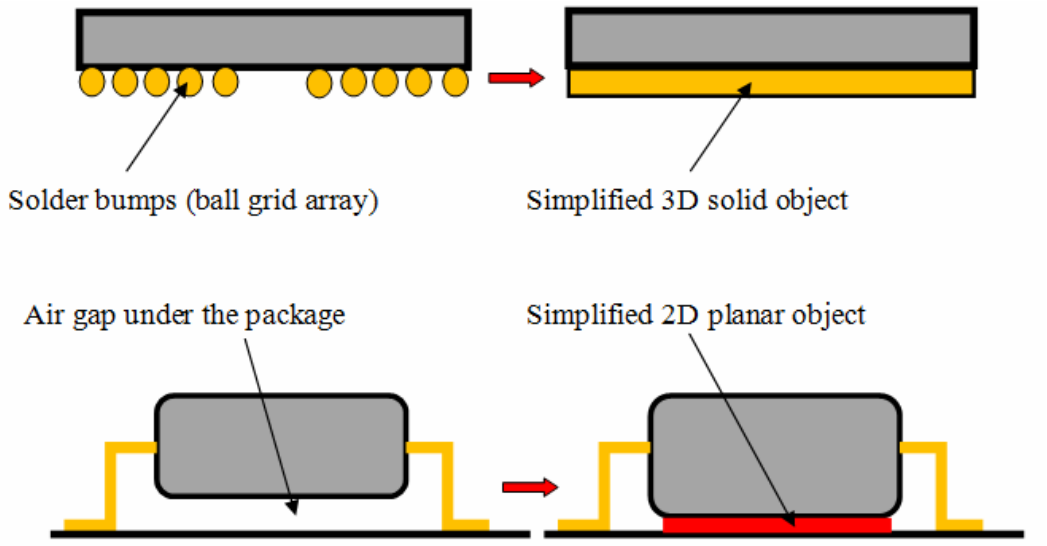

Figure 1.11 Simplified representation of solder bumps and air gap

According to author's knowledge, such a simplification was first proposed by Cooley and Razani in 1991 for a Leadless Chip Carrier (LCC) electronic component [15].

They described their simplification process as homogenization of solder bumps and air gap. Later on Rosten and et al. had used such simplifications for internal-external leads and die attach in their pioneering study about thermal modelling of a QFP [16]. Although these studies are forerunners of simplification efforts, they didn't offer a complete conduction based compact thermal model.

CCM concept as used in this study was first proposed in a study by Karimanal and Refai-Ahmed in 2002 [17], where they tried to validate the use of CCM for a BGA application. They used volume average based formulations to lump distinct parts of BGAs (Figure 1.12) such as die, die flag, die attach array of wire bonds, encapsulation surrounding the die, substrate with layers of copper traces, array of solder balls, air material in ball suppress region and thermal ball region and to determine effective thermo-physical properties of these lumped pats.

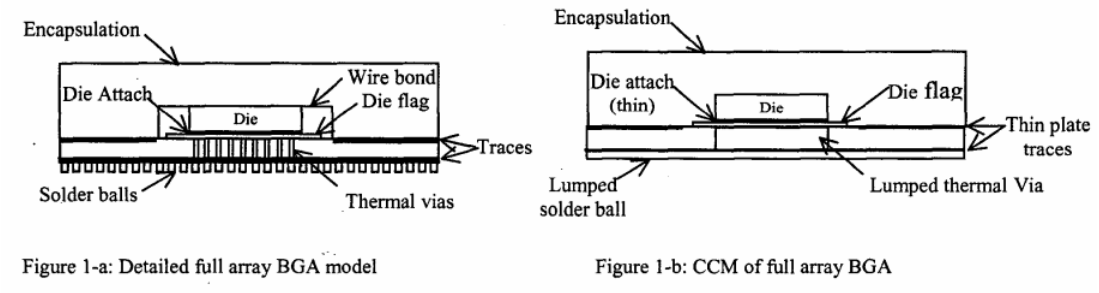

Figure 1.12 Detailed and lumped BGA models [17]

CCM modelling of Karimanal and Refai-Ahmed was based on the following procedure [17].

"

1) Identify distinct objects or array of objects forming the segments of possible conduction pathways.

2) Lump each of these segments to a single block with effective properties

3) After simplification, consider using thin plate objects as much as possible in order to minimize the unaligned edges and sources of thin computational cell elements."

They computed isotropic effective density and specific heat of various parts of their CCM using

$$\rho_{eff} = \frac{\sum \rho_i V_i}{\sum V_i} \tag{1.2}$$

$$C_{p,eff} = \frac{\sum C_{p,i} m_i}{\sum m_i} \tag{1.3}$$

which makes use of density, specific heat, mass and volume of individual parts that constitute the lumped volumes. They also identified effective conductivities in parallel and series pathways (bidirectional) for stacked structures based on the orientation of materials forming the composite entities which as shown in Figure 1.13.

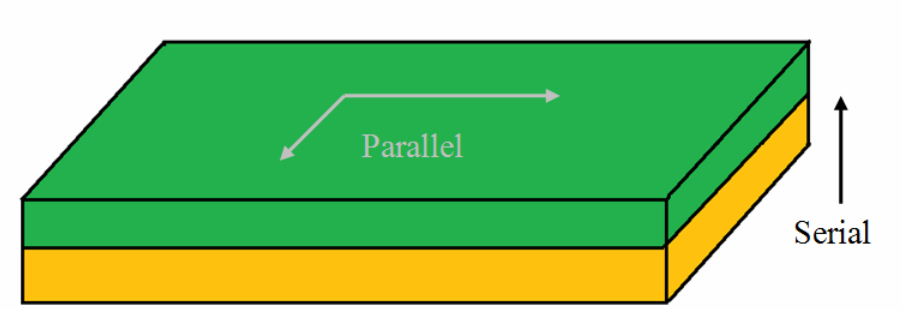

Figure 1.13 Resistance directions of parallel and serial pathways for stacked structures

They defined orthotropic effective (bidirectional) conductivities for stacked structures as follows

$$k_{parallel} = \frac{\sum k_i A_i}{\sum A_{total}} \tag{1.4}$$

$$k_{serial} = \frac{t_{total}}{\sum \frac{t_i}{k_i}} \tag{1.5}$$

where k_i, A_i and t_i are the conductivities, cross sectional areas and thicknesses of individual parts. Finally in order to get an isotropic effective conductivity for composite entities they used volume based averaging as follows.

$$k_{eff-isotropic} = \frac{\sum k_i V_i}{\sum V_{total}} \tag{1.6}$$

CHAPTER 2

LITERATURE REVIEW

One of the earliest studies about simplified thermal modelling of electronic component was conducted by Cooley and Razani [15], in which the commonly used linear package thermal resistance parameter. R_{jC} (junction to case), was investigated in detail. They applied a homogenization technique using two approaches. In the first one, stated to be more accurate, solder bumps along each edge of the package was lumped, whereas in the second one all solder bumps and air gap under the package were lumped into a single thin block. They performed finite element based simulations for the first model and calculated R_{jC} values. They also performed experiments and measured R_{jC} values using Mil-Std and SEMI fluid bath techniques. Numerical calculations provided an effective R_{jC} of 18 °C/W for a surface integrated leadless chip carrier. But the value of R_{jC} found in the Mil-Std or SEMI standard test was 3 °C/W. They claimed that the value found in the Mil-Std or SEMI is misleading because of measuring location of case temperature on the outside face of the package and this was seen as the main reason of the discrepancy between simulations and experiments. At the end of their study they drew a conclusion as "single parameter R_{jC} is very limited in its applicability and is becoming a thing of the past for thermal analysis of complex microelectronic systems requiring three dimensional modelling of the entire system. Finite element modelling provides an accurate method for temperature prediction in microelectronics and is particularly attractive if justified simplifications are made to a model for time and money savings" [15].

Guenin et al. analyzed thermal performance of a SuperBGA, which is a thermally enhanced BGA, using non-linear lumped parameter model [18]. To obtain a simplified thermal model (what they called thermal circuit diagram) of SuperBGA as shown Figure 2.1, each component of the package, the board and boundaries were represented with resistances. At the end of study, they claimed that simulated values agree with the measured ones for all conditions including radiation and the method can be used at development stages of similar packages for thermal evaluations [18].

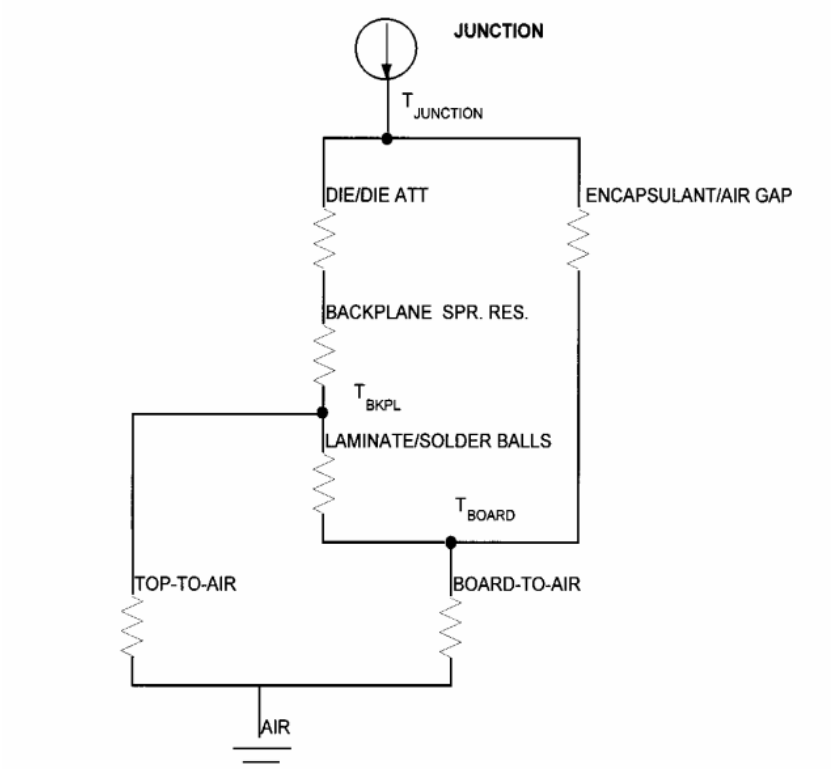

Figure 2.1 Thermal circuit diagram for the SuperBGA package [18]

One of the most detailed studies about standardized thermal model of an electronic package was performed by Rosten et al. [16], with support of DELPHI. In this pioneering study a detailed thermal model was developed for a Plastic Quad Flat Package (PQFP) using the commercial CFD software Flotherm. Main goal of the study was to illustrate the applicability of their thermal model and to promote component manufacturers to supply similar thermal models of their packages to their

customers. Detailed thermal model was validated with experiments, in which junction to ambient thermal resistances were measured in a still air environment (JEDEC and SEMI natural convection test setups). Also surface temperatures were measured using an infrared camera. One of the important points of this study was the use of both lumped (compact) and zero thickness components in the detailed thermal model. For internal leads they used a continuous layer of material as shown in Figure 2.2 with effective material properties such as effective thermal conductivity computed using the properties of mold compound and copper leads (Eq. 1.4-1.5). Similar continuous layers were also used for external leads.[16].

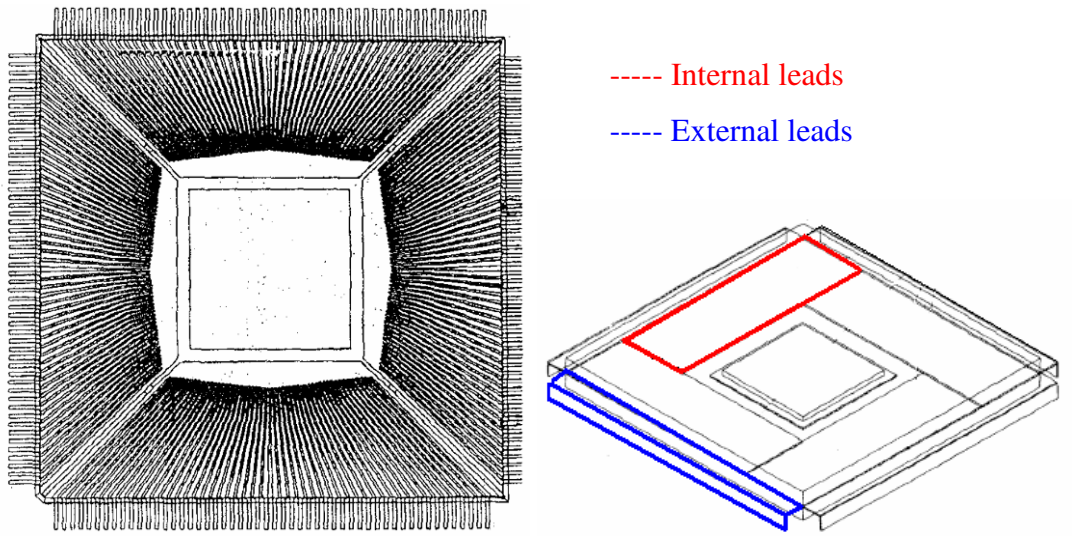

Figure 2.2 Representation of internal and external leads [16]. Real diagram of lead frame (left), lumped (compact) continuous layers (right)

As a result of their study, Rosten et al. claimed that "the predicted values (junction to ambient) were only 3.5 % lower than experimental results for both the JEDEC and SEMI tests. This was within the range of experimental error and demonstrated that the computational model is able to predict the thermal resistance to within the range of the experimental error" [16].

Another DELPHI supported study was presented by Parry et al. for a single-chip package [19], in which simplified resistance models were generated with using data fitting and analytic techniques. In the first step a detailed model was created to serve as a base model. The die, C4 substrate and the ball grid arrays were represented with cubic blocks in the detailed thermal model. Two simple resistance based CTMs were tested, one of which is of star network type and the other was an original design of the authors. CTMs were examined at different environmental conditions where air was forced with 0.5, 1.0, 2.0, 4.0 m/s uniform velocities. At the end of the study authors claimed that CTM designed by them was superior to star network model when die junction temperature results were compared with the detailed thermal model.

Lee and Mahalingan used a detailed thermal model to investigate thermal limits of a plastic Pin Grid Array (PGA) package [20]. They first validated their DTM based CFD simulations using experiments and then performed extra numerical tests using DTM to study the thermal limits of the PGA. They asserted that the procedure of generating DTM can be applied to any single chip electronic package.

Due to increasing use of CFD tools for numerical simulations of electronic cooling applications, Zahn performed a comparative study of two popular CFD software, Icepak and FloTHERM [21]. He investigated the performance of these two software for package level thermal analyses and compared them based on accuracy and ease of use. Zahn reported that the maximum difference between experiments and simulations is less than 10 % for both Icepak and FloTHERM. He added that junction and highest case temperature results of Icepak is more precise. Zahn found Icepak to be superior due to its user friendly graphical interface and efficient grid generator. On the other hand he added that Icepak's simulation models take much more space in the computer's hard drive. Zahn concluded as "the scope of this study is somewhat narrow and should not be used by the reader as the only basis for selecting a CFD tool. The user is instead encouraged to perform a benchmark study

which emphasizes their own level of electronic thermal analysis, whether it is package, printed circuit board, or system level".

One of the pioneering studies about system level thermal modelling was conducted by Rodger et al., in which thermal behaviour of a multi-component PCB is studied numerically [22]. They used one Plastic Quad Flat Package (PQFP), one Thin Small Outline Package (TSOP) and two Small Outline (SO) electronic packages to construct a multi-component PCB as shown in Figure 2.3. Components of this PCB assembly were modelled with both detailed and compact strategies. For detailed modelling they used Rosten et al's approach as explained above. For compact modelling they preferred Adams et al.'s Block on Lead (BoL) technique [23], which consists of an inner and outer single layer block with heat dissipation confined to the inner one. Effective thermal conductivities of inner and outer blocks are computed based on volumetric averaging. Rodger et al. indicated that number of grid cell in computational domain can be reduced by a factor of two with the use of compact modelling. They showed that detailed modelling of multi-component PCB causes unnecessarily fine grid in the far field region. The study concluded that compact modelling can predict package junction temperatures and surface temperature gradients with good accuracy [22].

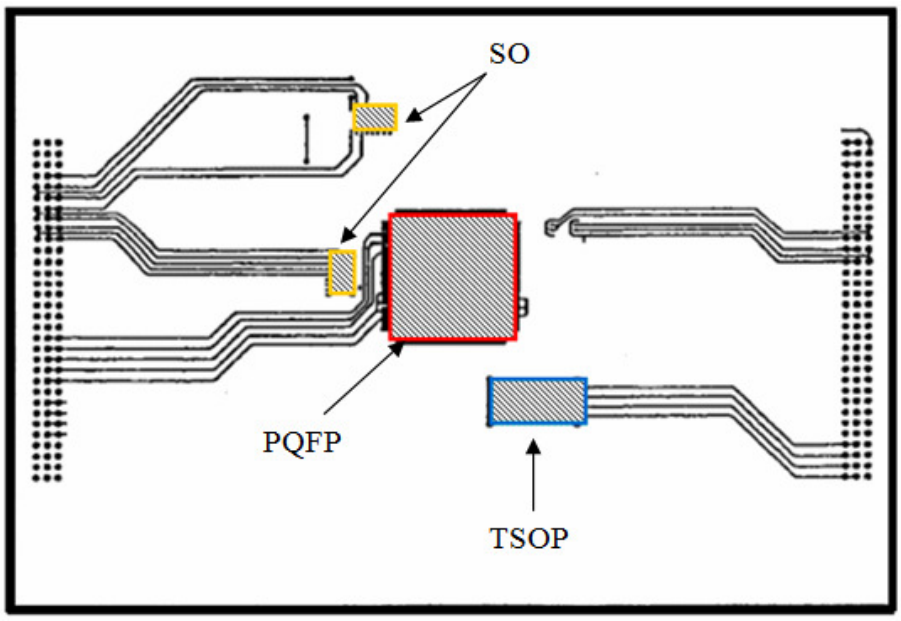

Figure 2.3 Multi-component test PCB component location and copper traces [22]

Although most of the printed circuit boards and electronic packages are cooled with forced convection, conduction cooling to a cold plate is preferred especially for applications in defence industry to satisfy reliability demands. One of the leading studies relevant to the use of compact modelling for conduction cooling was presented by Aranyosi et al. [24], in which the primary concern was to create boundary condition independent CTMs for steady-state problems. A genetic algorithm based technique was used to extract the CTM parameters of star resistor and shunted resistor CTMs. To simulate a conduction-only case, weak radiative and convective transports were ignored. In the simulation part resistance values of star and shunt network topologies were obtained by the help of detailed thermal models. According to the results of this study star-shaped CTMs accurately predict the junction temperatures, but usually give insufficient accuracy for the heat flux values.

In conduction cooled electronic packages, where PCB is used as a heat sink, heat transfer path from die to PCB through ball grid array or external leads becomes important. Most of the researchers modelled PCB and BGA of such cases using single layer blocks with anisotropic effective conductivities without taking the

spreading resistance into account. The concept of spreading resistance is used whenever a heat source is located on top of a component having an area larger than the source. Ying and Toh worked on this subject with the aim of obtaining anisotropic spreading resistance formulation that can be included in CTMs [25]. At the end of study authors claimed that important parameters which effect spreading resistance were ratio of in plane-through plane thermal conductivity, PCB geometry and thermal boundary conditions.

Lasance presented a study that introduces generic benchmark models for two of the commonly used components, a leaded package (TQFP) and an area-array package (BGA) [26]. The ultimate aim of Lasance was to establish a common framework that can be used by other researchers. These benchmark models contain sufficient details to make them suitable for parametric studies but extreme care is required for grid independence.

Mostly due to changing ambient conditions, electronic systems and components may be exposed to transient operating conditions. Although electronics cooling simulations are usually carried to be steady state there are studies focusing on the transient aspects. One of the noticeable studies in this respect was performed by Eveloy et al. [27], who used FloTHERM to investigate the accuracy of transient simulations in still air and forced air flow (1 and 2.25 m/s) ambients. Different transient operating conditions such as component dynamic power dissipation in fixed ambient conditions, passive component operation in dynamic ambient conditions and combined component dynamic power dissipation in varying ambient conditions were analyzed. Numerically and experimentally obtained junction and PCB surface temperatures were compared. Component and PCB modelling methodologies were based on Rosten et al.'s approach [16]. It was shown that junction temperatures can be predicted with good accuracy in both steady and transient ambient conditions. Also it was pointed out that CFD tools could be used for evaluation of performance of electronic packages at critical boundary conditions.

In another transient CTM study Mohammadi and Marami modelled a BGA package [28]. First a standard CTM was built with a resistor network topology. Then this CTM is converted into a dynamic CTM by introducing capacitors that represent thermal mass of the component. Transient junction temperatures and heat flux values were used to evaluate the performance of dynamic CTM against a detailed dynamic model. An optimization algorithm was employed to modify the resistance model so that the difference between the results of detailed and compact models can be minimized. The authors concluded that the developed dynamic CTM is able to capture the transient behaviour of the BGA package efficiently and accurately.

Garcia and Chiu [29] used CTM idea to simplify multi (stacked) die packages, where two or more dies are used in one package as shown Figure 2.4. Their first approach was conduction based compact modelling (CCM) of Gemal and Refai, where die attach was simplified to be a 2D (zero thickness) object and solder balls and vias were lumped into simplified blocks. In the second approach additional simplifications such as lumping stacked dies into a single die were performed. As a third alternative a simple two resistor CTM consisting of a junction to case resistance (R_{jc}) and a junction to board resistance (R_{jb}) was used. These CTMs were compared with a detailed model under different boundary condition scenarios such as still air enclosure (JESD51-2a) [30], ring cold plate test (JESD51-8) [31], and top cold plate test. It was observed that the first CTM could reasonably simulate thermal performance of the package and it was pointed out that CTMs of this study should be validated with an experimental study where a real thermal test dice is used.

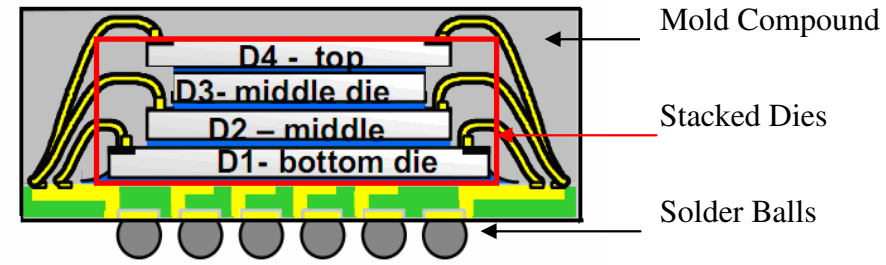

Figure 2.4 Representation of multi-die package [29]

Dhinsa et al. evaluated commonly used turbulence models in terms of computational efficiency and accuracy of heat transfer problems [32]. Turbulence models such as LVEL, CAP, Wolfshtein, k-ε, k-ω, hybrid k-ε k-l and Shear-Stress Transport (SST) were examined with PHYSICA finite volume code for the Meinders' single test cube benchmark problem. In addition to the evaluation of commonly used turbulence models a new transitional turbulence model was also offered. The new transitional model was a hybrid technique that uses suitable turbulence models near the wall regions and the standard k-ε model elsewhere. The authors pointed out that "As the recirculation vortices develop they encapsulate heat from a package and restrict further heat being extracted and removed from the system". Also it was concluded that it is difficult to obtain accurate predictions using the standard k-ε turbulence model for real word problems. At the end there was no obvious winner, but other investigated models gave better results compared to the standard k-ε.

Although thermal performance of BGA and QFP type electronic components have been investigated extensively, power modules and their thermal characteristics has not been examined in detail in the literature. Pang devoted his PhD dissertation to this issue by investigating embedded power modules and composing a guideline that can be used by power module designers [33]. Interestingly he used I-DEAS for the numerical simulations. First numerical models were validated with experiments and then different cooling techniques for embedded power modules were studied. Important thermal design variables such as chip-to-chip distance, copper trace area, polyimide thickness, ceramic materials, etc. were examined in detail. It was observed that temperature of hot spots on the power models can be reduced by 24 % with simple design changes and even more reduction can be achieved by a double sided cooling strategy.

In order to investigate static and dynamic effects of heat dissipation on an electronic component, electrical simulation tools can be coupled with CFD tools to perform electro-thermal simulations. Vellvehi et al. performed such a study to simulate the electro-thermal behaviour of a DC/DC converter [34]. A relaxation method was used

to couple electrical and thermal simulation tools. Vhdl-Ams and FloTHERM were used for electrical and thermal modelling, respectively. These software are coupled using a relaxation method, in which “electrical and thermal equations are solved separately exchanging temperature and power parameters periodically until thermal and electrical convergence is reached” [34]. Although such a coupled simulation provided more accurate temperature values, it also resulted in longer run times. DC/DC converter was modelled in two stages. In the first stage only power devices, MOSFETs and Schottky diodes, were included for the validation of methodology. In the second stage other inactive parts such as self-inductances, capacitors and transformers were also modelled. Results of simulations were evaluated with respect to infrared thermography experiments to get a good agreement.

CHAPTER 3

PROBLEM STATEMENTS AND EXPERIMENTAL STUDIES

In this chapter first the three problems that are studied will be described. Next details of the experimental setups used for the first two problems will be provided. Finally experimental results will be presented and discussed.

3.1 Problem Statement

In this study a number of conduction based compact thermal models (CCM) with varying details of a Thin-Shrink Small Outline Package (TSSOP) type and module type DC/DC converters are designed and used to simulate steady state operating conditions. The motivation is to understand the level of geometrical and material property simplifications that can be tolerated in obtaining numerical results of acceptable accuracy. CCM alternatives are tested for three different problems corresponding to component, board and system level arrangements as described below.

Component level simulations made use of a single TSSOP type DC/DC converter located on a PCB which is cooled by natural convection. Five different CCMs are designed with varying degrees of geometrical simplification. Numerical results obtained by Icepak (ANSYS Inc.) software are compared against experiments in which temperatures at several locations of the PCB are measured. Both the experimental setup and the corresponding numerical model are designed in accordance to the JEDEC 51-2a standard [30].

In the second problem cooling characteristics of a module type DC/DC converter, which is a common electrical component used in electro-optical systems, is investigated through both experimental and numerical studies in a board level arrangement. Temperatures at multiple locations of the PCB and DC/DC converter assembly are measured using thermocouples. Three different CCMs are developed and effects of CCM selection, grid size and quality and turbulence modelling are examined by comparing numerical results against experimental data.

For system level arrangement, presented here as the third problem, thermal management of a typical air transport rack chassis is studied only numerically. A single PCB with a number of heat generating components including the TSSOP type DC/DC converters studied previously is located in a sealed box that is cooled from outside using forced convection. Considering the results of the case with least amount of simplification to be the most accurate, performance of CCMs designed previously are evaluated.

3.2 Experimental Studies

Two experiments are conducted to analyze the accuracy that can be obtained by the use of different CCMs. The first experimental setup is for natural convection cooling of TSSOP type DC/DC converter and the second one is for forced convection cooling of a matrix of module type DC/DC converters. During the experiments temperature measurements at several locations of the PCB and DC/DC converter surfaces are made.

3.2.1 Natural Convection Experimental Setup

For the first validation experiment JEDEC 51-2a (Integrated Circuits Thermal Test Method Environmental Conditions - Natural Convection (Still Air)) standard procedure is followed [30].

In the experiment an evaluation module of a Thin-Shrink Small Outline Package (TSSOP) type integrated circuit working as a DC/DC converter is used. Surface temperatures at various locations are measured and stored until steady conditions are reached.

Figure 3.1 presents a general view of the natural convection setup. All components used in this setup are explained below in detail.

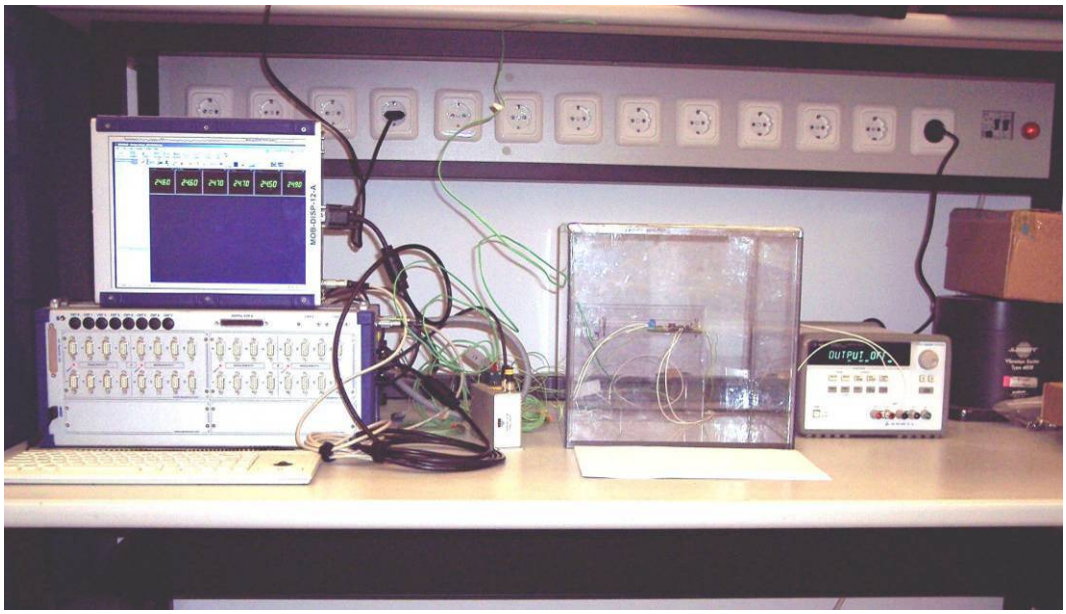

Figure 3.1 General view of the natural convection experimental setup

TPS54610EWM Evaluation Module

TPS54610EVM is an evaluation printed circuit board (PCB) with a TSSOP type DC/DC converter, produced by Texas Instruments. As shown in Figure 3.2 the main heat generating component on it is a TSSOP type buck regulator DC/DC converter. It is defined in its data sheet as “The TPS54610 evaluation module (EVM) uses the TPS54610 synchronous buck regulator to provide a 3.3-V output over an input range of 4.0 V to 6.0 V and over a load range of 0 A to 6 A.” [40].

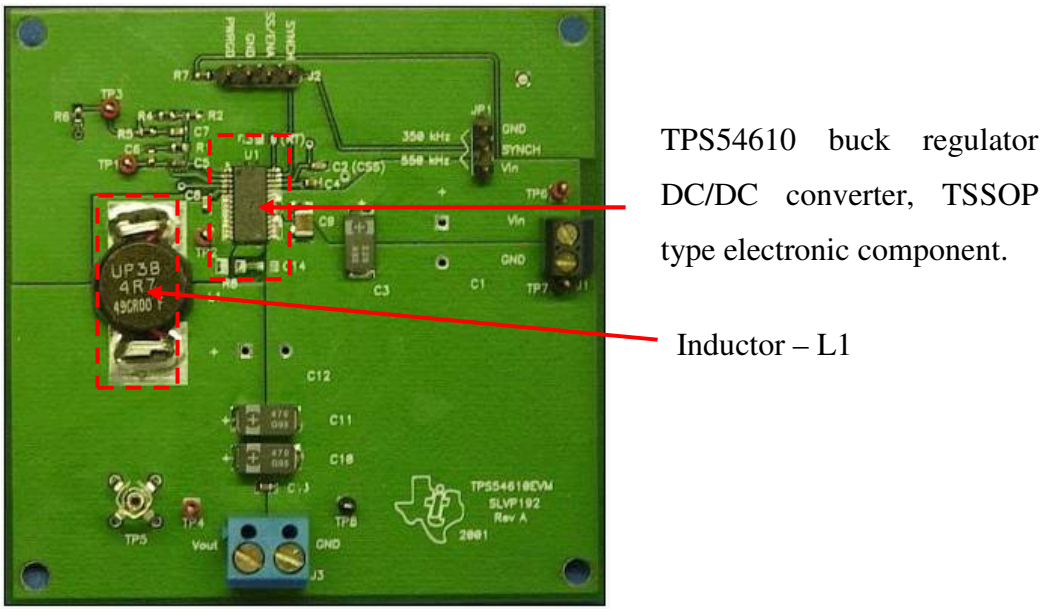

Figure 3.2 Evaluation Module with the DC/DC Converter

As sketched in Figure 3.3 printed circuit board of TPS54610EVM is a standard 2P2S (2 signal and 2 power (ground) planes) board, which is compatible with the JEDEC 51-2a test standards. The stack up layer of the PCB is explained in its vendor documents as “The top and bottom layers are 1.5 oz. copper, while the two internal layers are 0.5 oz. copper. The two internal layers are identical and are used as quiet ground planes” [40].

Figure 3.3 Stack up layers of the *TPS54610EVM* PCB

TPS54610 Buck Regulator DC/DC Converter

Shown inFigure 3.4, TPS54610 is a low-input voltage, high-output current, synchronous buck power module [41]. Thermal enhancement options are available

for TPS54610 with PowerPAD™ package, which is used in the experiments of the current study. It is the major heat generating component of the first experiment.

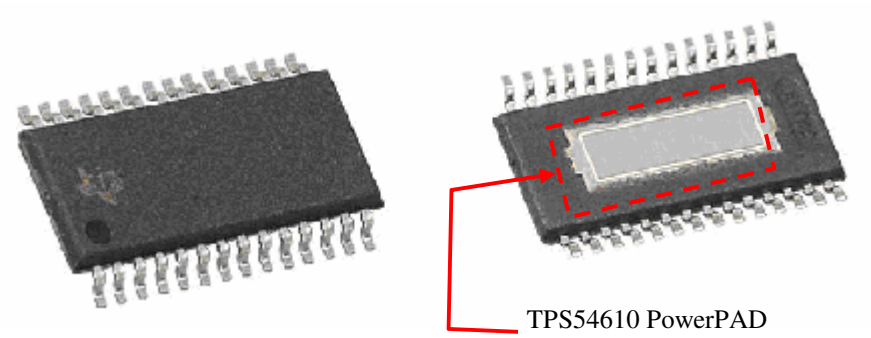

Figure 3.4 TPS54610 buck regulator DC/DC converter IC [41]

Test Enclosure Assembly

Test enclosure assembly, shown in Figure 3.5, is produced in ASELSAN A.Ş. It is made of polycarbonate, which is a transparent material with low thermal conductivity (0.179W/mK). The material itself and the dimensions of the enclosure, as shown in Figure 3.6, are consistent with JEDEC 51-2a standard. All edges of the enclosure are thoroughly sealed to ensure no airflow through it.

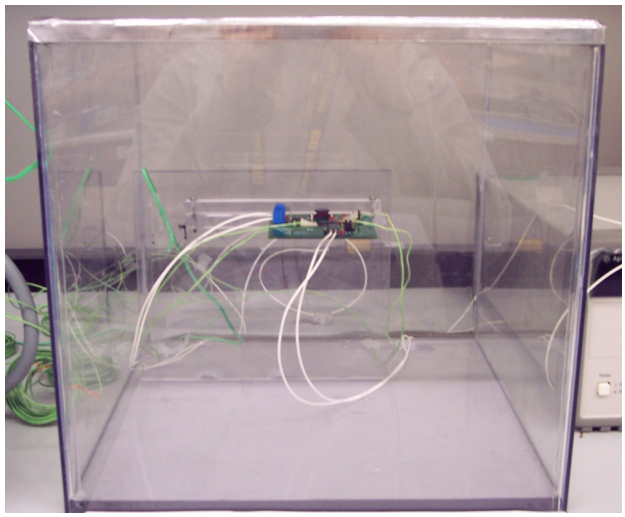

Figure 3.5 Test Enclosure Assembly

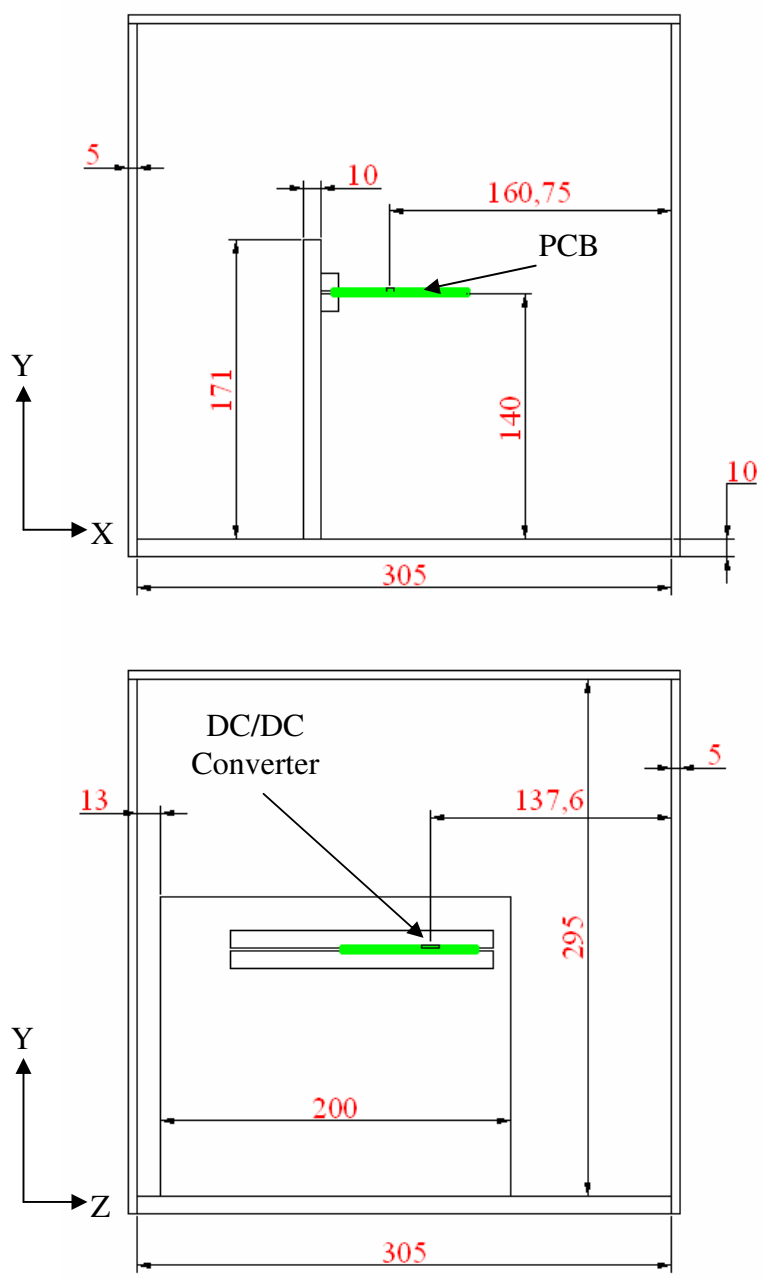

Figure 3.6 Dimensions (in mm) of the Test Enclosure Assembly

Data Acquisition System and Thermocouple Interface Pad (TIP)

In order to store measured temperature values, a 32 channel data acquisition system, shown in Figure 3.7 is used. Also shown in the same figure, a thermocouple interface

pad is used to connect K type thermocouples to the system. The sampling rate of data acquisition system is set to be 0.1 s.

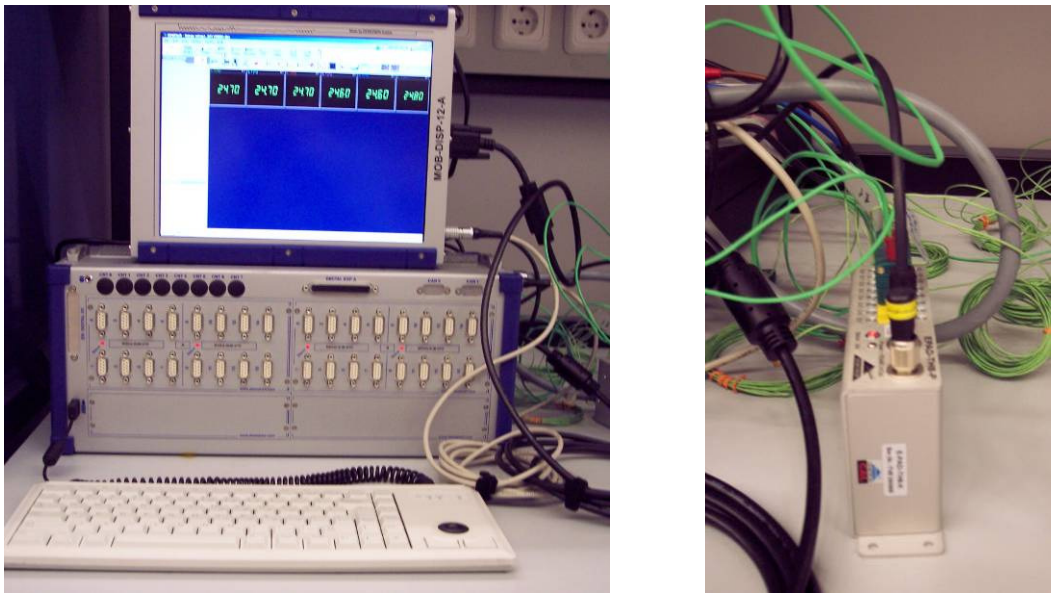

Figure 3.7 Data Acquisition System (left) and Thermocouple Interface Pad (right)

Thermocouples

While K-type, surface-mount fast-response (less than 0.15 s) thermocouples are preferred for surface temperature measurements, general purpose K-type thermocouples are used for air temperature measurements (Figure 3.8 Fast response thermocouples are made of 30 AWG (0.0254 mm) thermocouple wire with a temperature sensitivity of ± 1.1 °C [42]. General purpose ones are made of 20 AWG (0.81 mm) nickel-chromium wire with a temperature sensitivity of ± 1.5 °C [43], [44].

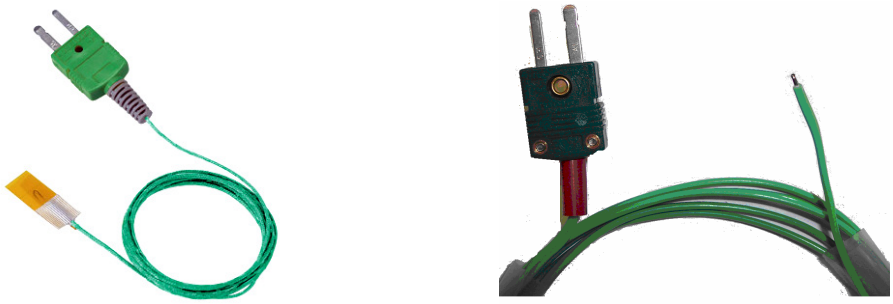

Figure 3.8 Fast response (left) and general purpose (right) K-type thermocouples [42]

Electric Load and Power Supply

Electric Load is a kind of resistor and used to simulate output electrical behaviour of electronic systems in experiments. A resistance with aluminium fins, as shown in Figure 3.9 is used as the electric load. Its resistivity is 1 Ω and it is extremely durable at high temperatures [45].

Figure 3.9 Wirewound resistor (Mil-prf-18546 Qualified aluminium housed) [45]

Finally an Agilent E3634A 25V-7A power supply, shown in Figure 3.10, is used in order to satisfy power demand of TPS54610 evaluation board.

Figure 3.10 Agilent Power Supply

3.2.2 Procedure of the Natural Convection Experiment

As a first step, *TPS54610EVM* input output connections are linked up as pointed out in EVM data sheet [40]. A diagram showing connection points (Voltage input, voltage output, ground J1 (GND) and ground J3) is given in Figure 3.11. Power supply is connected to J1 and V_{in} through a pair of 20 AWG wires. Similarly, electric load (1 Ω resistor) is connected to J3 and V_{out} through a pair of 20 AWG wires. Wires are kept as short as possible to minimize losses in them. After these connections the evaluation board is placed in the test enclosure assembly, keeping the power supply and the electric load outside.

Next, thermocouples are attached to locations shown in Figure 3.12, using Kapton (polymide) double side sticky tape labels. Thermal conductivity and thickness of these labels are 0.12 W/mK and 0.064 mm. As seen, five thermocouples are used for temperature measurements, but actually only three of them (1, 2, 5) are required by JEDEC 51-2a standard. The first thermocouple is located at the centre of the top surface of the DC/DC converter. The second one is placed as on the PCB surface, as close as possible to the external leads as pointed out by JEDEC 51-2a. The third thermocouple is located at the centre of the top surface of PCB and the forth one is placed at the bottom surface of the PCB as close as possible to the via structure. Finally the fifth thermocouple is used to measure air temperature inside the enclosure and placed as stated by JEDEC 51-2a. All the thermocouples are connected to TIP, which is further connected to the data logger.

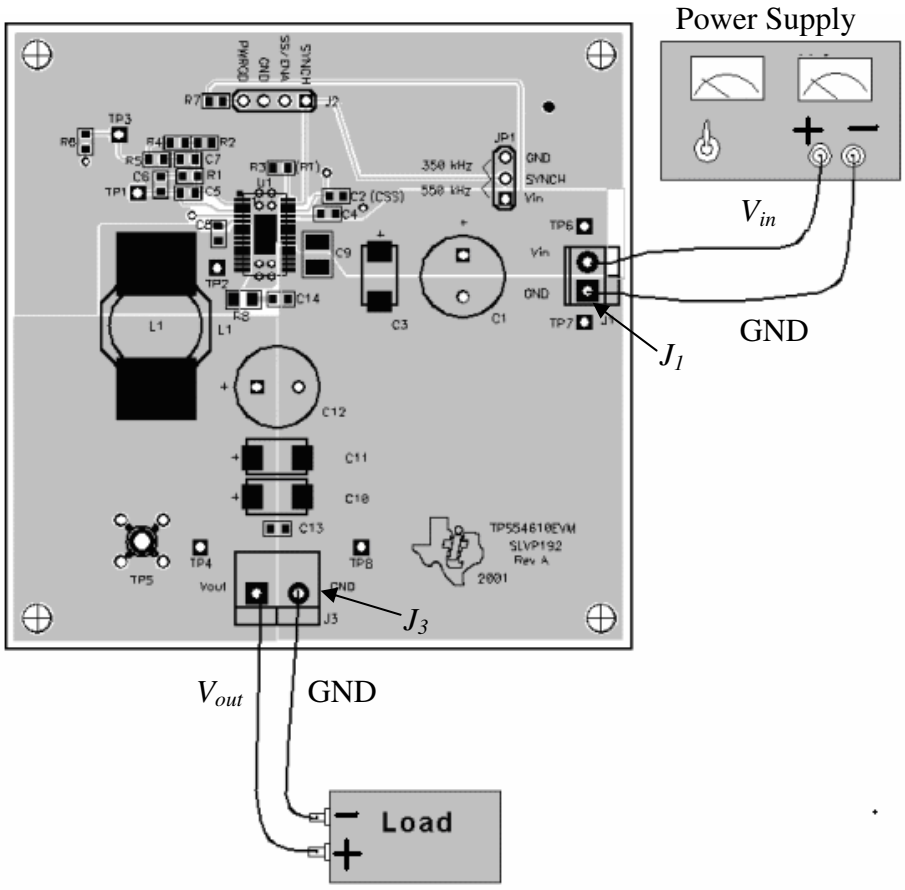

Figure 3.11 EVM connections [40]

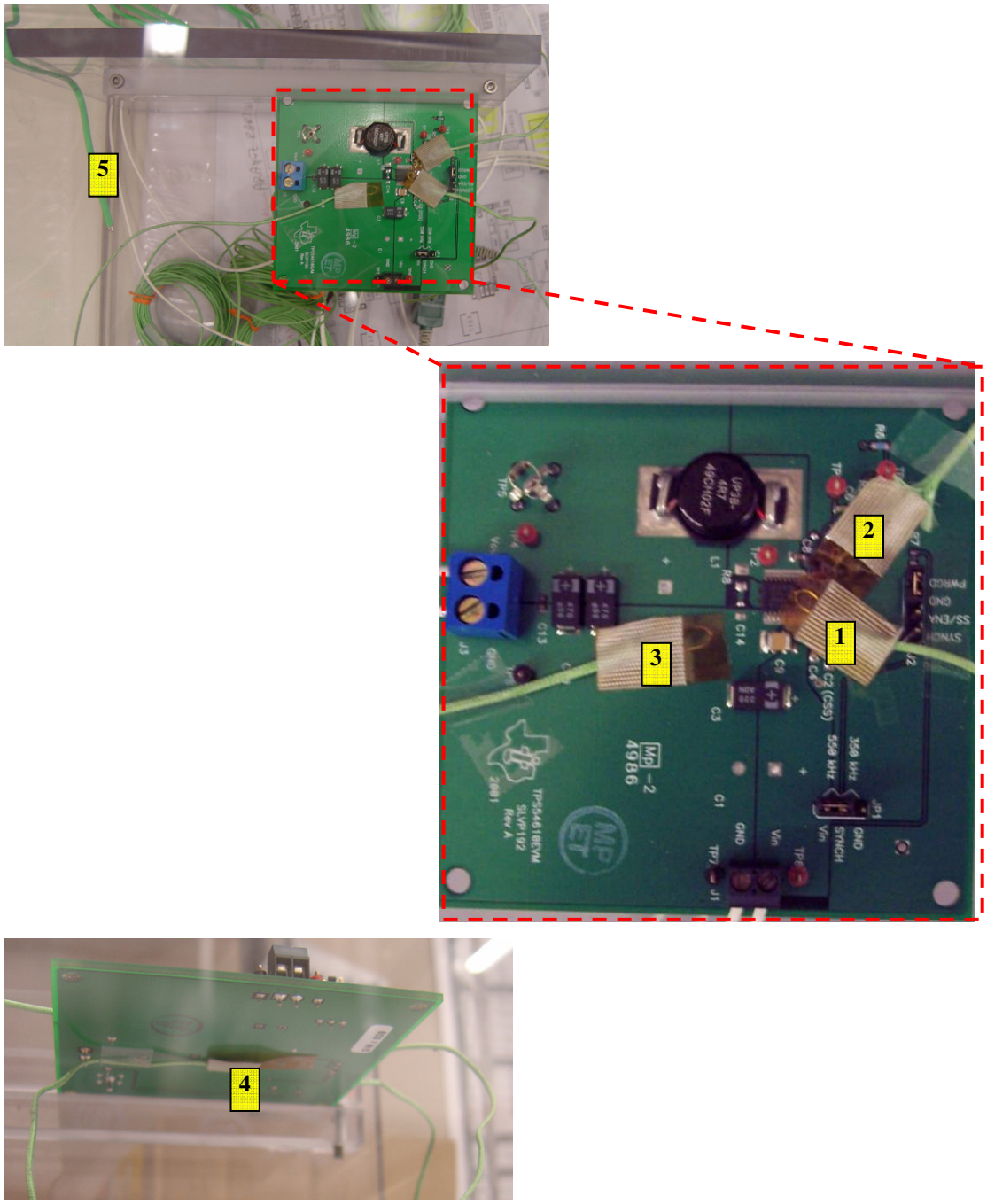

Figure 3.12 Thermocouple locations and identification numbers

As mentioned in the data sheet of the evaluation board, input voltage and current values are adjusted using the power supply as 5 Volt and 6 Ampere, respectively [40]. But these are not the actual values used by the board. Input voltage and current values read from the power supply while the board is in operation are given in Table

3.1. Output voltage given in the same table is measured using a standard multimeter. Output current and output power values are calculated by the help of the electric load as follows

$$P_{out} = I_{out}.V_{out} = I_{out}{}^{2}.R_{electric\ load} \quad (3.1)$$

Using the known resistance of the electric load, which is 1 Ω, output current value is calculated to be the same as the output voltage value. Finally output power given in Table 3.1 is calculated by the help of the above equation.

Table 3.1 Input / Output voltage, current and power values of the evaluation board

	Voltage (V)	**Current (A)**	**Power (W)**
Input	4.996	2.232	11.151
Output	3.270	3.270	10.693

Difference between input and output powers is 0.458 W, which can be considered to be the total heat dissipated by the evaluation board. This heat is not only dissipated by the DC/DC converter, but also by other components such as the inductor L1 shown in Figure 3.2. To determine the heat dissipated by the DC/DC converter only, heat dissipated by the inductor is taken into account. Internal resistance of the inductor is given as 11.4 mΩ at a maximum current of 7.7 A [46]. In our case the current passing through L1 is approximately 3.0 A. Based on the current difference, inductor's internal resistance is assumed to be 4.5 mΩ, which provides a heat dissipation value of $(3^2)(0.0045) = 0.0405$ W. Therefore the heat dissipated by the DC/DC converter only can be computed to be approximately $0.458 - 0.0405 \approx 0.42$ W. This is the value used in the numerical simulations.

To make sure that the board is working as expected efficiency graph provided by the manufacturer is used [41]. As seen in Figure 3.13, efficiency of the evaluation board at 2.232 A input current is approximately 96 %. Note that this graph is given for 5V input and 3.3 V output voltages, whereas these values are measured in the experiment to be 4.996 V and 3.27 V, respectively. Using the power values given in Table 3.1, the board actually operates at an efficiency of 10.693/11.151 * 100 = 95.9 %, which is very similar to the value read from the graph. Therefore it can be said that the board is working as expected.

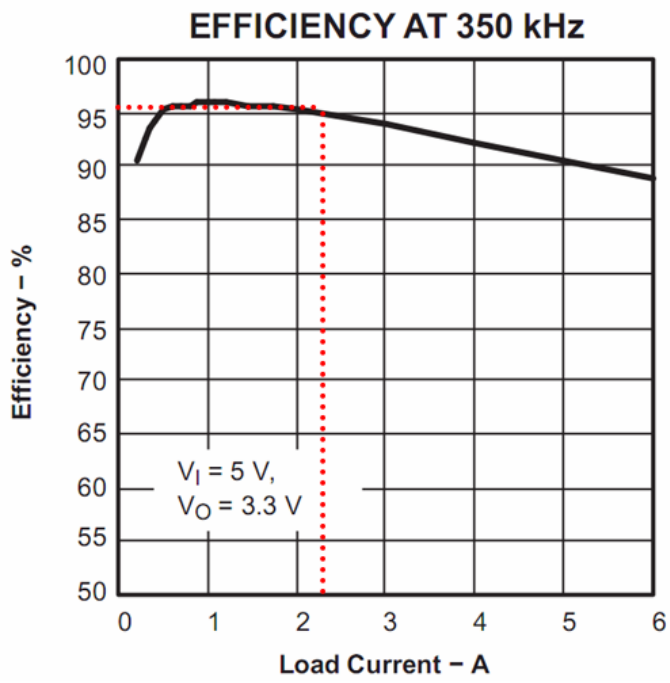

Figure 3.13 Efficiency graph of the TPS54610 DC/DC converter [41]

3.2.3 Measurements of the Natural Convection Experiment

Data acquisition system is started to record temperatures from test enclosure just before power supply is turned on. Temperatures are recorded at every 0.1 s for two hours. Results of the measurements are given in Figure 3.14.

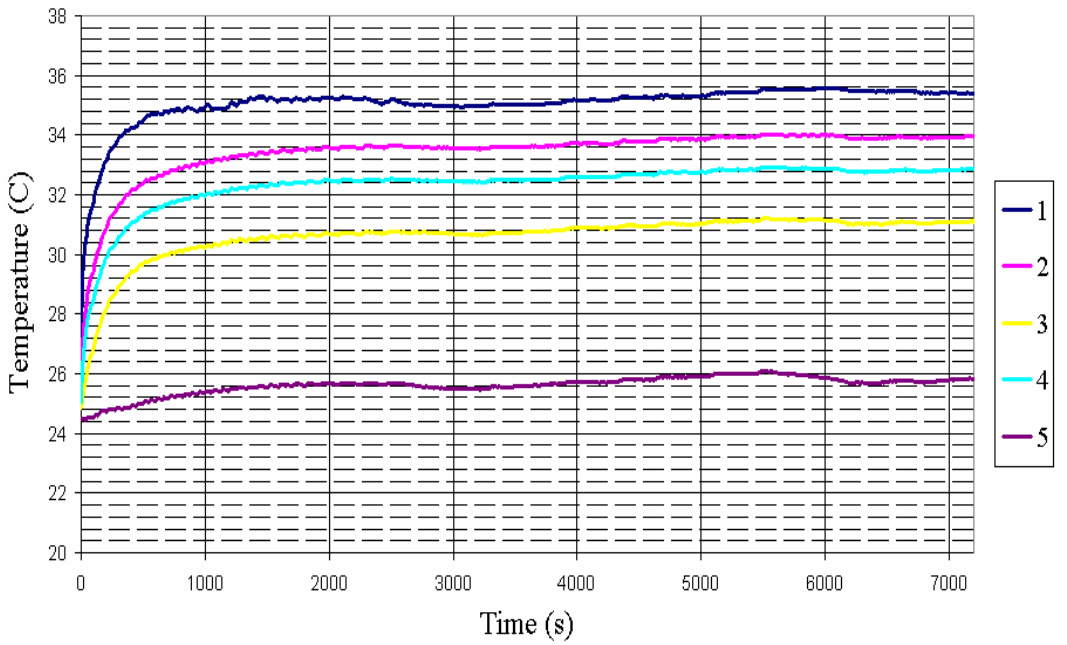

Figure 3.14 Measurements of the natural convection experiment. Coloured lines and corresponding numbers represent thermocouples.

As seen from the graph maximum temperature value is recorded by thermocouple 1 as expected, which is directly attached to the DC/DC converter. All five measurements show a similar increasing trend for the first 1500 s, after which temperatures stabilize with small fluctuations due to the fluctuations of the outside ambient temperature. Steady state temperatures, shown in Table 3.2, are taken to be the average values corresponding to the last 1000 s of the experiment.

Table 3.2 Temperature results of the first experiment (ºC)

Thermocouple (TC) No				
1	**2**	**3**	**4**	**5**
35.4	33.9	31.1	32.8	25.7

3.2.4 Forced Convection Experimental Setup

In the second validation experiment a board level thermal analysis is studied under forced convection conditions. In the experiment a power card that is a part of a real electro-optical system is used. The card is composed of nine identical MGDM-150 series module type DC/DC converters and a 12 layer printed circuit board.

Figure 3.15 presents a general view of the forced convection experimental setup. Each of the components used in the experiment is described below in detail.

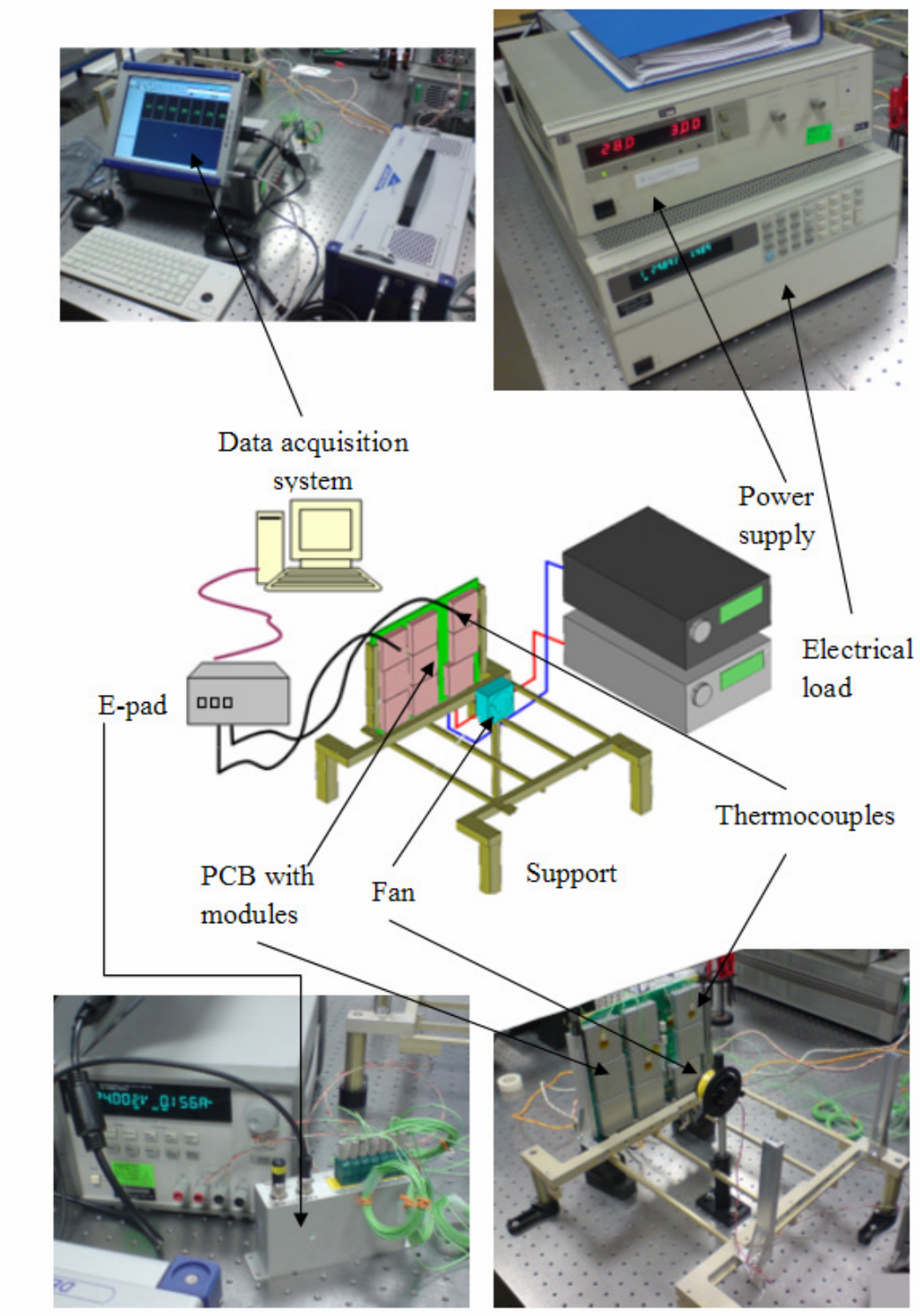

Figure 3.15 General view of the forced convection experimental setup

The Power Card

Power card, which is a part of a real electro-optical system, is an assembly of 12 layer PCB and 9 identical MGDM-150 series module type DC/DC converters. DC/DC converters are produced by GAIA Converter Inc. and attached to the PCB as shown in Figure 3.16 at ASELSAN Inc.. PCB of the power card has external dimensions of 3.4 x 210 x 250 mm and contains 12 tracing layers, each containing different ratios of FR-4 and copper. Copper trace thicknesses are very high compared to a standard PCB, due to which electrical output of the card could reach to values as high as 400 W.

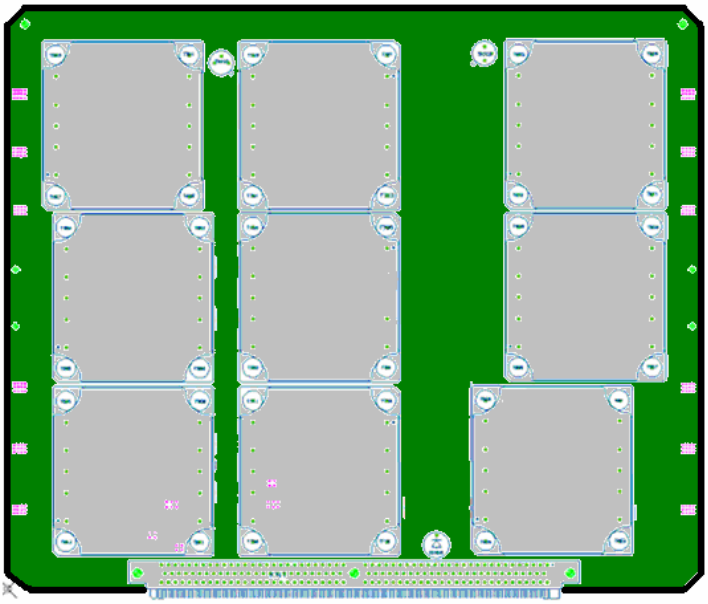

Figure 3.16 Power Card with 9 Module type DC/DC converters

MGDM-150 Series Module Type DC/DC Converter

This converter, produced by GAIA Inc., is described in its data sheet as "The MGDM-150 low input voltage series is a complete line of high density wide input range DC/DC power modules designed for aerospace, military and high-end industrial applications. These modules use a patented fixed switching topology at

420 KHz providing ultra wide input range, low noise characteristics and high power density. Standard models are available with ultra wide input voltage range of 9-45, 16-80 volts. The series include single output voltage choices of 3,3, 5,12, 15, 24, 28 volts" [42].

Similar to the natural convection experiment, DC/DC converters of this experiment are also the major heat generating components. To spread and remove undesired heat the converter has an aluminium shield as shown in Figure 3.17. By the help of this shield, which is called base plate by the manufacturer, working temperature of the converter can go up to +105 ^{o}C.

Figure 3.17 MGDM-150 Series Module Type DC/DC Converter [47]

Fan

An Ametek Rotron ½ Aximax 28 V DC (3162SF) fan, shown in Figure 3.18, is selected as a cooling element of the forced convection experimental setup. It has a maximum speed of 10000 rpm and a free flow rate of 25.2 cfm [48].

Figure 3.18 Ametek Rotron ½ Aximax 28VDC Fan [48]

Support

Support, shown Figure 3.15, is produced from aluminium at ASELSAN A.Ş. Power card and fan are placed on it. It is fixed on an optical table with mechanical fasteners.

Data Acquisition System, Thermocouple Interface Pad and Thermocouples

These are the same as the ones used in the natural convection experiment (see Figure 3.7 and Figure 3.8) .

Electric Load and Power Supply

Agilent 6050A electric load (Figure 3.19) is used to simulate the output electrical behaviour of the power card. HP 6010A DC power supply used in the experiments is also shown in Figure 3.19 to supply electricity to power card.

Figure 3.19 Agilent 6050A Electric Load (left) and HP 6010A Power Supply (right)

3.2.5 Procedure of the Forced Convection Experiment

First the power card input/output connections are established as shown in Figure 3.20. Power supply and the electric load are connected to input and output pins of the power card through two pair wires. Wires are kept to be short to minimize losses. An important point is that power is supplied to the card from two separate channels. The first channel supplies electricity to the DC/DC converters numbered as 1-5, while the second channel supplies to converters numbered as 6-9. Although DC/DC converters are identical in structure different amounts of heat is dissipated on them due to this difference.

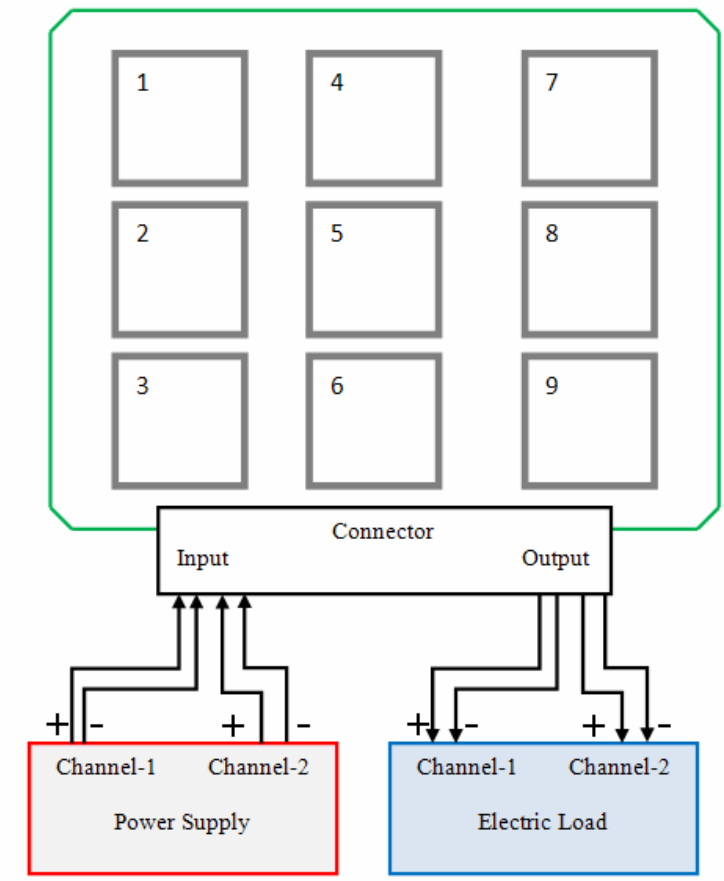

Figure 3.20 Connection of Power Card, Power Supply and Electric load

For the forced convection experiment temperatures are measured by six thermocouples shown in Figure 3.21. As seen, six different thermocouples were used for measurements and attached to locations using Kapton (polymide) double side sticky tape labels. The first thermocouple is placed at the centre of the top surface of the first DC/DC converter, the second one is placed on the PCB between the first and fourth DC/DC converters. The third and fourth thermocouples are attached to the side and top surfaces of the fifth converter, respectively. The fifth thermocouple is directly attached to the PCB and the last one is set to measure temperature of the top surface of the seventh DC/DC converter.

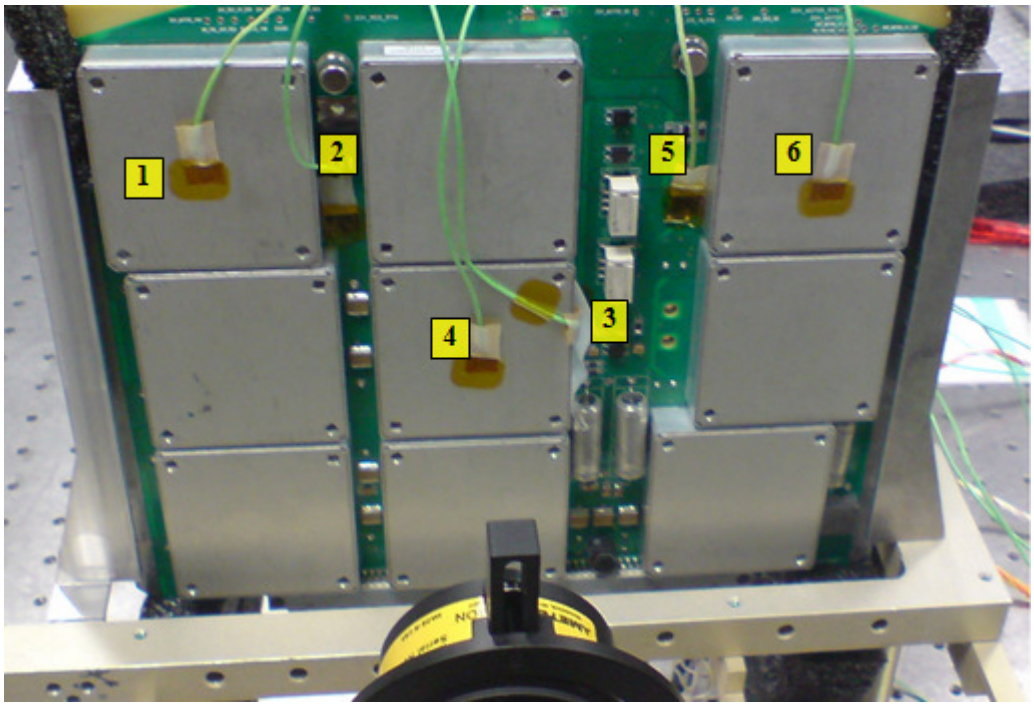

Figure 3.21 Thermocouple locations and numbers

After connecting the power card, data logger and the thermocouple interface pad, power supply is set to the input voltage and current values given in Table 3.3.

Table 3.3 Input / Output voltage, Current and Power Values of the Forced Convection Setup

		Voltage (V)	**Current (A)**	**Power (W)**
Input	Channel-1	28	2.28	63.84
	Channel-2	28	0.602	16.87
Output	Channel-1	29.88	1.39	41.53
	Channel-2	29.76	0.255	7.59
Difference	Channel-1			22.31
	Channel-2			9.28

* The channel-1 supplies electricity to the DC/DC converters numbered as 1-5

* The channel-2 supplies to converters numbered as 6-9.

Difference between input and output powers, as shown in Table 3.3, are 22.31 W and 9.28 for channel-1 and channel-2, which can be considered to be the total heat dissipated by the power card. As declared previous sections the first channel supplies electricity to the DC/DC converters numbered as 1-5, while the second channel supplies to converters numbered as 6-9. So (22.31 / 5 = 4.46 W) 4.46 W is the value used in the numerical simulations for each DC/DC converter numbered as 1-5 and (9.28 / 4 = 2.32 W) 2.32 W is the value used in the numerical simulations for each DC/DC converter numbered as 6-9.

3.2.6 Measurements of the Forced Convection Experiment

Temperatures are recorded at every 0.1 s for one and a half hours. Results of the measurements are given in Figure 3.22.

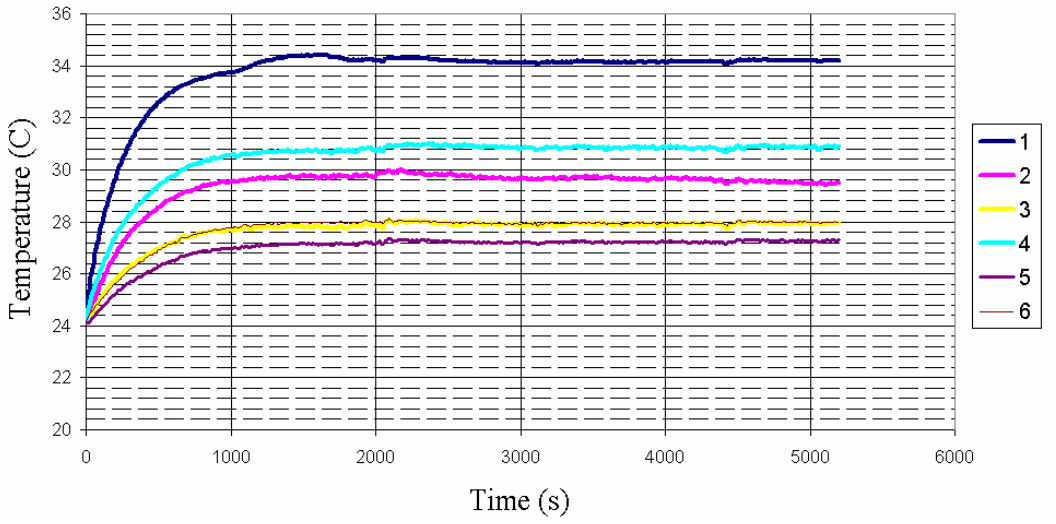

Figure 3.22 Measurements of the forced convection experiment. Coloured lines and corresponding numbers represent thermocouples.

As expected highest temperatures are recorded by the first and the fourth thermocouples, which are mounted on upper surfaces of the converters that produce more heat. All the measurements show a similar increasing trend for the first 1800 s,

after which they stabilize. Steady state temperatures, shown in Table 3.4 are calculated as averages of the last 1000 s of the experiment.

Table 3.4 Steady state temperatures measured in the second experiment (^{o}C)

Thermocouple (TC) No					
1	**2**	**3**	**4**	**5**	**6**
34.2	29.7	27.9	30.9	27.2	28.0

CHAPTER 4

NUMERICAL STUDIES and RESULTS

As mentioned in Chapter 3, this study involves experimental and numerical investigation of three heat transfer problems. The first one is a component level study for the natural convection cooling of a TSSOP type DC/DC converter. The second one is a board level study of forced convection cooling of module type DC/DC converters attached to a PCB. And the last problem is about the use of compact thermal models developed for the first problem in a more complicated system level arrangement. This chapter is about the numerical simulations performed for each of these problems.

All simulations described below are performed using Icepak 4.4.8 (ANSYS Inc.), which is a CFD software that solves mass, momentum and energy conservation equations to simulate fluid flows with heat transfer. For problems involving natural convection it employs the Boussinesq model. In conducting solid regions it solves a simple conduction equation that includes the heat flux due to conduction and volumetric heat sources within the solid.

In addition to the three conservation equations, radiative transport equation is also included in the computations. Discrete ordinate method is used to transform this additional equation into a set of simultaneous partial differential equations [35], [36], [38].

For turbulence computations Icepak offers several modelling options. In this study a number of different RANS based models are used and compared for the second and third problems [35], [36], [37], [38], [39].

4.1 Numerical Study of the First Problem (Natural Convection Cooling)

Computational model of natural convection experimental setup described previously in Chapter 3 is shown in Figure 4.1. Main parts of the setup, namely the PCB, TPS54610 DC/DC converter and the test enclosure assembly are involved in the computational model. All geometrical details, except some non-essential parts of the PCB such as small resistors, inductors and capacitors, are included in the numerical model.

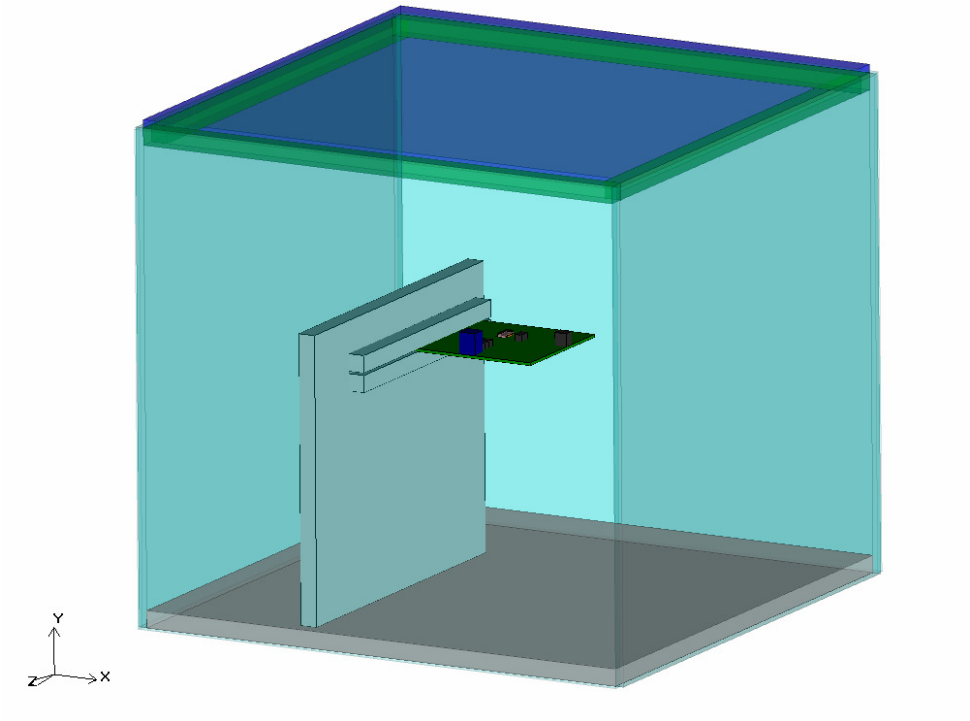

Figure 4.1 Computational model of the natural convection experiment setup

Five different conduction based compact thermal models (CCM) of the DC/DC converter are created based on previous studies of Ahmed and Karimanal [17]. These

compact models are obtained by applying different levels of simplification to a more realistic detailed thermal model (DTM). Details of these compact and detailed models will be given in the coming section.

Other than the modelling of the DC/DC converter, all simulations are identical in terms of dimensions, geometrical details, material properties, etc. In all models PCB is modelled as a solid cubic block of dimensions 76 x 1.6 x 76 mm. In order to prevent small grid cells, tracing (signal and power) planes of printed circuit board are omitted. But the effect of these omitted copper tracing layers is taken into account by modifying the material properties of the PCB properly. Effective material properties, shown in Table 4.1 are computed as a combination of the properties of FR-4 and copper using Eqns. (1.2 - 1.5).

Table 4.1 Effective material properties of PCB

Effective Conductivity x-direction (W/m-K)	**Effective Conductivity y-direction (W/m-K)**	**Effective Conductivity z-direction (W/m-K)**	**Effective Specific Heat (J/kg-K)**	**Effective Density (kg/m^3)**
32	0.3	32	1213	1890

Also common in all simulations, test enclosure assembly is modelled according to real dimensions using cubic blocks with real material properties of polycarbonate (k = 0.179 W/mK).

4.1.1 Detailed Thermal Model (DTM) of TPS54610 DC/DC Converter

As mentioned in the first chapter, a standard electronic package such as QFP, BGA or TSSOP involves some common parts as shown in Figure 1.4. In addition to these common parts, TPS54610 DC/DC converter has a particular part called powerPAD, which is a thermal enhancement used to eliminate bulky heat sinks and slugs (Figure 4.2). In these designs lead frame die pad (or thermal pad) is exposed to the bottom of

the IC. This provides an extremely low thermal resistance (R_{JC}) path between the die and the exterior of the package [41].

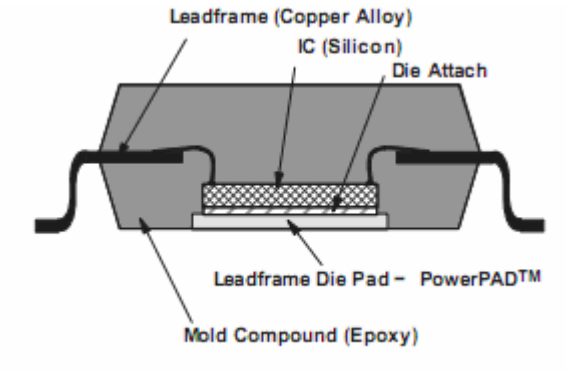

Figure 4.2 Section view of the package with powerPAD

Structural items of the TPS54610 DC/DC converter included in DTM are the die, die attach, die pad (powerPAD), vias and leads with all items encapsulated in a cubic volume of plastic mould compound (mold). Different views of the created DTM are given in Figure 4.3. Material specifications and dimensions of these different items are given in Table 4.2. Important aspects of modelling each item used in the DTM are described below.

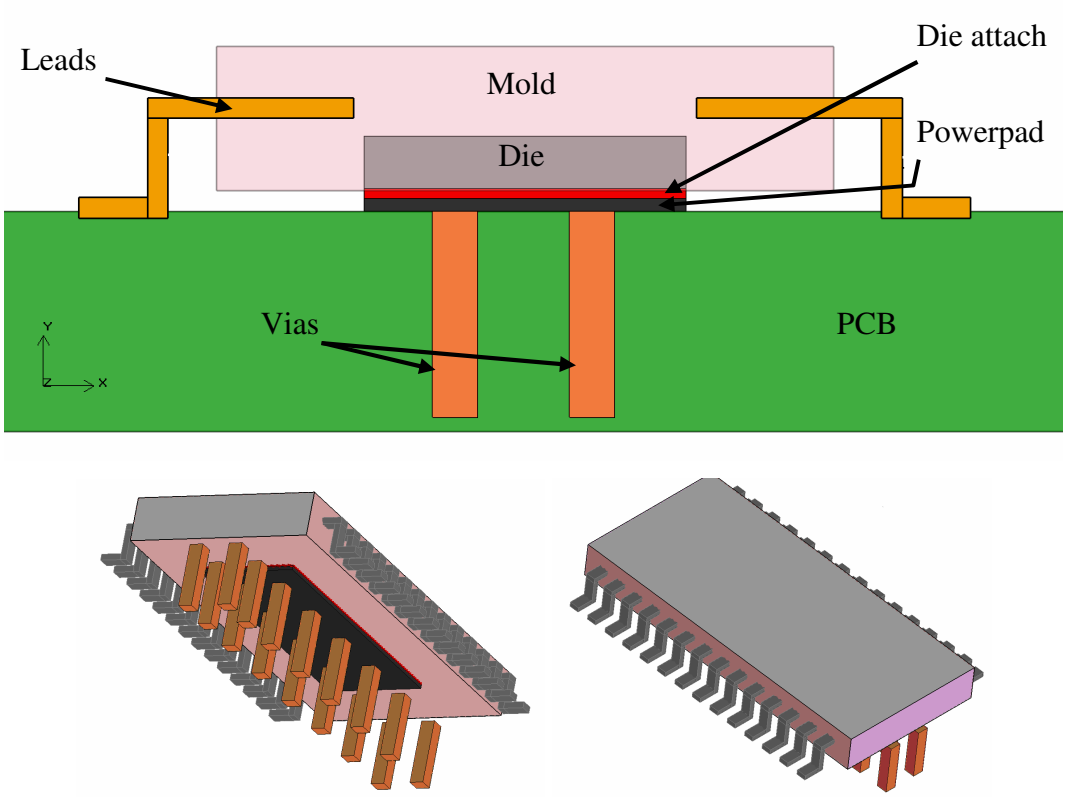

Figure 4.3 Different views of DTM of TPS54610 DC/DC converter

Table 4.2 Material specifications and dimensions of different items used in the DTM of TPS54610 DC/DC converter

Feature	Material	Dimensions (mm)	Thermal Characteristics		
			Thermal Conductivity (W/mK)	Density (kg/m^3)	Specific Heat (J/kgK)
Mold	Epoxy-silica filled	4.5 x 1.05 x 9.8	0.63	1800	1004
Die	Silicone	2.35 x 0.381 x 6.46	144	2330	712
Die Attach	Die attach material of ICEPAK	2.35 x 0.0727 x 6.46	2.5	1900	795
PowerPAD	Lead	2.35 x 0.09 x 6.46	35	130	11210
Leads	Copper		387.6	385	8933
Vias	Copper	0.33 x 1.5 x 0.330.	387.6	385	8933

Plastic Encapsulate(Mold)

Mold is modelled as a solid cubic block of dimensions 4.5 x 1.05 x 9.8 mm. Of all parameters used in the model, the most important one is the thermal conductivity of the mold, because in a plastic package it has the dominant thermal resistance. Epoxy silica-filled material properties are used from Icepak libraries.

Die

Silicon die is modelled as a cubic block of dimensions 2.35 x 0.381 x 6.46 mm. It is placed on top of the die attach as seen in Figure 4.3. Silicon material properties provided by the ICEPAK libraries are used. In the numerical model 0.42 W amount of heat dissipated by the TPS54610 DC/DC converter is assigned to the die.

Die Attach and PowerPAD

Die attach is a very thin layer of adhesive material that sticks the die to the powerPAD. It is modelled as a cubic block of dimensions 2.35 x 0.0727 x 6.46 mm. Lead frame powerPAD is modelled as a cubic block of dimensions 2.35 x 0.09 x 6.46 mm and placed between die attach and PCB.

Leads and Vias

Leads and vias are modelled as cubic blocks. Detailed dimensions of leads are given in Figure 4.4. Both structures are modelled as copper. An important point is that vias, which are actually cylindrical objects, are modelled as cubic prisms (0.33 x 1.5 x 0.33 mm) due to mesh generation concerns.

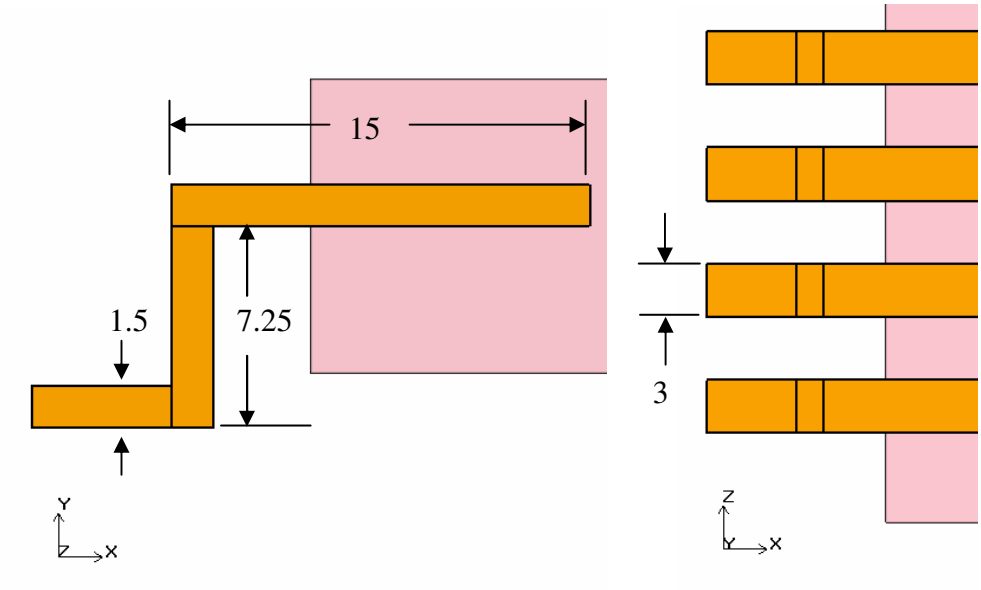

Figure 4.4 Detailed dimensions of leads (all dimensions are in mm)

4.1.2 Compact Thermal Models of the TPS54610 DC/DC Converter

Following the procedures described in previous studies, five different conduction based compact thermal models (CCM) of the DC/DC converter are generated [17], [26], [29], [51]. Each CCM is designed to be simpler than the previous one using the logic suggested by Ahmed and Karimanal [17]. Details of these CCM are explained in the coming sections.

4.1.2.1 First CCM (CCM 1)

As a first simplification leads and vias are lumped into continuous layer of materials as shown in Figure 4.5 with effective material properties computed using equations (1.2 - 1.5). Leads are separated into two as external and internal. While copper and epoxy (silica filled) material properties are used for internal lead effective material property computations, air and copper material properties are used for external leads. Details of effective material properties are given in Table 4.3.

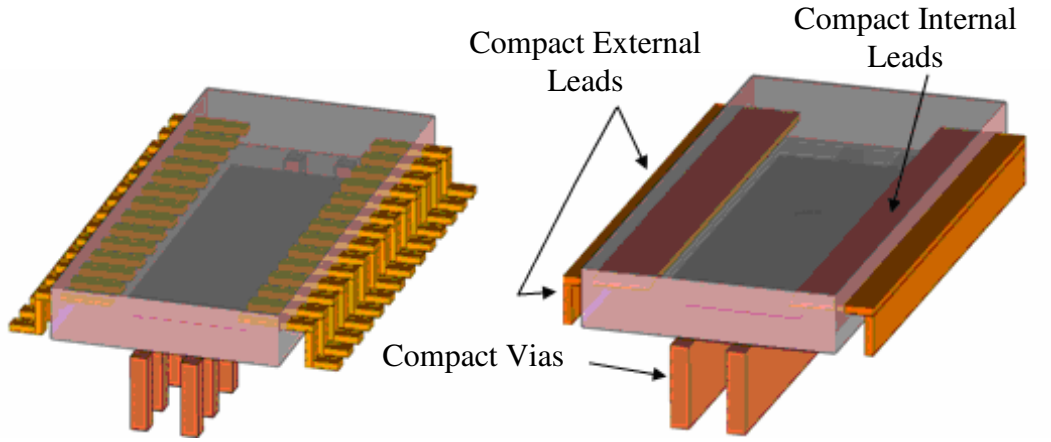

Figure 4.5 First conduction based compact thermal model (CCM 1)

Table 4.3 Effective material properties for CCM 1

Compact Feature	Effective Conductivity x-direction (W/m-K)	Effective Conductivity y-direction (W/m-K)	Effective Conductivity z-direction (W/m-K)	Effective Specific Heat (J/kg-K)	Effective Density (kg/m^3)
Internal Leads	186.4	186.4	1.21	706	5223
External Leads	186	186	0.05	706	4911
Via	95.25	95.25	0.33	1076	3122

4.1.2.2 Second CCM (CCM 2)

In addition to the simplifications implemented in CCM 1, thin air gap separating the package from the board is modelled as a planar (zero thickness) object in CCM 2 as shown in Figure 4.6. Zero thickness planar object has the thermal conductivity of air (0.0261 W/mK) and an effective thickness (0.15 mm). This simplification is done to eliminate the necessity of creating very fine mesh in the original thin air gap. As a result of this simplification, height of the mold is increased but height of the DC/DC converter from PCB is not changed.

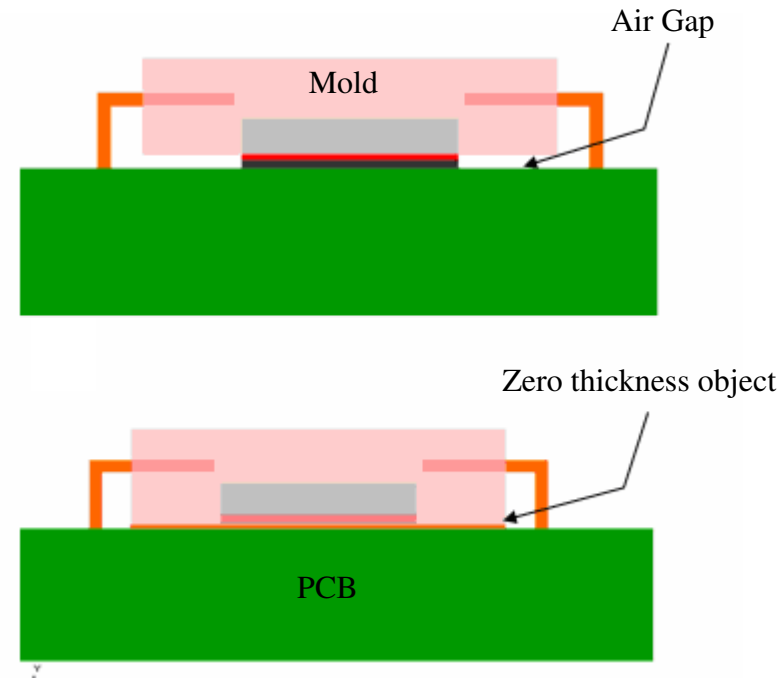

Figure 4.6 Second conduction based compact thermal model (CCM 2)

4.1.2.3 Third CCM (CCM 3)

In addition to the previous simplifications, die, die attach and powerPAD, which were 3D prismatic objects in previous models, are lumped into a single modified die as shown in Figure 4.7. 0.42 W of heat dissipation is assigned to this new modified die. Its material properties, shown in Table 4.4, are obtained by combining those of die, die attach and powerPAD.

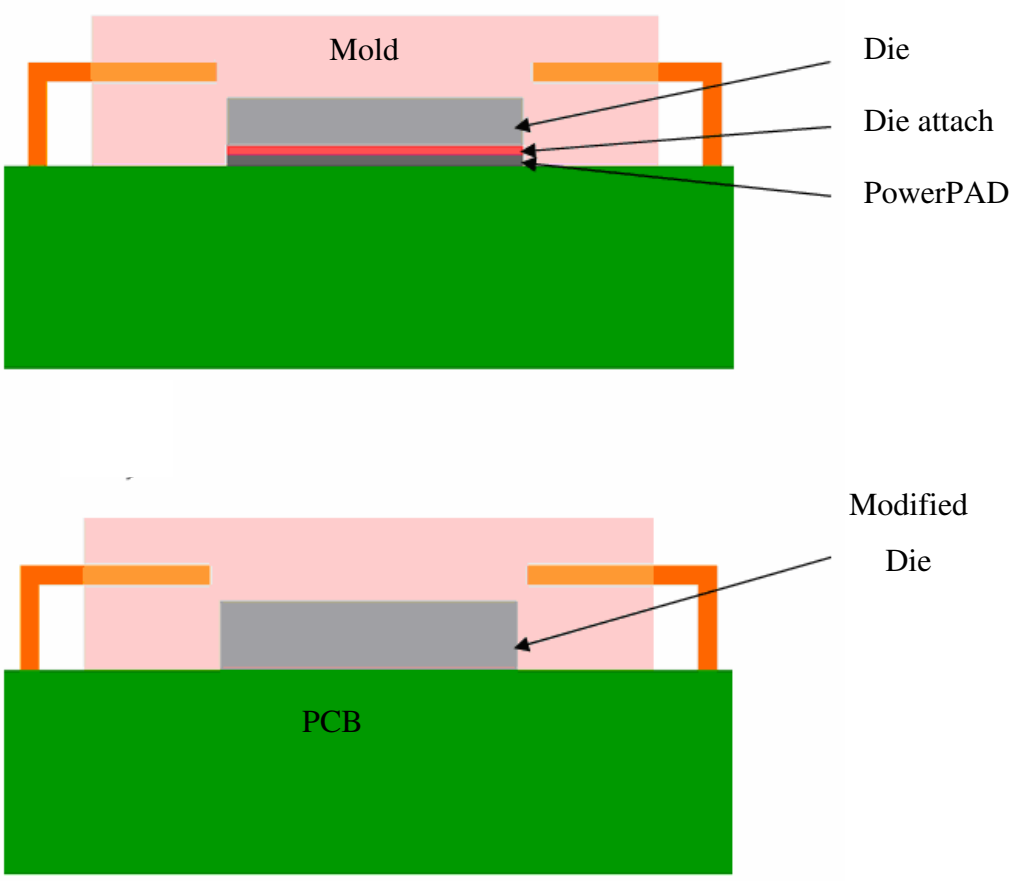

Figure 4.7 Third conduction based compact thermal model (CCM 3)

Table 4.4 Material properties and dimensions of die, die attach, powerPAD and modified die used to create CCM 3

Feature	Material	Thickness (mm)	Conductivity (W/m-K)	Density (kg/m^3)	Specific heat (J/kg-K)
Die	silicone	0.381	144	2330	712
Die attach	*	0.0727	2.5	1900	715
Power pad	Lead	0.09	35	11210	130
Modified die	----	0.5437	Serial : 106.00 Parallel : 13.35	3446	634

* Icepak material library was used for die attach material properties.

4.1.2.4 Fourth CCM (CCM 4)

As shown in Figure 4.8 external leads, vias and zero thickness planar object that represents the effect of air gap under the package are omitted. Internal leads are also extracted from the model, but mold material properties are recomputed by considering the effect of the removed leads, as given in Table 4.5. Last physical representation of CCM 4 can be seen at Figure 4.8. Such a compact model, which is called Block on Lead (BoL), was previously used by Adams et. al [23].

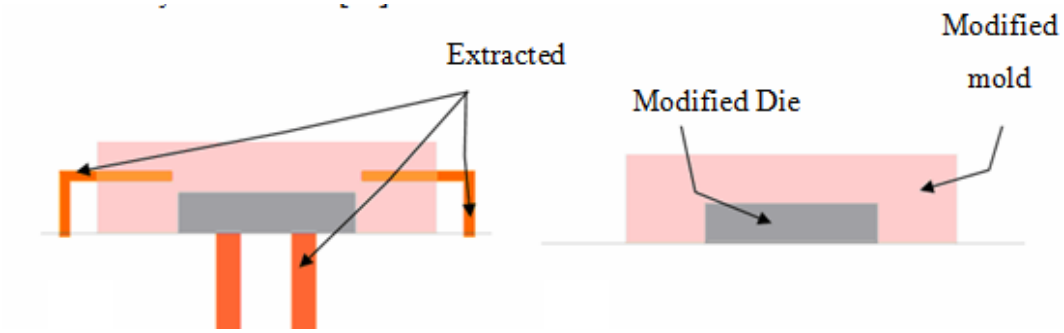

Figure 4.8 Fourth conduction based compact thermal model (CCM 4)

Table 4.5 Material properties of internal leads, mold and modified mold used to create CCM 4

Feature	Material	Conductivity (W/m-K)	Density (kg/m^3)	Specific heat (J/kg-K)
Internal leads	Copper	386	8960	385
Mold	Epoxy-silica	0.63	1800	1004
Modified Mold	--------	11.5	2001	986

4.1.2.5 Fifth CCM (CCM5)

In this last compact model geometry of the DC/DC converter is simplified one step further to its possible simplest status. All internal components (internal leads, die, die attach, powerPAD) are lumped into a single block called “modified mold 2” as shown in Figure 4.9. 0.42 W of heat dissipation is assigned to modified mold 2 uniformly. The effective material properties were computed with the same equations of previous CCMs, Table 4.6.

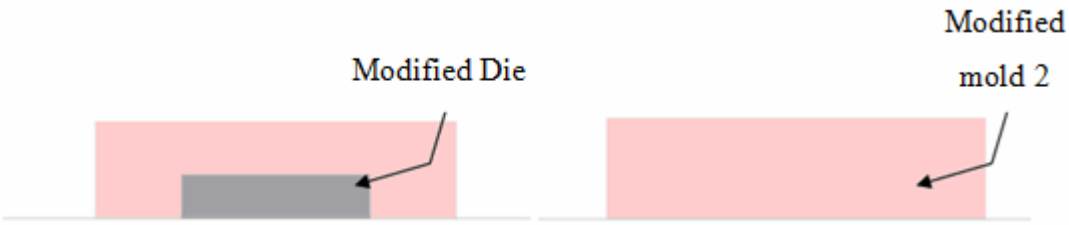

Figure 4.9 Fifth conduction based compact thermal model 5 (CCM5)

Table 4.6 Material properties of die, die attach, powerPAD, internal leads, mold and modified mold 2 used in creating CCM 5

Feature	Material	Conductivity (W/m-K)	Density (kg/m^3)	Specific heat (J/kg-K)
Die	Silicone	144	2330	712
Die attach	-----	2.5	1900	715
Power pad	Lead	35	11210	130
Internal leads	Copper	386	8960	385
Mold	Epoxy-silica	0.63	1800	1004
Modified Mold 2	--------	26.25	2227	931.65

4.1.3 Boundary Conditions and Solver Settings

Figure 4.10 shows the computational domain which includes the previously described test enclosure assembly with the printed circuit board placed inside a 3D rectangular volume called cabinet. Dimensions of cabinet are selected to be 355 x 355 x 355 mm. Spacing between the cabinet and the test enclosure assembly (except y=0 plane) are 20 mm for x and y directions and 50 mm for the z direction. All surfaces of the cabinet, except the bottom (y=0) one, are open to the surrounding air for heat and mass transfer. Bottom surface of the computational domain is defined as adiabatic at the ambient air temperature of 25 °C. No slip boundary condition is used at all solid surfaces inside the domain.

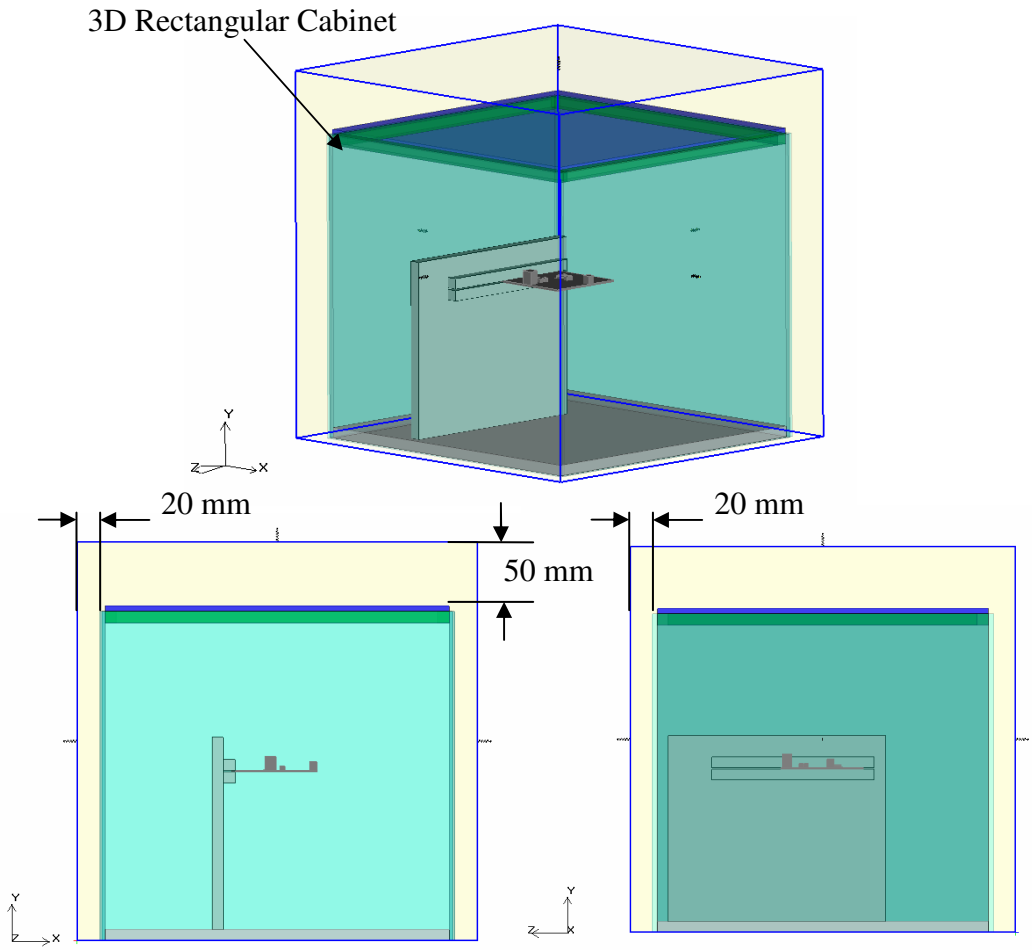

Figure 4.10 Computational domain of the first problem

In order to determine flow regime a Rayleigh number calculation was performed.

$$Ra = \frac{g\beta(T_w - T_\infty)L^3}{\gamma\alpha} \tag{4.1}$$

Unknowns of equation (4.1) were assumed due to performed experimental study. Mean wall temperature (T_w) was assumed 34 ºC at the top wall of TPS54610 DC/DC converter and ambient temperature (T_∞) was 25 ºC. Gravity (g) is 9.81 m/s, the volumetric thermal expansion coefficient (β) was calculated according to the fluid temperature (T_f, which is a mean of T_w and T_∞) of 29.5 ºC is $3.31 \times 10^{-3} K^{-1}$. The length ($L$) of the top wall of TPS54610 DC/DC converter was 9.8 mm, the kinematic viscosity (γ) is 16.14×10^{-6} m^2/s and the thermal diffusivity (α) is 22.87×10^{-6} m^2/s at T_f. So that;

$$Ra = \frac{(9.81)(3.31x10^{-3})(307-298)(9.8x10^{-3})^3}{(1.614x10^{-5})(2.287x10^{-5})} = 745157$$

Since $Ra < 10^8$, the flow is laminar [35].

Other solver settings are summarized in Table 4.7. Convergence criterion is set to the default suggested value of 0.001 for solution residuals. Additionally top surface temperature of the DC/DC converter is monitored during the simulations to check whether it reaches to a constant value or not. Default Icepak under relaxation factors of 0.3 and 0.7 are used for pressure and momentum respectively. Different approaches are tried and compared for pressure and momentum discretizations.

Table 4.7 Solver settings summary for the first problem

Settings		**Selection 1**	**Selection 2**
Flow Regime		Laminar	
Under Relaxation	Pressure	0.3	
	Momentum	0.7	
Pressure Discretization		1st order	Body force
Momentum Discretization		1st order	2nd order
Pressure – Velocity Coupling		SIMPLE	SIMPLE

4.1.4 Grid Generation on Numerical Models of the First Case

Although Icepak automates the mesh generation process, it allows modification of certain meshing parameters in order to refine the mesh and optimize trade-offs between computational cost and solution accuracy. User can apply such customizations at the global level, i.e. same for the entire computational domain, or use different parameters for mesh portions around different items of the domain [35].

Icepak mesh generator operates on a cocooning methodology whereby each object is meshed individually. Each object is meshed as close to the specifications defined by users as possible. Mesh elements are smaller near objects to take into account thermal and velocity gradients that are often present near the boundaries of objects. In contrast open spaces between objects are meshed with large elements, to minimize computational costs [35].

Although in Icepak hexahedral, tetrahedral and hex-dominant mesh types are available, hexahedral unstructured mesh type, which is used for this problem, is presented as default and seen suitable for most applications (Figure 4.11). To generate a proper mesh parameters presented in Figure 4.12 are used.

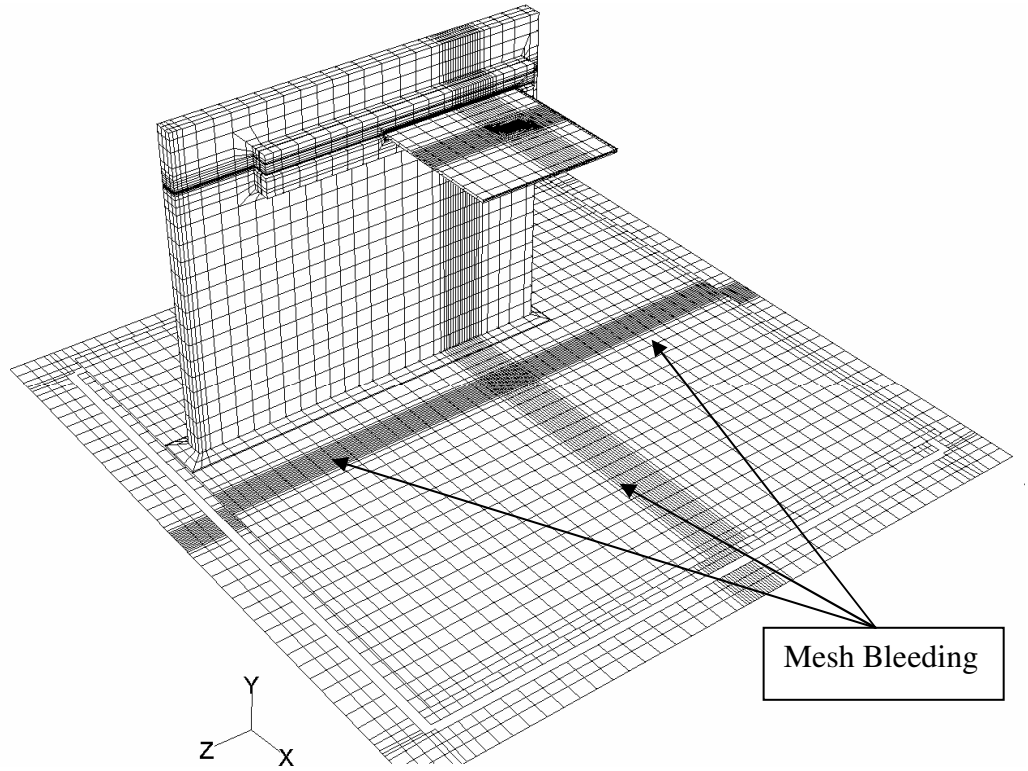

Figure 4.11 A sample hexa-unstructured grid used in the first problem demonstrating undesired mesh bleeding.

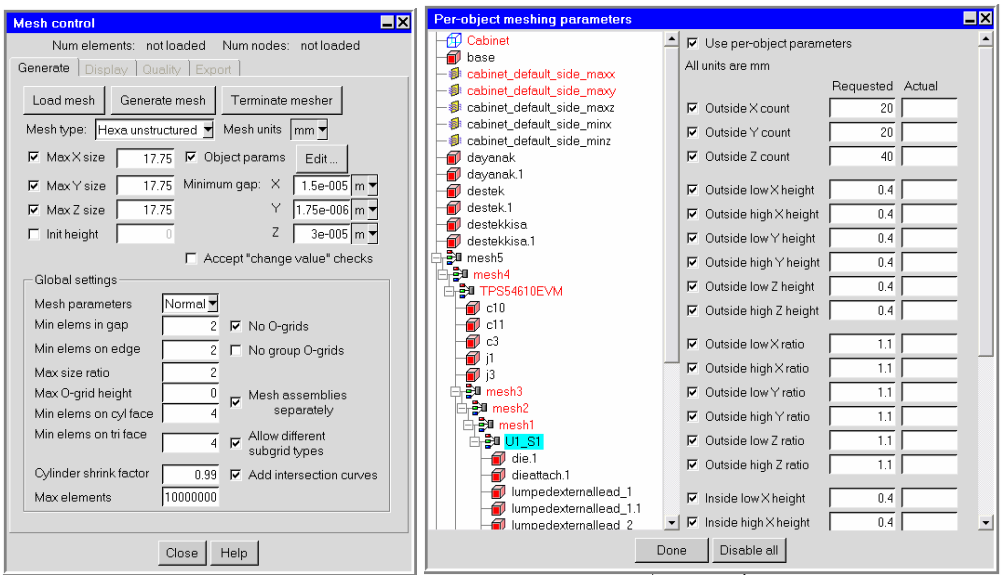

Figure 4.12 Icepak grid generation interfaces with default (left) and local (right) mesh refinement parameters used for the first problem

As shown in Table 4.8 the first numerical model, where detailed thermal model is used for the DC/DC converter, has maximum grid count. In this model very fine details of the DC/DC converter required the use of very small sized elements and due to the limitations of Icepak mesh generator, these small elements affect grid quality at far field regions of the computational domain, which is an undesired process known as mesh bleeding, demonstrated in Figure 4.11.

Table 4.8 Mesh count summary of the first case

# of Numerical Model	**Thermal model of TPS54610 DC/DC converter**	**Explanation**	**Total mesh count on the computational domain**	**Total mesh count inside the non-conformal domain**
NM-1	DTM	All Conformal	892810	N/A
NM-2	DTM	N-C is used	539307	120320
NM-3	CCM1	N-C is used	459945	36540
NM-4	CCM2	N-C is used	456542	32928
NM-5	CCM3	N-C is used	452114	28224
NM-6	CCM4	N-C is used	426204	5852
NM-7	CCM5	N-C is used	403160	1230

In order to reduce grid count and minimize undesired mesh bleeding, an additional strategy known as non-conformal (N-C) meshing is used. In this technique, as shown in Figure 4.13, , a region around the DC/DC converter, which is the most critical part of the computational domain is defined and it can be meshed independently of the mesh outside it. Grid points belonging to the meshes inside and outside a N-C region do not coincide at a N-C interface and hanging nodes appear. However, these nodes are handled automatically by the flow solver [35]. As seen in Table 4.8 N-C strategy is very effective in reducing the overall mesh count.

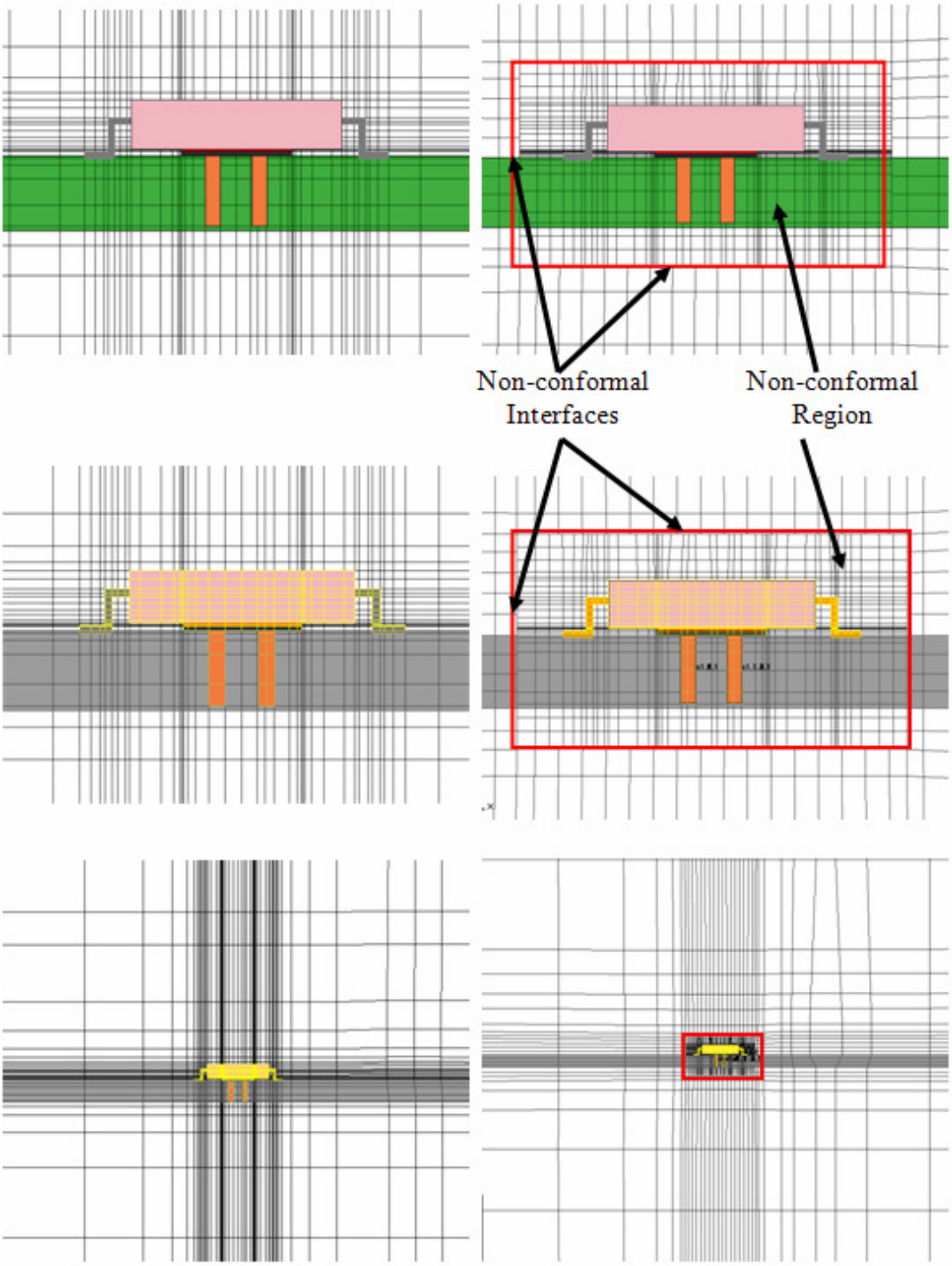

Figure 4.13 Conformal (left) and non-conformal (right) meshing

4.1.5 Numerical Simulations

Using the DTM and 5 CCMs described in the previous sections, 14 different simulations, given in Table 4.9 are performed to evaluate the performance of CCMs. The first two simulations correspond to the use of DTM with conformal and non-conformal meshes coupled with first order discretization for pressure and momentum terms of the governing equations. Simulations 8 and 9 are similar to the first two, the difference being the use of alternative discretization schemes. Simulations 3-7 and 10-14 make use of compact models with different discretization strategies. As will be discussed below, all simulations with CCMs use N-C meshes.

Table 4.9 Simulations performed for the first problem

Simulation Number	**TPS54610 DC/DC Converter Thermal Model**	**Discretization Scheme**	
		pressure	**momentum**
1	DTM with conformal mesh	1st order	
2	DTM with N-C mesh	1st order	
3	CCM 1	1st order	
4	CCM2	1st order	
5	CCM 3	1st order	
6	CCM 4	1st order	
7	CCM 5	1st order	
8	DTM with conformal mesh	Body force Weight	2nd order
9	DTM with N-C mesh	Body force Weight	2nd order
10	CCM 1	Body force Weight	2nd order
11	CCM 2	Body force Weight	2nd order
12	CCM 3	Body force Weight	2nd order
13	CCM 4	Body force Weight	2nd order
14	CCM 5	Body force Weight	2nd order

In order to compare numerical results with the experimental ones, temperatures at five thermocouple locations are recorded during the simulations. Temperature values obtained experimentally and numerically are given in Table 4.10, Table 4.11 and Table 4.12.

Table 4.10 Temperature measurements of natural convection problem (ºC)

Thermocouple (TC) No				
1	**2**	**3**	**4**	**5**
35.4	33.9	31.1	32.8	25.7

Table 4.11 Simulation results using 1st order discretization schemes.
T (ºC) : Temperature %: Percent deviation with respect to experiment

Simulation Number		**Thermocouple (TC) No**				
		1	**2**	**3**	**4**	**5**
1	T (ºC)	35.4	32.4	30.2	31.3	25.2
	%	0.0	-4.4	-2.9	-4.6	-1.9
2	T (ºC)	35.2	32.2	30.1	31.4	25.2
	%	-0.6	-5.0	-3.2	-4.3	-1.9
3	T (ºC)	34.4	31.9	30.1	31.3	25.2
	%	-2.8	-5.9	-3.2	-4.6	-1.9
4	T (ºC)	34.3	31.9	30.1	31.3	25.2
	%	-3.1	-5.9	-3.2	-4.6	-1.9
5	T (ºC)	34.0	31.9	30.1	31.3	25.2
	%	-4.0	-5.9	-3.2	-4.6	-1.9
6	T (ºC)	38.8	33.1	30.2	30.5	25.2
	%	9.6	-2.4	-2.9	-7.0	-1.9
7	T (ºC)	36.5	32.0	30.1	31.1	25.2
	%	3.1	-5.6	-3.2	-5.2	-1.9

Table 4.12 Simulation results using 2nd order discretization schemes.
T (ºC) : Temperature % : Percent deviation with respect to experiment

Simulation Number		Thermocouple (TC) No				
		1	**2**	**3**	**4**	**5**
8	T (ºC)	35.5	32.5	30.3	31.4	25.2
	%	-0.3	-4.1	-2.6	-4.3	-1.9
9	T (ºC)	35.3	32.2	30.2	31.5	25.2
	%	-0.3	-5.0	-2.9	-4.0	-1.9
10	T (ºC)	34.5	32.0	30.2	31.4	25.2
	%	-2.5	-5.6	-2.9	-4.3	-1.9
11	T (ºC)	34.4	32.0	30.2	31.4	25.2
	%	-2.8	-5.6	-2.9	-4.3	-1.9
12	T (ºC)	34.1	32.0	30.2	31.4	25.2
	%	-3.7	-5.6	-2.9	-4.3	-1.9
13	T (ºC)	38.9	33.3	30.3	30.7	25.2
	%	9.9	-1.8	-2.6	-6.4	-1.9
14	T (ºC)	36.6	32.1	30.2	31.2	25.2
	%	3.4	-5.3	-2.9	-4.9	-1.9

4.1.6 Discussion and Comparison of the First Case

The first and second simulations make use of DTM of DC/DC converter with conformal and N-C meshing options, respectively. According to Table 4.8 grid count and solution time can be reduced on the order of 40 % by the use of the N-C strategy, without making any physical modifications to the numerical model. Comparing simulations 1 and 2 in Table 4.11, temperature difference between conformal and N-C grids is less than 0.6 %. A similar observation can be made by comparing simulations 8 and 9 of Table 4.12 which use 2nd order discretization.

Based on these comparisons it was decided that N-C mesh, which is far more efficient computationally can be used for all simulations which use CCMs. Figure 4.14 and 4.15 can be used to compare velocity fields obtained from simulations 1 and 2. It is seen that N-C grid, which has less far field grid resolution compared to the conformal grid predicts lower velocities in general. Although not mentioned previously a third grid that is generated using a "max size ratio" parameter of 1.45 is also tested. The resultant grid count was over 3,000,000 but the results were very similar to those of simulation 1. Therefore this third grid alternative is not used anymore.

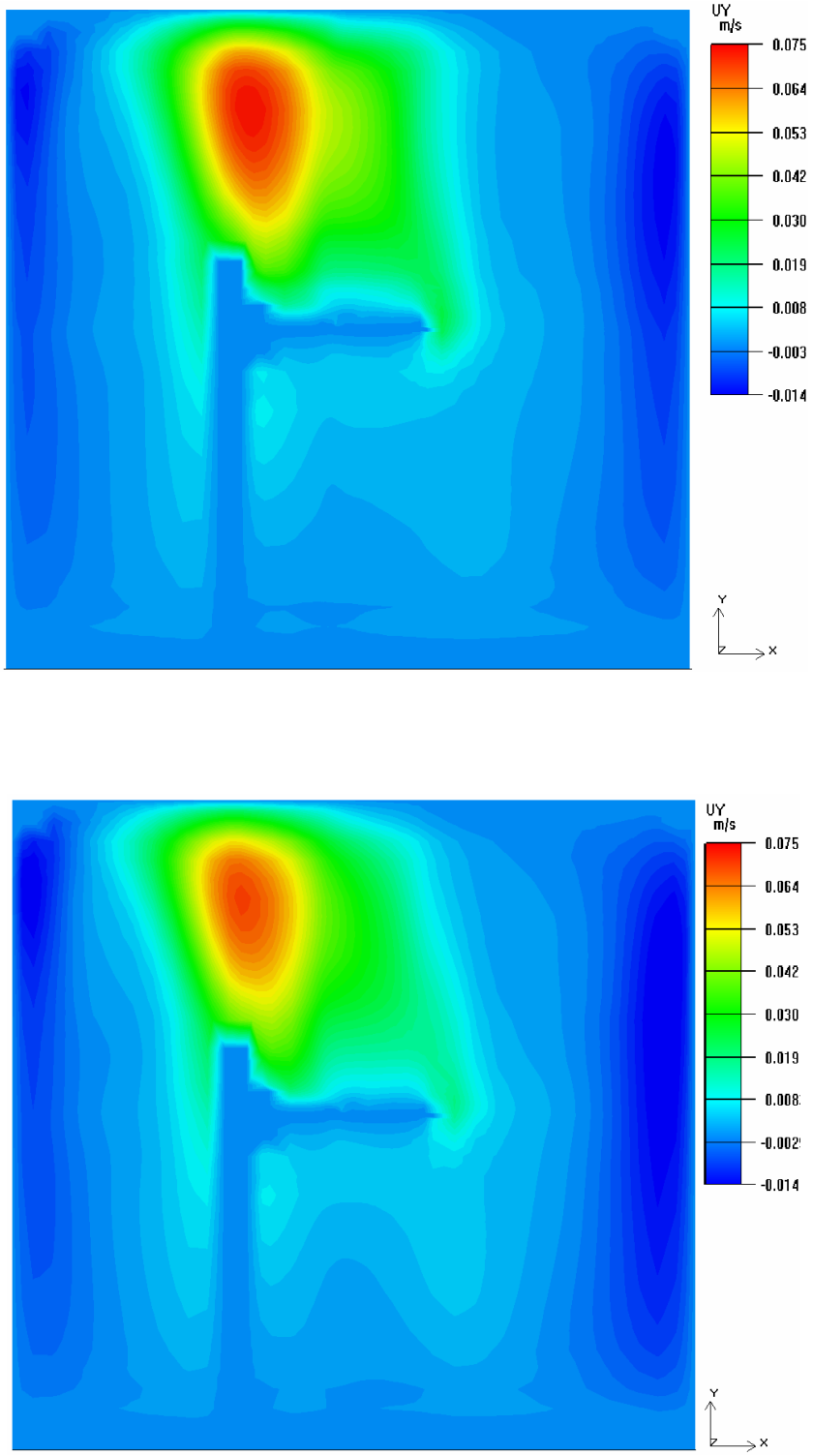

Figure 4.14 Vertical velocity component contours in the xy plane for the first (top) and second (bottom) simulations.

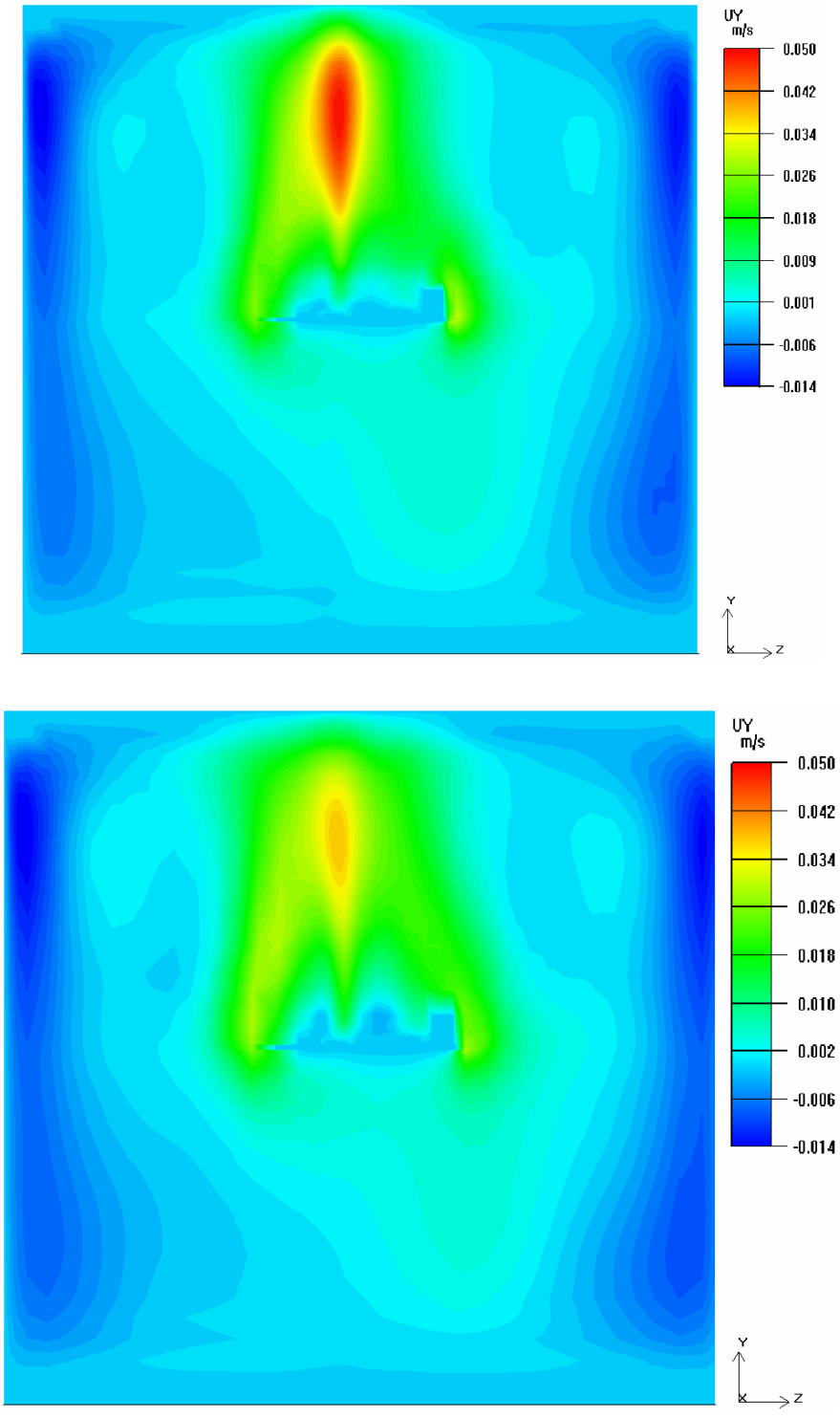

Figure 4.15 Vertical velocity component contours in the yz plane for the first (top) and second (bottom) simulations.

To compare the results obtained by using first and second order discretizations DTM based simulations of Table 4.11 and Table 4.12 can be compared. Temperature deviations for simulations 1 and 2 are less than 5.0 % for all temperature points. Upper surface temperature is the most critical one and it is predicted with a deviation less than 1 %. Although simulations 8 and 9 make use of 2nd order discretization the results are very similar to those of simulations 1 and 2. Therefore it is decided that simulations 1 and 2 can be used to evaluate CCM simulations together with experimental comparisons. As a final detail of DTM results temperature distribution on the DC/DC converter surface obtained by the first simulation is given in Figure 4.16. Surface temperature contours obtained by the second simulation are very similar.

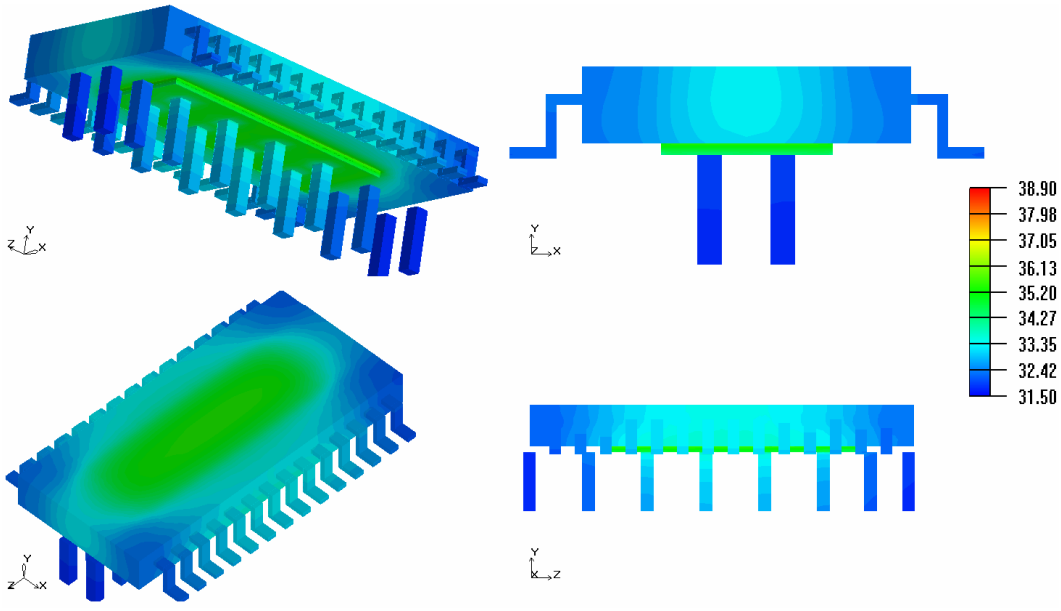

Figure 4.16 Surface temperature contours of the DTM of TPS54610 for AN 1

Percent temperature deviations obtained by the use of CCMs, given Table 4.11 and Table 4.12, can also be presented in a graphical form as shown Figure 4.17. These contours will be compared with the one given in

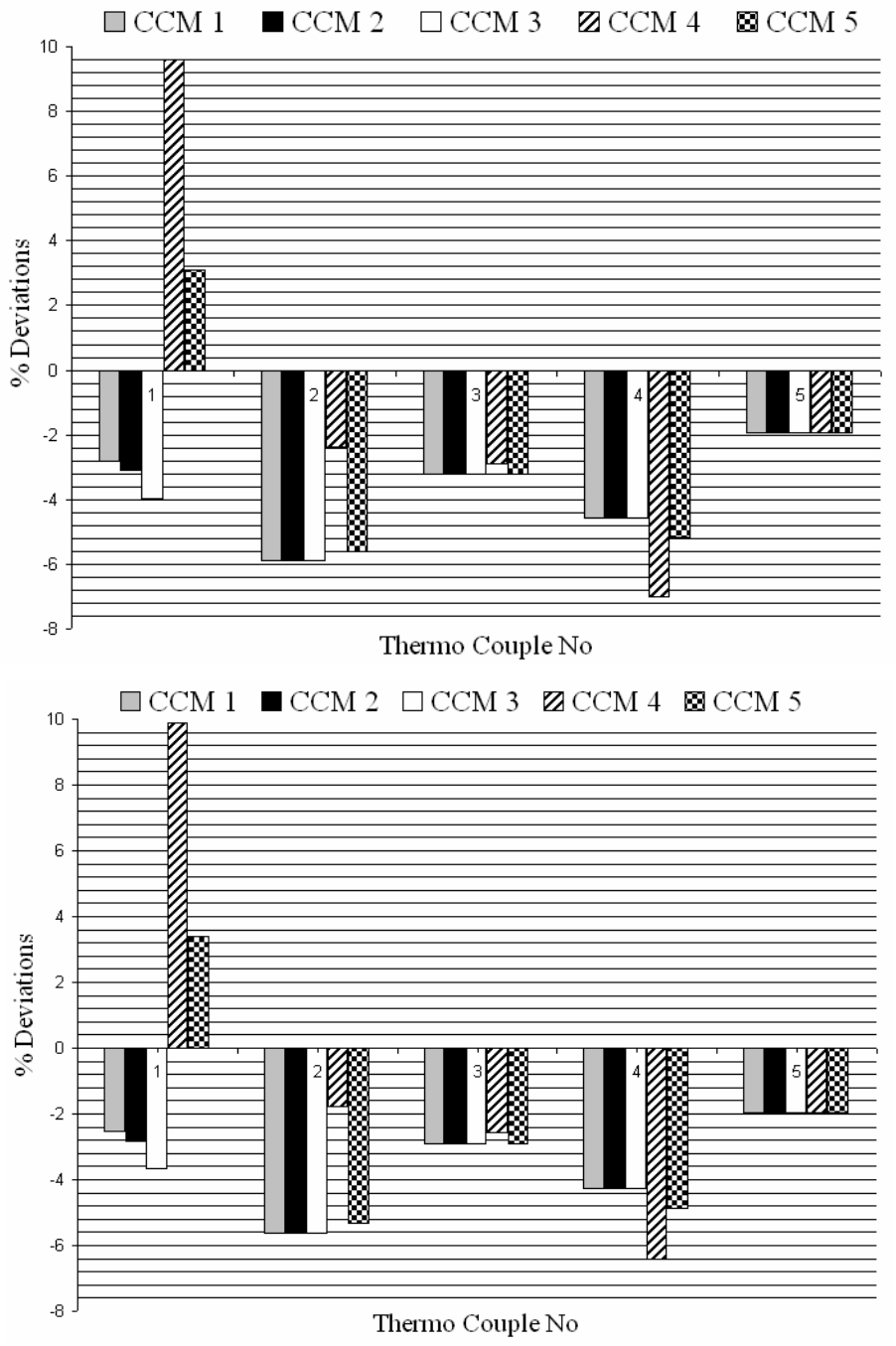

Figure 4.17 Percent deviations for different CCMs with 1st order (top) and 2nd order (bottom) discretizations

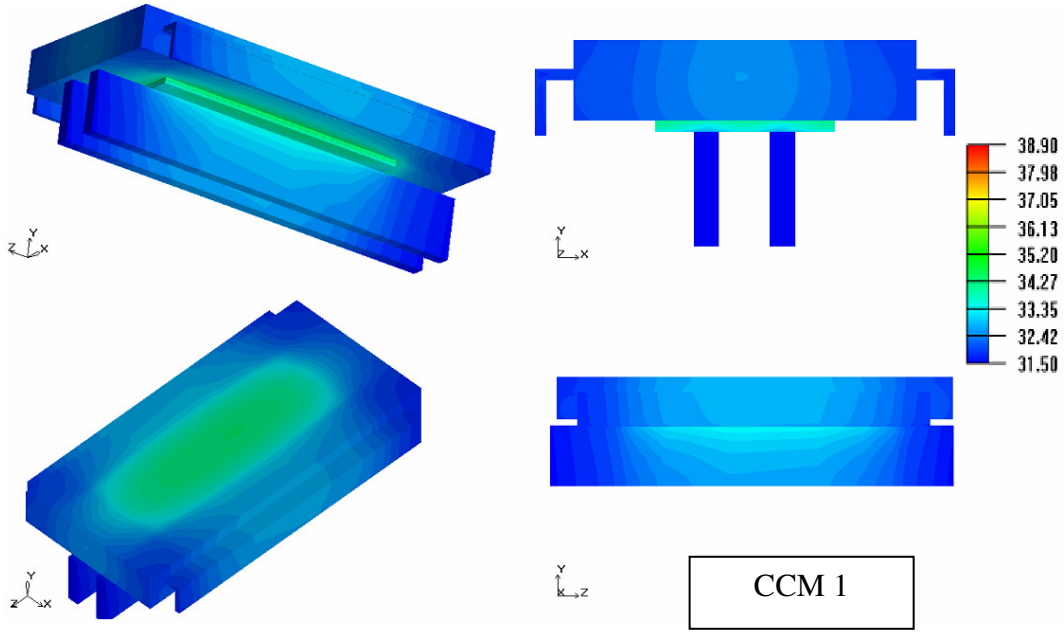

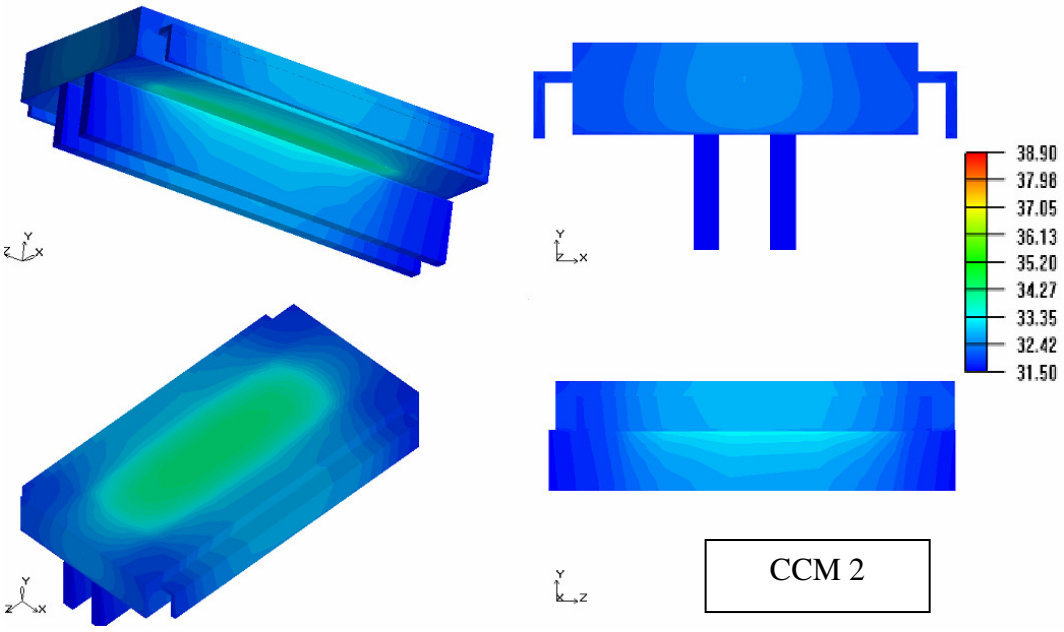

Figure 4.18 DC/DC converter surface temperature distributions obtained by different CCMs

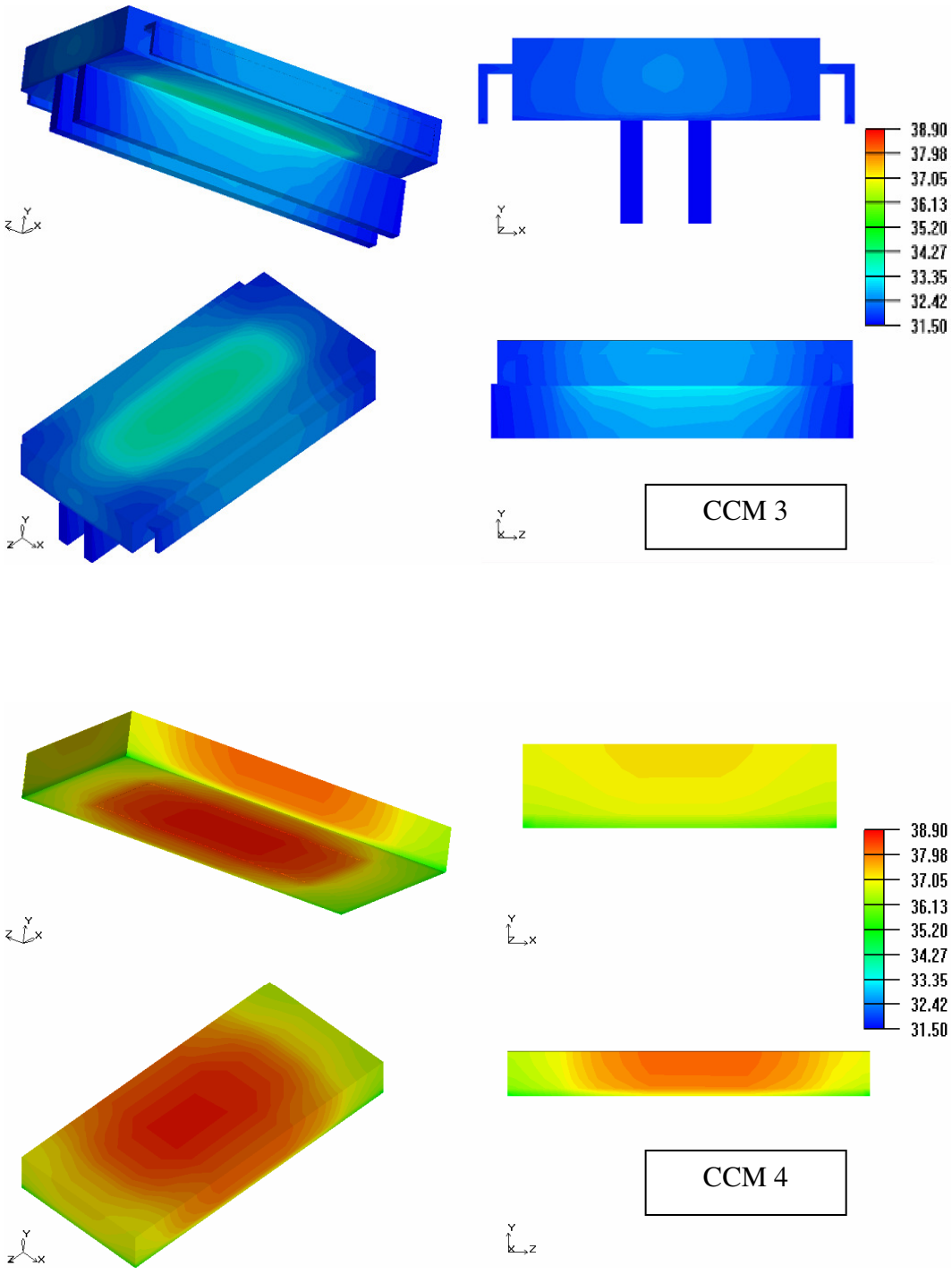

Figure 4.18 DC/DC converter surface temperature distributions obtained by different CCMs (continued)

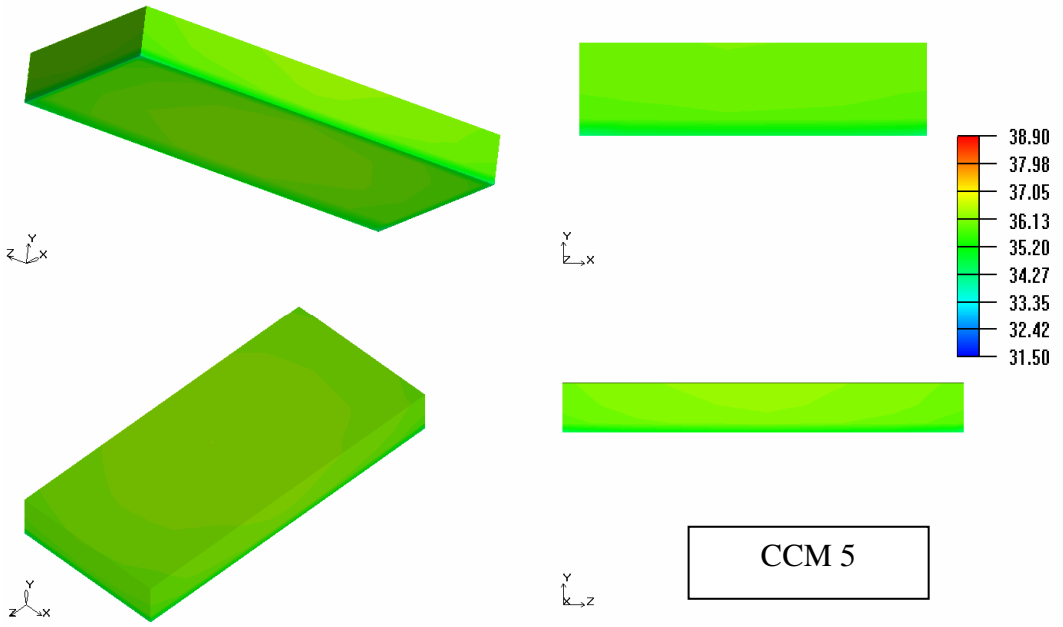

Figure 4.18 DC/DC converter surface temperature distributions obtained by different CCMs (continued)

In CCM 1 internal and external leads of DC/DC converter are lumped into simple blocks. Due to this lumping process temperature distribution over the converter becomes more uniform with reduced surface temperatures. As a result of this, deviations from experiments increase especially for TC points 1 and 2. Additional simplifications for CCM 2 and CCM 3 result in further slight decreases in surface temperatures. However, in general both point temperature and surface contour results are very similar for CCMs 1, 2 and 3.

However, simplifications done for CCMs 4 and 5, i.e. elimination of external leads and vias, modify heat transfer paths considerably, which results in very different (higher) surface temperature distributions compared to other CCMs. Parallel to this, point temperature results also increase, e.g. for CCM 4 temperature deviation at the first TC point reaches to 10 %. This sharp increase in CCM 4 is less in CCM 5 due to the assignment of heat dissipation to the whole modified mold 2.

Simplification efforts of CCMs also affect the temperature distribution on the PCB of the evaluation board as shown in Figure 4.19. Not for CCMs 1, 2 and 3, but for CCMs 4 and 5 PCB surface temperature distributions show remarkable differences compared to the detailed model.

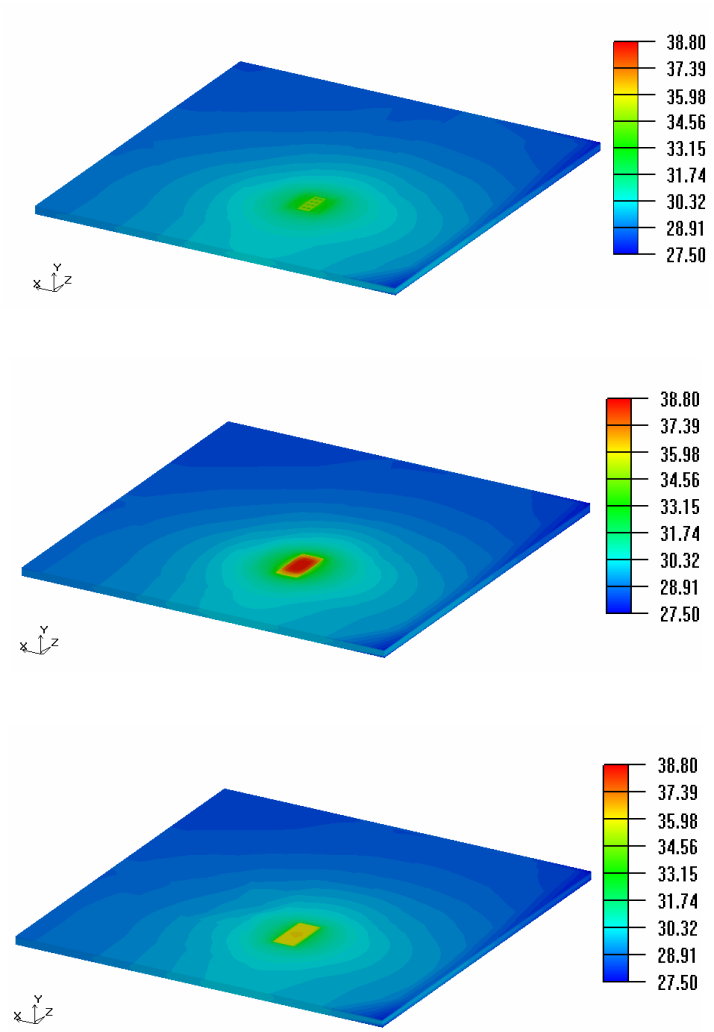

Figure 4.19 PCB surface temperature distributions using DTM of simulation 2 (top), CCM 4 of simulation 6 (middle) and CCM 5 of simulation 7 (bottom)

4.2 Numerical Study of the Second Problem (Forced Convection Cooling)

In the second problem a number of different compact thermal models of MGDM-150 series module type DC/DC converter are created. These CCMs are used in the simulations performed on the computational model of the forced convection cooling experiment shown in Figure 4.20. Main parts of forced convection experimental test setup, namely power card, fan and support are used in computational model. All details of the actual experimental setup, except some non-essential parts of the power card such as small resistors, inductors and capacitors, are modelled as they are.

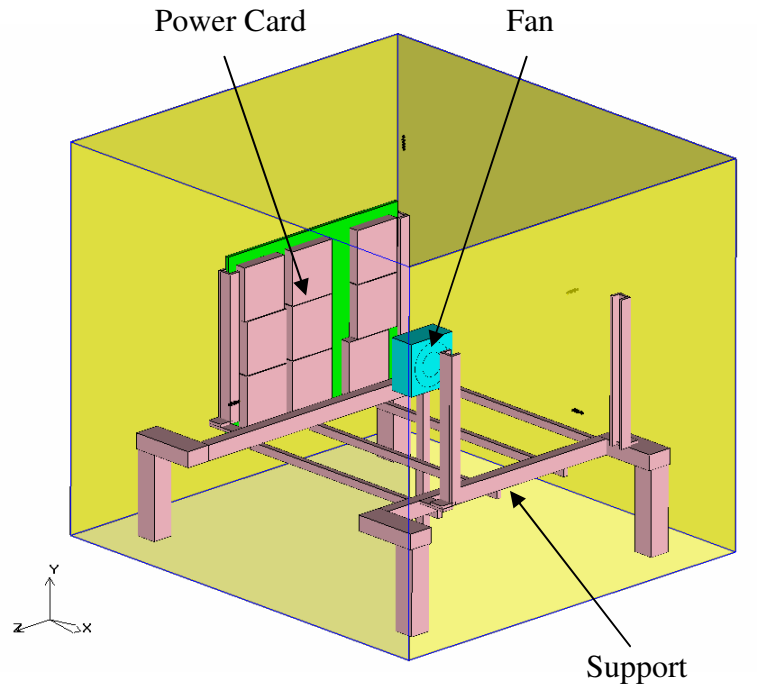

Figure 4.20 Computational model of forced convection experiment setup

Unlike the previous problem, no detailed thermal model is created for the module type converter of this problem, due to the lack of detail about the internal structure of the device. In creating CCMs, studies in the literature [16], [17], [33] and manufacturer's data sheets are used. Three physically different CCM alternatives are

created. In the numerical analyses all parts other than the CCMs are kept identical. Below details of these common parts will be given.

Support is modelled according to its real dimensions using prismatic blocks of aluminium. Fan is inserted into the numerical model using Icepak's fan interface feature. Fan properties such as outer and inner diameters, width and static pressure-air flow rate curve are defined according to the values taken from the manufacturer's data sheet [48], The fan properties are also given in appendix A. As described in Chapter 3 power card is an assembly of a PCB and 9 module type DC/DC converters as shown Figure 4.21. PCB of the power card is modelled as a solid block of dimensions 250 x 210 x 3.4 mm. In order to prevent small grid cells, tracing (signal and power) planes of PCB are omitted. Similar to the first problem discussed in the previous section this simplification is supported by using modified effective material properties for PCB as shown in Table 4.13.

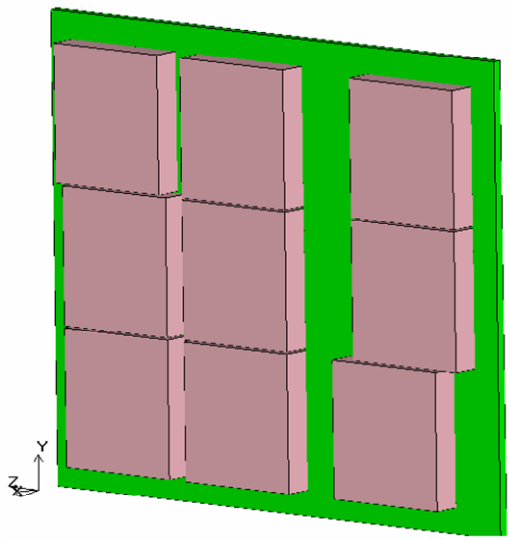

Figure 4.21 Numerical model of power card

Table 4.13 Effective material properties of the Power Card PCB

Effective Conductivity x-direction (W/m-K)	Effective Conductivity y-direction (W/m-K)	Effective Conductivity z-direction (W/m-K)	Effective Specific Heat (J/kg-K)	Effective Density (kg/m^3)
64	0.46	64	1127	2696

4.2.1 Compact Thermal Models of MGDM-150 DC/DC Converter

For the creation of CCMs described in this section dissertation of Pang [33] is studied in detail to understand internal structure of module type DC/DC converters and their heat generation mechanism. Three important parts of module type converters, namely mosfet, mold and external aluminium casing, shown in Figure 4.22, are taken into consideration in creating compact models. In all three CCMs these parts are modelled as simple, prismatic volumes with isotropic material properties.

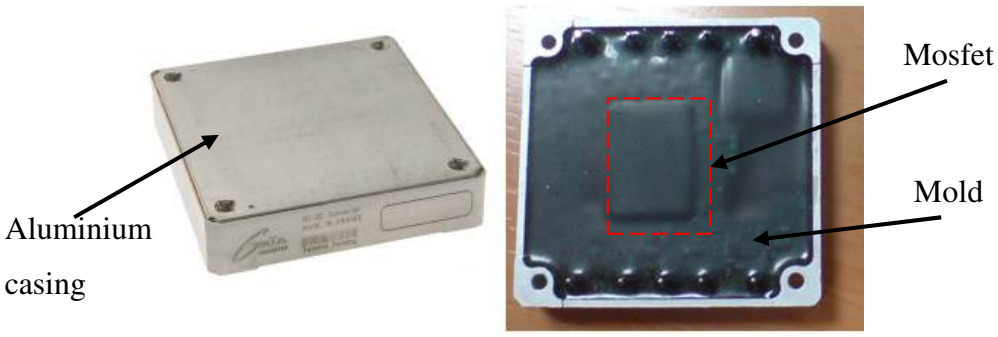

Figure 4.22 Important parts of MGDM-150 DC/DC converters

4.2.1.1 Single Volume CCM (CCM A)

Using a single volume is the simplest possible way to create a CCM. In this model module type DC/DC converter is modelled as a single prismatic geometry of

dimensions 56 x 60 x 12.7 mm as shown Figure 4.23. Isotropic properties of the single volume is computed using Eqns (1.2), (1.3) and (1.6) and properties of individual parts as listed in Table 4.14. In order to take the air gap between the PCB and converters into account in numerical models, a zero thickness planar object is used with thermal conductivity of air (0.0261 W/mK), and an effective thickness of 0.5 mm. The same zero thickness object is also used in the other models.

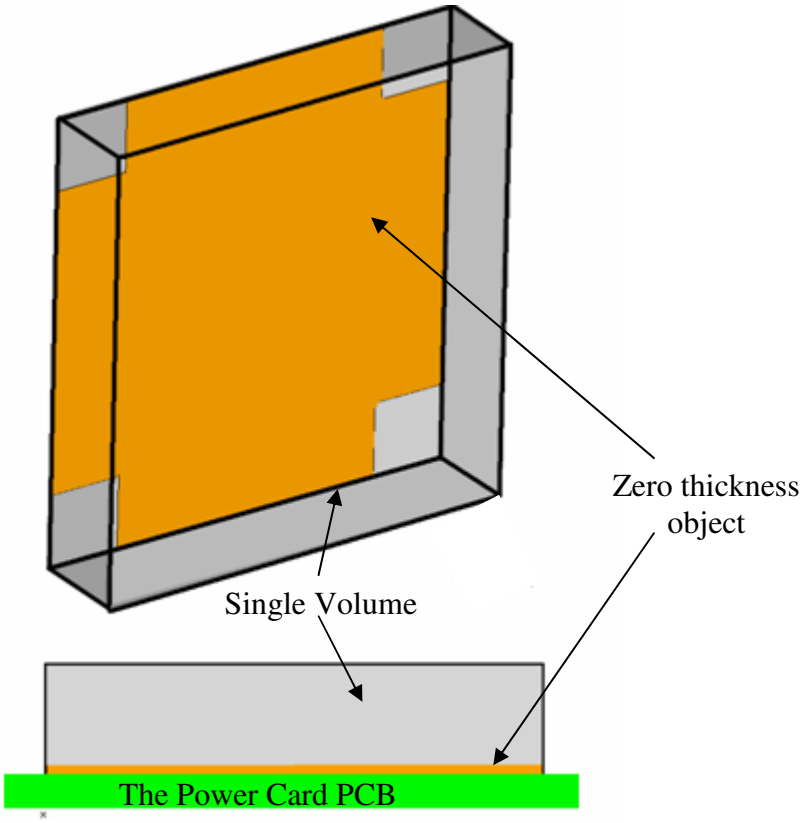

Figure 4.23 Single volume CCM (CCM A)

Table 4.14 Effective material properties for CCM A

Feature	Material	Volume (m^3)	Conductivity (W/m-K)	Density (kg/m^3)	Specific heat (J/kg-K)
Mosfet	Silicone	5350 x 10^{-9}	148.00	2300	712.00
Mold	Epoxy-Silica	29077.25 x 10^{-9}	0.63	1800	1005.00
Casing	Aluminium	11408.70 x 10^{-9}	205.00	2800	900.00
Single Volume	----------	45300 x 10^{-9}	69.51	2132.15	955.82

4.2.1.2 Multiple Volumes CCM (CCM B)

This time CCM is constructed as a combination of three simple volumes as shown in Figure 4.24. The first volume represents mosfet. It is the main source of heat generation and all the heat dissipation is associated with it. The other two volumes are used to model the mold and the external metallic casing. Dimensions of external casing and mold were determined due to vendor data sheets, but dimensions of mosfet are simply assumed to be 9.7 x 25 x 20 mm. Real material properties of silicone, epoxy-silica and aluminium are assigned to mosfet, mold and external casing respectively.

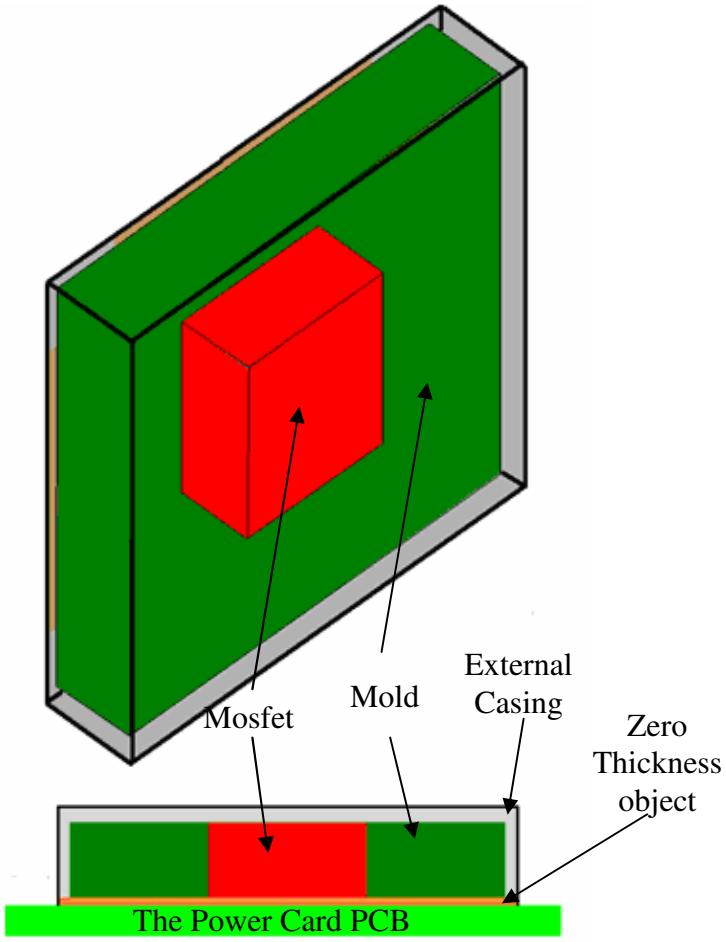

Figure 4.24 Multiple Volumes CCM (CCM B)

4.2.1.3 CCM with Combination of 2D and 3D Structures (CCM C)

In this final CCM mosfet is modelled as a 2D planar object and placed inside a single 3D prismatic volume as shown in Figure 4.25. No thermal conductivity value is assigned to the mosfet. Mean thermal conductivity value of 69.5 W/(mK) used for CCM A is assigned to the prismatic volume. To investigate the effect of this conductivity value another value which is 10 times smaller than the previous one, i.e. 6.95 W/(mK) is also used in the numerical tests. Similar mean thermal conductivity values were used previously by other researchers [52], [53].

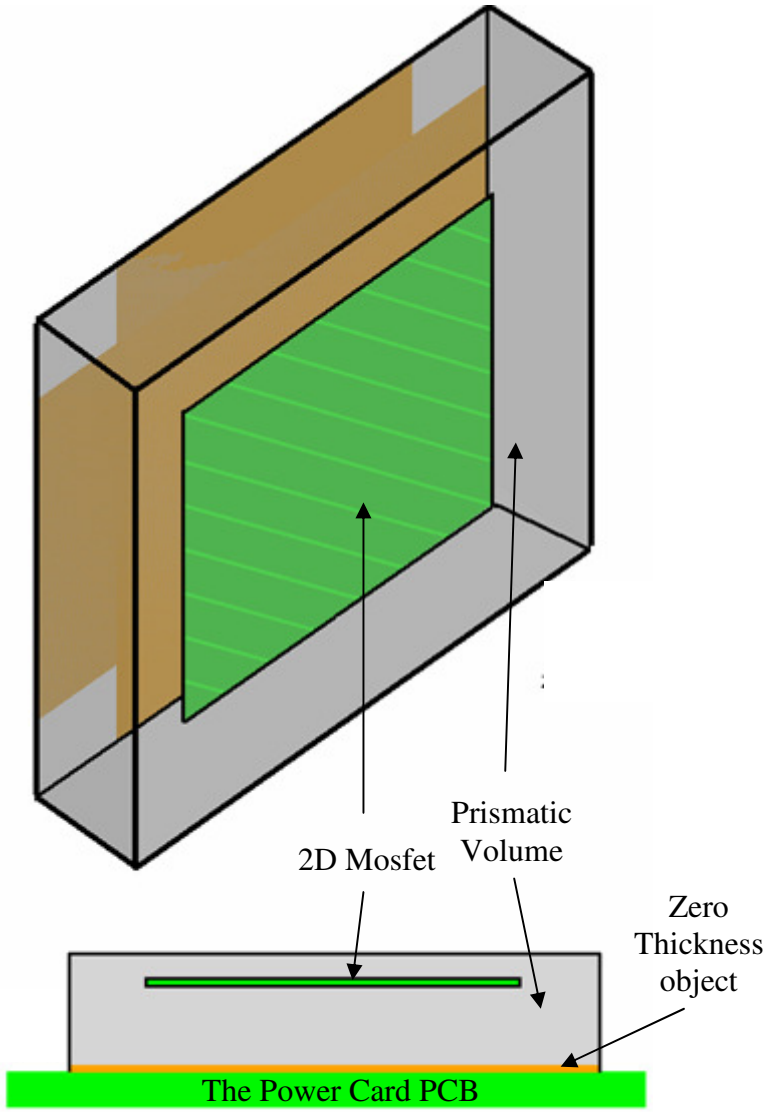

Figure 4.25 CCM with combination of 2D and 3D structures (CCM C)

4.2.2 Boundary Conditions and Solver Settings

Computational domain used for this problem can be seen in Figure 4.26 with the 3D rectangular cabinet created by Icepak. It has dimensions of 526 x 450 x 483 mm. Faces of the cabinet, except the bottom xz plane, are open to the surrounding air for heat and mass transfer. Bottom xz plane is defined as adiabatic and kept at the ambient temperature of 23 °C. No slip boundary condition is applied at all solid surfaces inside the computational domain.

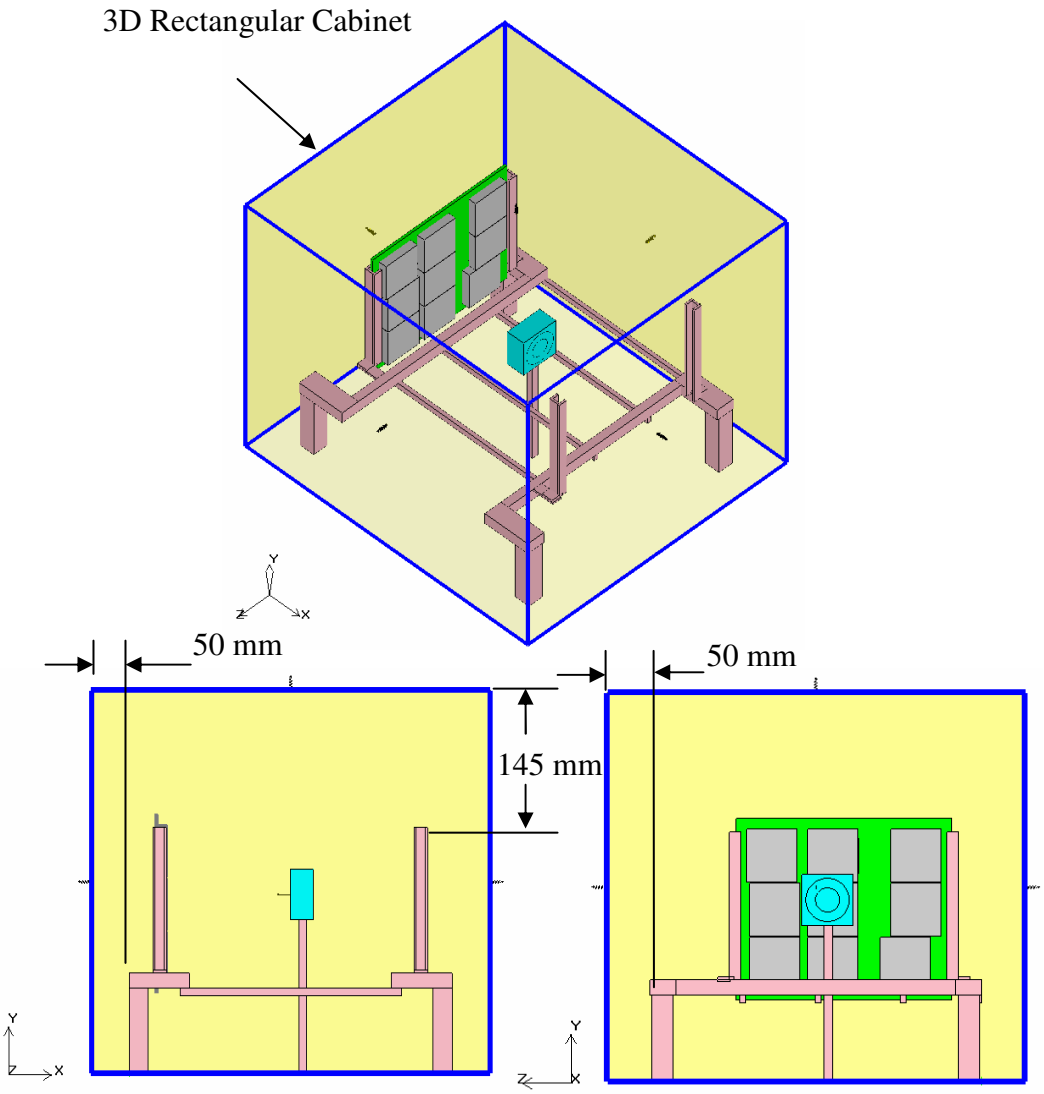

Figure 4.26 Computational domain inside a 3D cabinet for the second problem

Considering the irregularities and the swirling motion introduced by the fan the flow is considered to be turbulent. Other solver settings can be seen in Table 4.15. Convergence criterion is set to be 10^{-3} for solution residuals. Also the convergence is monitored by keeping track of the top surface temperature of the module type DC/DC converters during the simulations. Default Icepak under relaxation factors of 0.3 and 0.7 for pressure and momentum are used.

Table 4.15 Solver settings summary of second problem

Settings		Selection 1	Selection 2
Flow Regime		Turbulent	
Under Relaxation	Pressure	0.3	
	Momentum	0.7	
Pressure Discretization		1st order	2nd order
Momentum Discretization		1st order	2nd order
Pressure – Velocity Coupling		SIMPLE	SIMPLE

4.2.3 Grid Generation Details

Hexa-unstructured mesh generation technique is used to create meshes, a sample of which is shown in Figure 4.27. As seen in Figure 4.28, a non-conformal (N-C) domain is created around the power card and a denser grid is generated inside this region. By the help of N-C strategy grid count of the computational domain is roughly reduced by 45 % compared to a conformal grid.

To study the effect of grid resolution on the solution accuracy three different grids are created changing “max size ratio” parameter, which controls size ratio of adjacent elements for the whole model. Three different “max size ratio” values are used as 2.0 (default value), 1.35 and 1.3 to the control total grid count in the computational domain. Grid counts obtained with different “max size ratio” parameters are given in Table 4.16 with corresponding numerical model numbers.

In order to keep the y-plus value under 1 so that standard wall functions can be used with RANS type turbulence models, an initial height value of 0.05 mm is used for the cells adjacent to DC/DC converter surfaces. This value is determined by the help of a set of preliminary simulations that are not mentioned here.

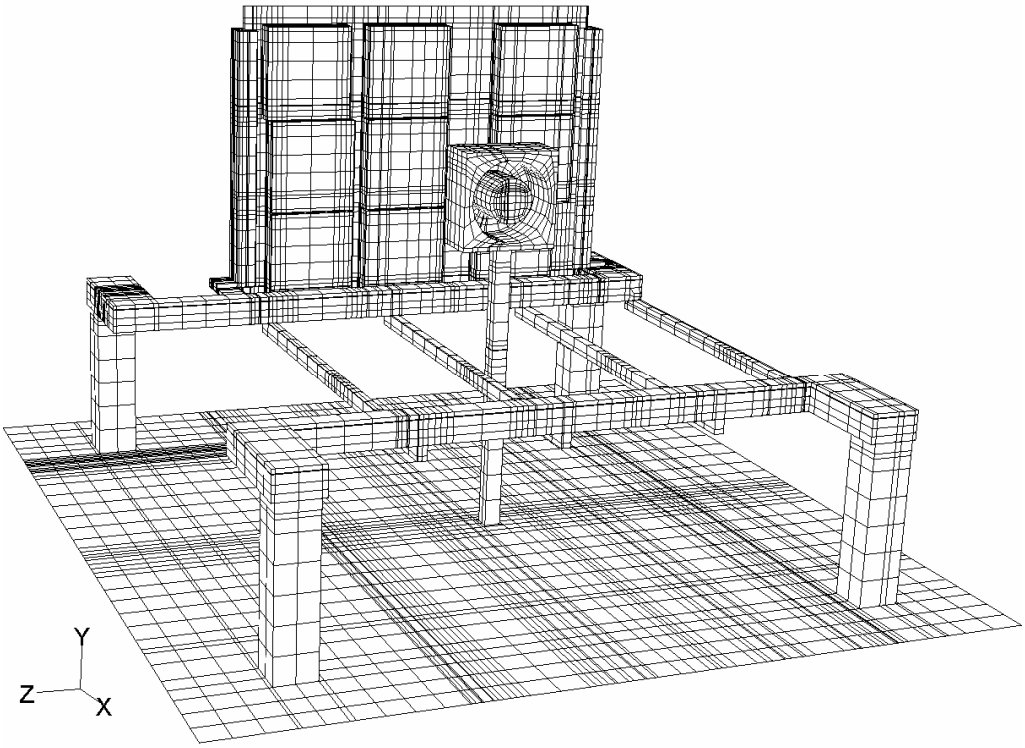

Figure 4.27 A sample hexa-unstructured grid generated for the second problem

Table 4.16 Grid counts used for different simulations of the second problem

# of numerical model	**Max size ratio**	**Thermal model of *MGDM-150* series module type DC/DC converter**	**Total mesh count inside the non-conformal domain**	**Total mesh count on the computational domain**
NM-8	2.0	CCM C	340233	573520
NM-9	1.35	CCM C	1241204	1812362
NM-10	1.3	CCM C	2572610	3132382
NM-11	2.0	CCM B	374682	604373
NM-12	1.35	CCM B	695413	1214600
NM-13	2.0	CCM A	248222	490727
NM-14	1.35	CCM A	581842	1621267

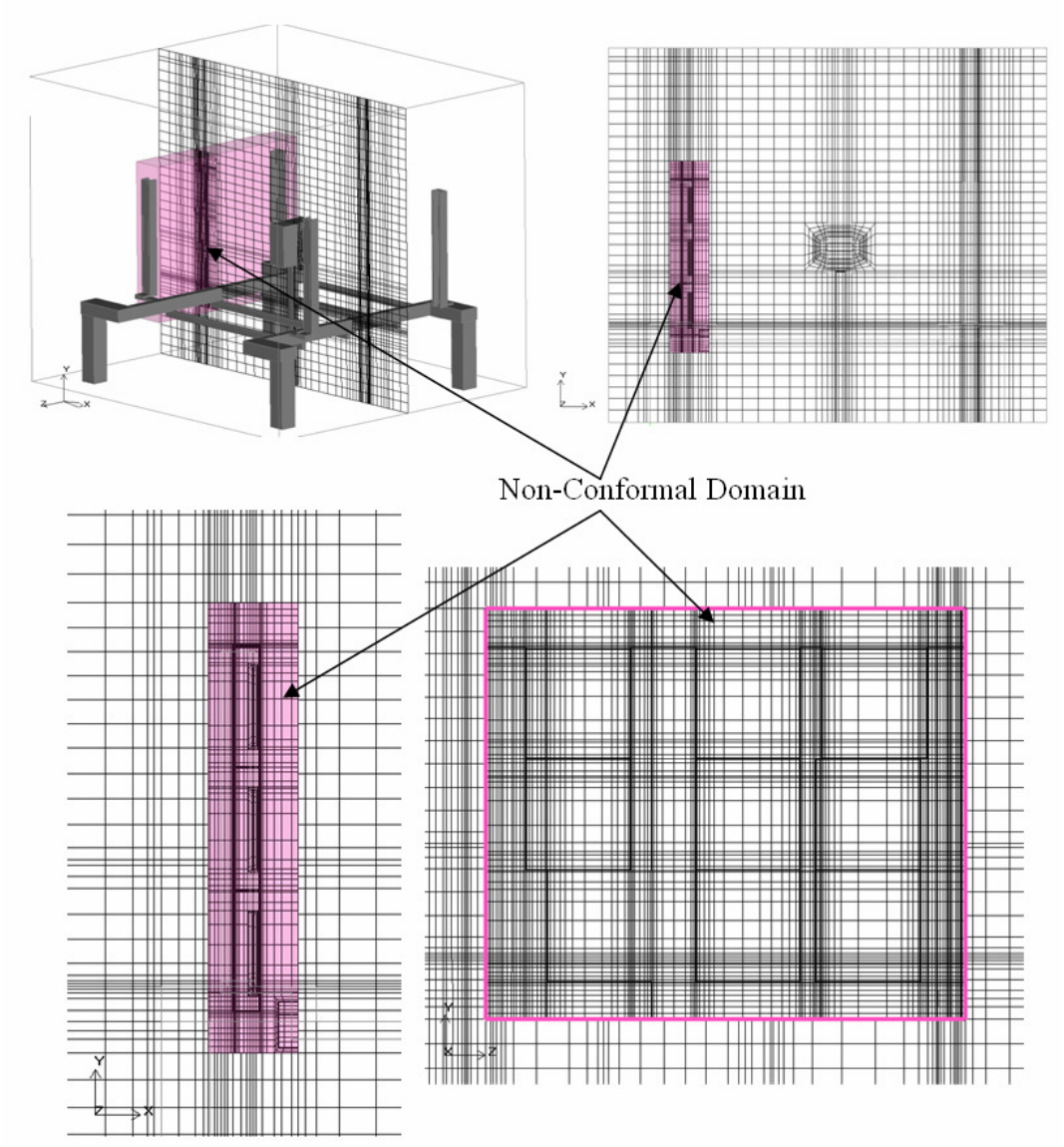

Figure 4.28 A sample non-conformal grid structure used for the second problem

4.2.4 Numerical Simulations

For the forced convection cooling of module type DC/DC converters 11 different simulations are performed in two steps. In the first step, as shown in Table 4.17 all CCM alternatives are analysed for two different “max size ratio” parameters which

are 2.0 and 1.35. Realizable k-ε is used as the turbulence model of these analyses. This selection is again based on a set preliminary studies that are not mentioned here.

In the second step of simulations CCM C is combined with two different turbulence models, two different discretization orders and two different thermal conductivity values as shown in Table 4.18.

Table 4.17 Summary of performed analysis of the second case (first step)

Simulation Number	**Thermal model**	**Max size ratio**	**# of numerical model**
15	CCM A	2.0	NM-13
16	CCM A	1.35	NM-14
17	CCM B	2.0	NM-11
18	CCM B	1.35	NM-12
19	CCM C	2.0	NM-8
20	CCM C	1.35	NM-9

Table 4.18 Summary of performed analysis of the second case (second step)

Simulation Number	Thermal model	Changed Parameter
21	CCM C	Max size ratio is set to 1.3
22	CCM C	Zero Equation turbulence model is used instead of Realizable k-ε
23	CCM C	6.95 W/mK is used instead of 69.5 W/mK for thermal conductivity of
24	CCM C	695 W/mK is used instead of 69.5 W/mK for thermal conductivity
25	CCM C	2^{nd} order discretization schemes are used instead of 1^{st} order schemes

4.2.5 Comparison of Results and Discussion

As described in Chapter 3, temperatures are measured for this problem using thermocouples at 6 different locations. During the simulations temperatures of these points are recorded so that point temperature comparisons can be made. Measured temperatures are given in Table 4.19. Numerically obtained temperatures and deviations from experimental ones are given in Table 4.20 and Table 4.21.

Table 4.19 Measured temperatures of the natural convection setup (ºC)

Thermocouple (TC) No					
1	**2**	**3**	**4**	**5**	**6**
34.2	29.7	27.9	30.9	27.2	28.0

Table 4.20 Results of the first step of simulations

T (ºC) : Temperature %: Percent deviations with respect to experiment

Simulation Number		**Thermocouple (TC) No**					
		1	**2**	**3**	**4**	**5**	**6**
15	T (ºC)	33.6	30.2	31.6	31.7	27.9	29.4
	%	-1.8	1.7	13.3	2.6	2.6	5.0
16	T (ºC)	32.3	29.1	30.8	30.8	27.0	28.5
	%	-5.6	-2.0	10.4	-0.3	-0.7	1.8
17	T (ºC)	36.6	29.0	32.1	33.4	27.1	31.2
	%	7.0	-2.4	15.1	8.1	-0.4	11.4
18	T (ºC)	35.4	28.6	31.5	32.9	26.9	30.2
	%	3.5	-3.7	12.9	6.5	-1.1	7.9
19	T (ºC)	33.5	30.0	31.4	31.7	27.8	29.4
	%	-2.0	1.0	12.5	2.6	2.2	5.0
20	T (ºC)	32.5	29.0	30.7	31.1	27.0	28.7
	%	-5.0	-2.4	10.0	0.6	-0.7	2.5

Table 4.21 Results of the second step of simulations

T (ºC) : Temperature %: Percent deviations with respect to experiment

Simulation Number		Thermocouple (TC) No					
		1	**2**	**3**	**4**	**5**	**6**
21	T (ºC)	32.3	28.9	30.5	30.9	26.8	28.4
	%	-5.6	-2.7	9.3	0.0	-1.5	1.4
22	T (ºC)	36.3	33.3	35.9	36.4	30.8	31.9
	%	6.1	12.1	28.7	17.8	13.2	13.9
23	T (ºC)	36.4	28.4	30.6	33.6	26.5	30.8
	%	6.4	-4.4	9.7	8.7	-2.6	10.0
24	T (ºC)	32.6	29.5	31.4	31.4	27.4	28.9
	%	-4.7	-0.7	12.5	1.6	0.7	3.2
25	T (ºC)	32.0	28.6	29.8	30.1	26.8	28.7
	%	-6.4	-3.7	6.8	-2.6	-1.5	2.5

To get a feeling of the flow field path lines obtained for simulation 19 are given in Figure 4.29. Temperature contours of the power card obtained by the same simulation can be seen in Figure 4.30.

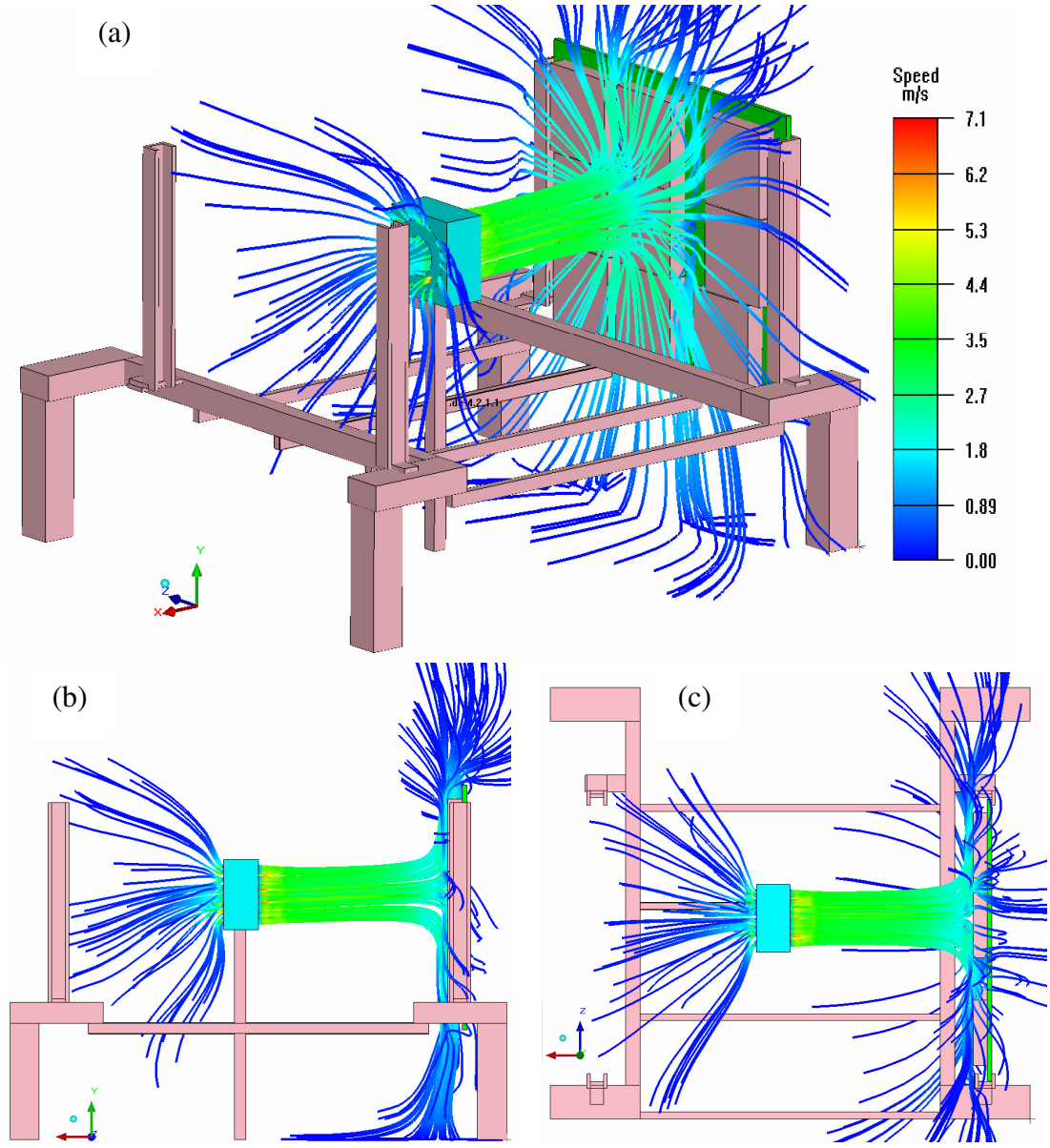

Figure 4.29 Speed (m/s) coloured path lines for fan derived flow

a) Isometric view, b) Z-plane view, c) Y-plane view

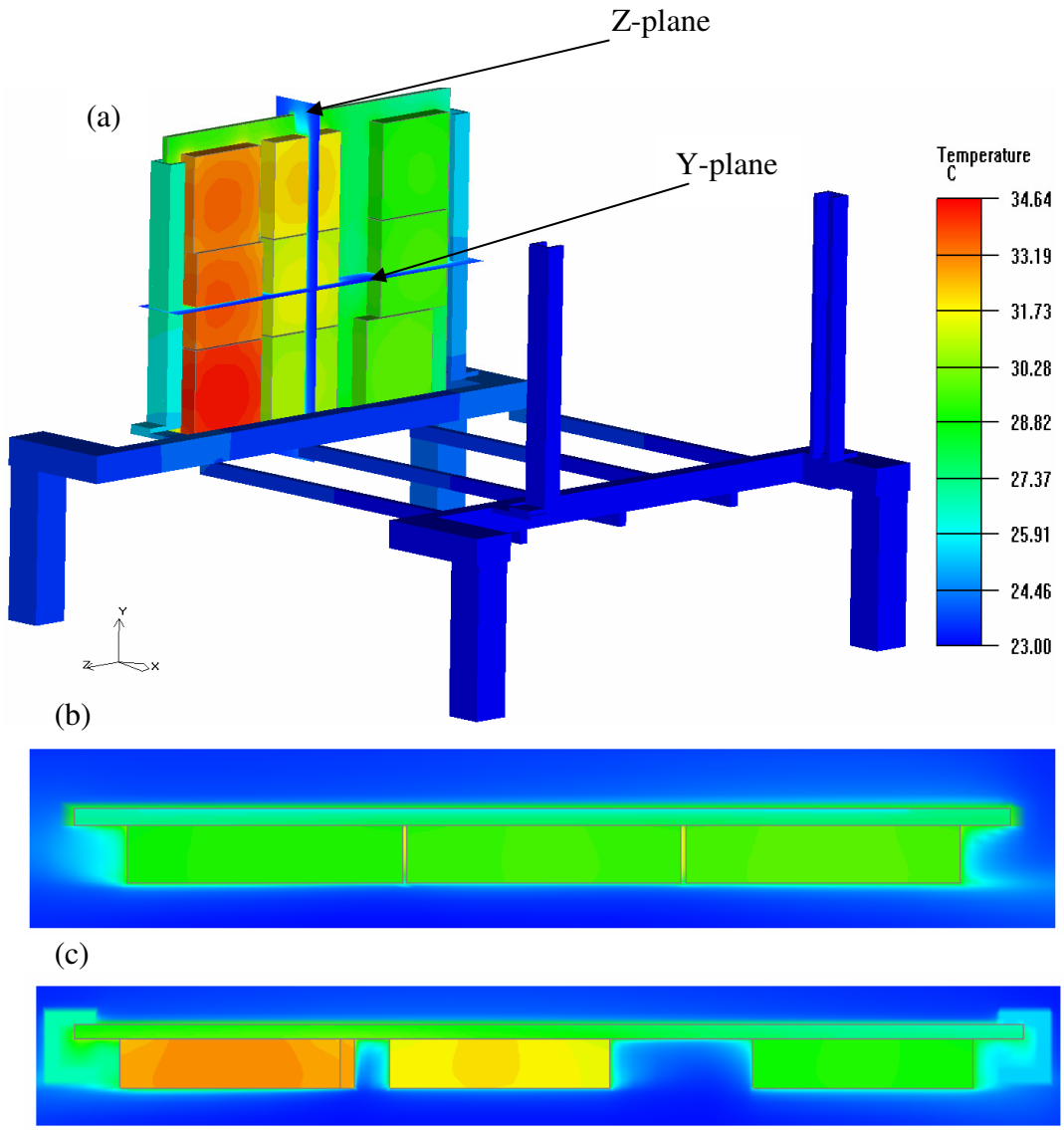

Figure 4.30 Temperature contours on the power card.

a) Isometric view, b) Z-plane view, c) Y-plane view

Figure 4.31 show temperature contours of the power card surface obtained by the first step simulations.

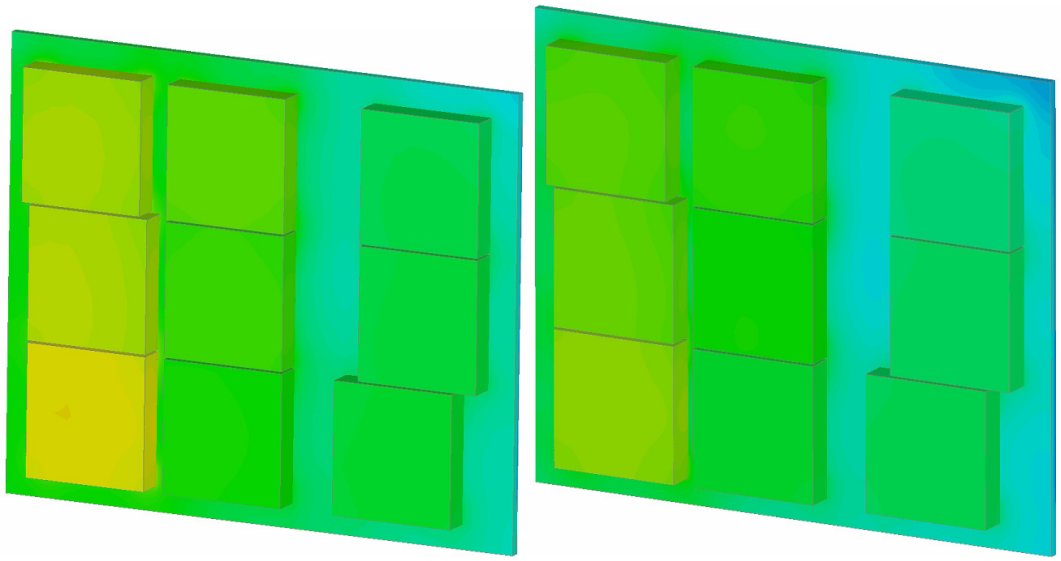

Simulation 15 Simulation 16

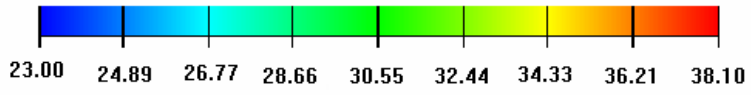

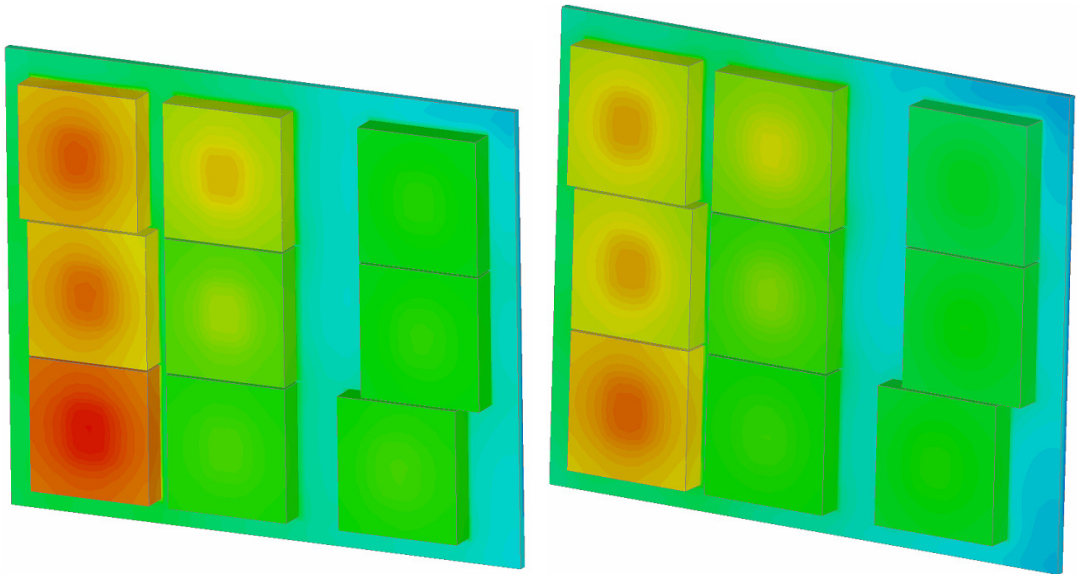

Simulation 17 Simulation 18

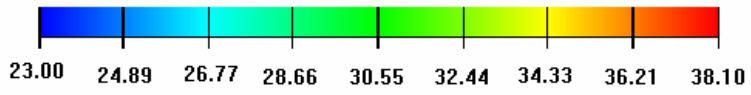

Figure 4.31 Temperature (ºC) contours of the power card surface obtained by different simulations

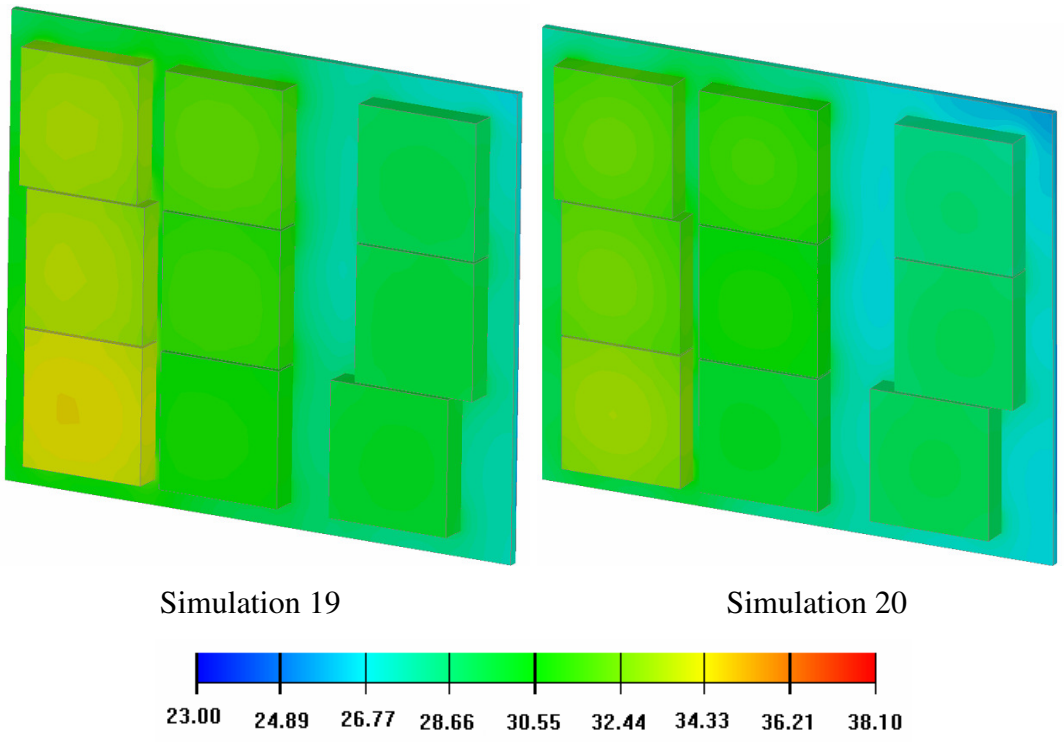

Figure 4.31 Temperature (ºC) contours of the power card surface obtained by different simulations (continued)

As seen in Figure 4.31 and Table 4.20 use of 1.35 for max size ratio (which results in a denser grid structure than the default value of 2.0) provides slightly lower temperatures at all temperature point locations for all CCMs. Upper surface temperatures (TC points 1, 4 and 6) can be obtained in 10 % deviation for all CCMs except at TC point 6 of simulation 17 that uses CCM B. Because of volume averaged lumping processes, temperature gradients for CCM A and CCM C are lower compared to CCM B. In other words CCM A and CCM C results in more uniformly distributed surface temperatures.

Highest deviations between the numerical and experimental results are observed at the third thermocouple location for all CCMs. Actually this is expected because the third thermocouple is attached to the thin side wall of a DC/DC converter module, which is a difficult spot to take accurate measurements. Also simulation results show

a trapped and slowly moving fluid body at this location, which may not be the actual case.

In the second step simulations effect of turbulence modelling, thermal conductivity value and discretization schemes are investigated. In this manner zero equation turbulence model is used instead of realizable k-ε, two different thermal conductivity values (6.95 and 695 W/mK) are examined instead of 69.5 W/mK and second order discretization schemes are used for pressure, momentum, turbulence kinetic energy and turbulence dissipation rate. Simulation 20 is chosen as a base model for comparisons where relative percent deviations are lower than 10 % for all TC points (Table 4.20) Temperature contours obtained by the second step simulations are shown in Figure 4.32.

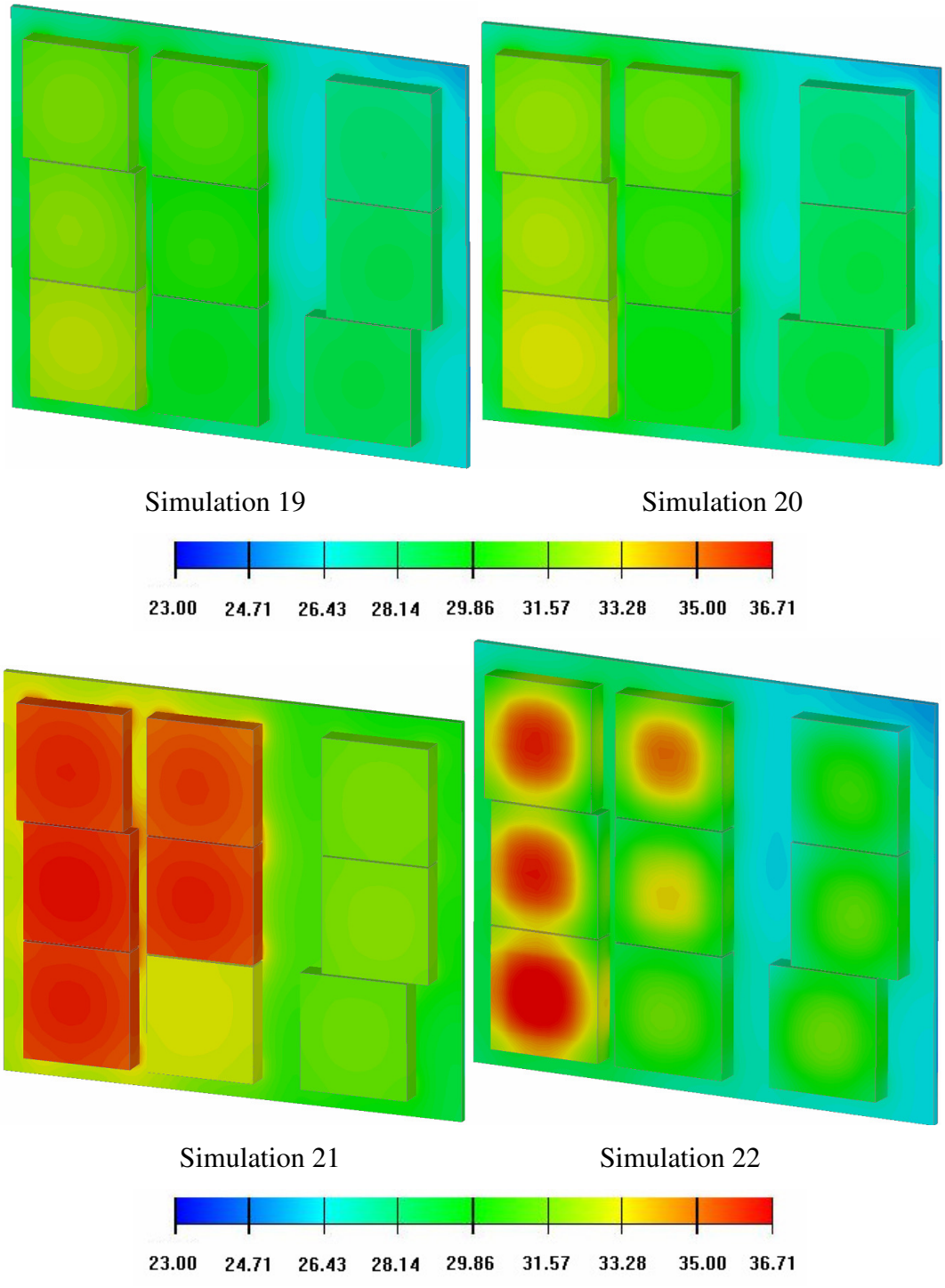

Figure 4.32 Temperature (ºC) contours of the power card surface obtained by different simulations

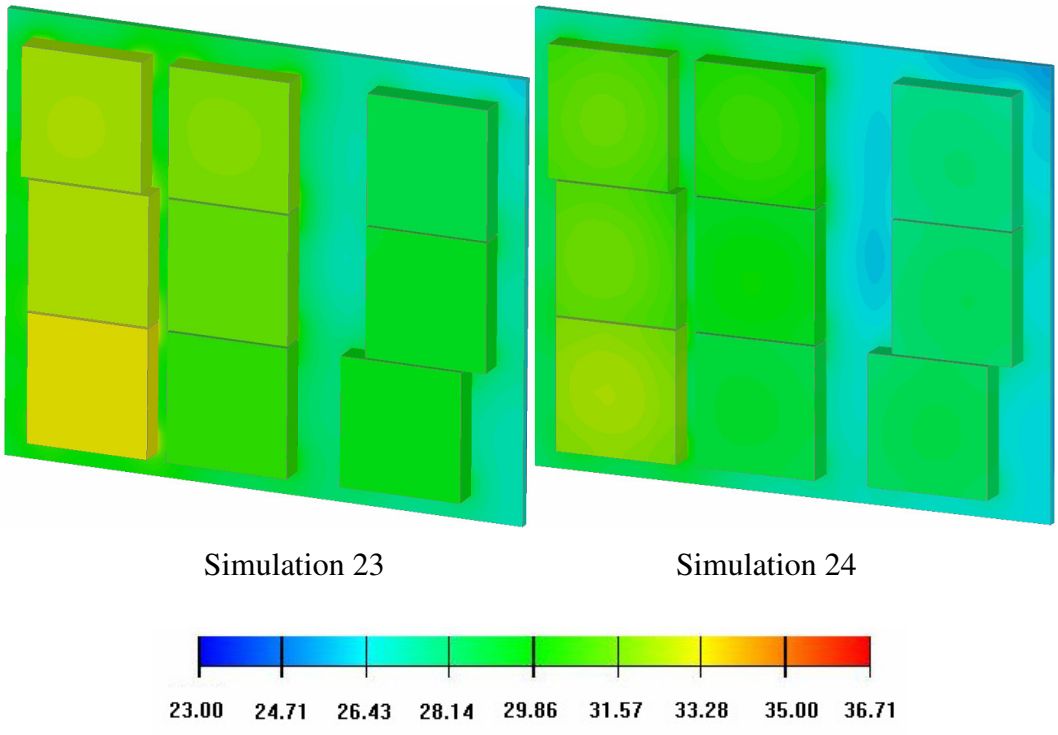

Figure 4.32 Temperature (ºC) contours of the power card surface obtained by different simulations (continued)

As seen in Table 4.21 and Figure 4.32, use of zero equation as turbulence model causes higher temperatures for all thermocouple points compared to realizable k-ε model. Although not mentioned here, temperatures obtained by laminar simulations were even worse than those provided by the zero equation model. As seen from Figure 4.32, the use of lower thermal conductivity value increases the internal resistance against dissipation of heat. So that high temperature gradients are seen on DC/DC converters and surface temperatures (TC point 1, 4 and 6) increase due to increasing spreading resistance. Higher thermal conductivity value decreases the internal resistance as expected and more uniform temperature distributions are seen on DC/DC converters. Due to this result the percent relative difference at TC point 3 increases according to base model (k = 69.5 W/mK). Second order discretization doesn't show drastic changes on surface temperature contours, but the lowest relative percentage error is obtained at TC point 3 (Table 4.21).

4.3 Numerical Study of the Third Problem (Realistic Avionic Box)

Third problem includes system level simulations of an electronic box which includes a PCB with 12 electronic packages. This PCB is located in an air-sealed box which is cooled from outside by the help of a fan. Computational domain used for the simulations can be seen in Figure 4.33 of the 12 items located on the PCB are selected to be the same as the TSSOP type DC/DC converter studies as the first problem. The idea is to use the already developed thermal models directly in this study. Specifically DTM and CCMs 3, 4 and 5 developed in the first study are used. Remaining 4 items located on the PCB are Plastic Quad Flat Package (PQFP), which are common elements of realistic avionic applications.

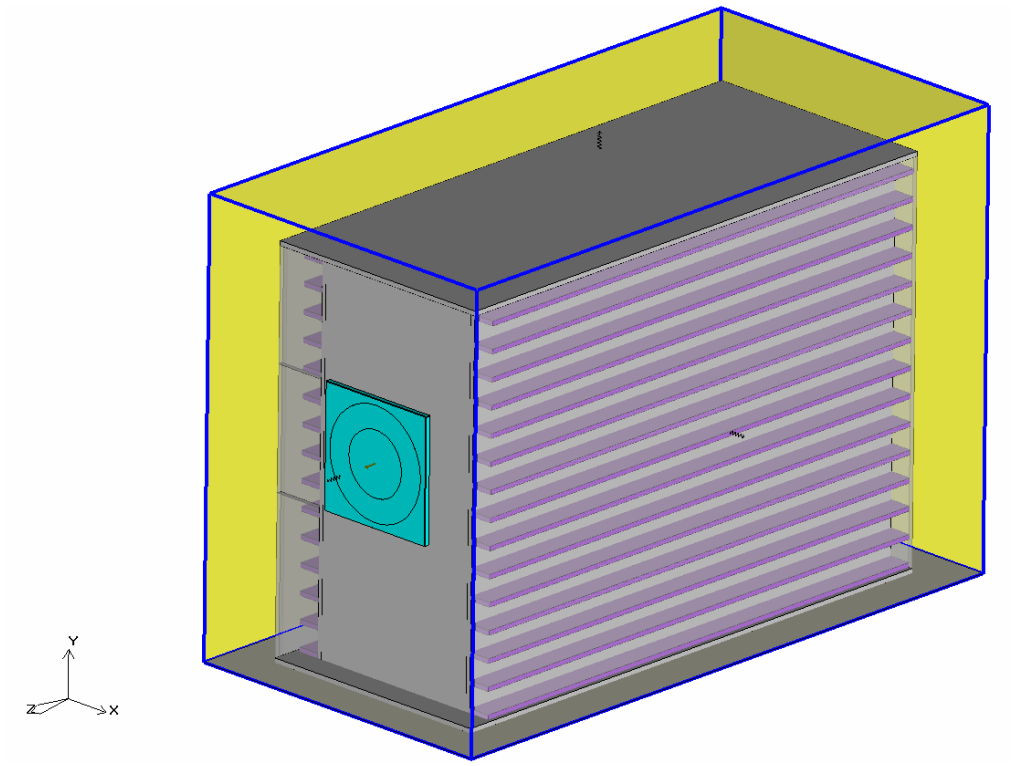

Figure 4.33 Computational model of the third problem (inside details cannot be seen)

In the following paragraphs details of the parts of the system that are identical in all simulations are presented.

Electronic box

Electronic box (also known as ATR chassis), seen in Figure 4.34, is made of aluminium and it is modelled using prismatic blocks. Its external dimensions are decided according to ARINC 404A Air Transport Equipment Cases and Racking Standard [5]. Standard ½ Short Air Transport Rack limit dimensions of 123.95 x 320.5 x 193.5 mm are selected as envelope dimensions. Electronic box has an air sealed enclosure, heat sinks and air channels.

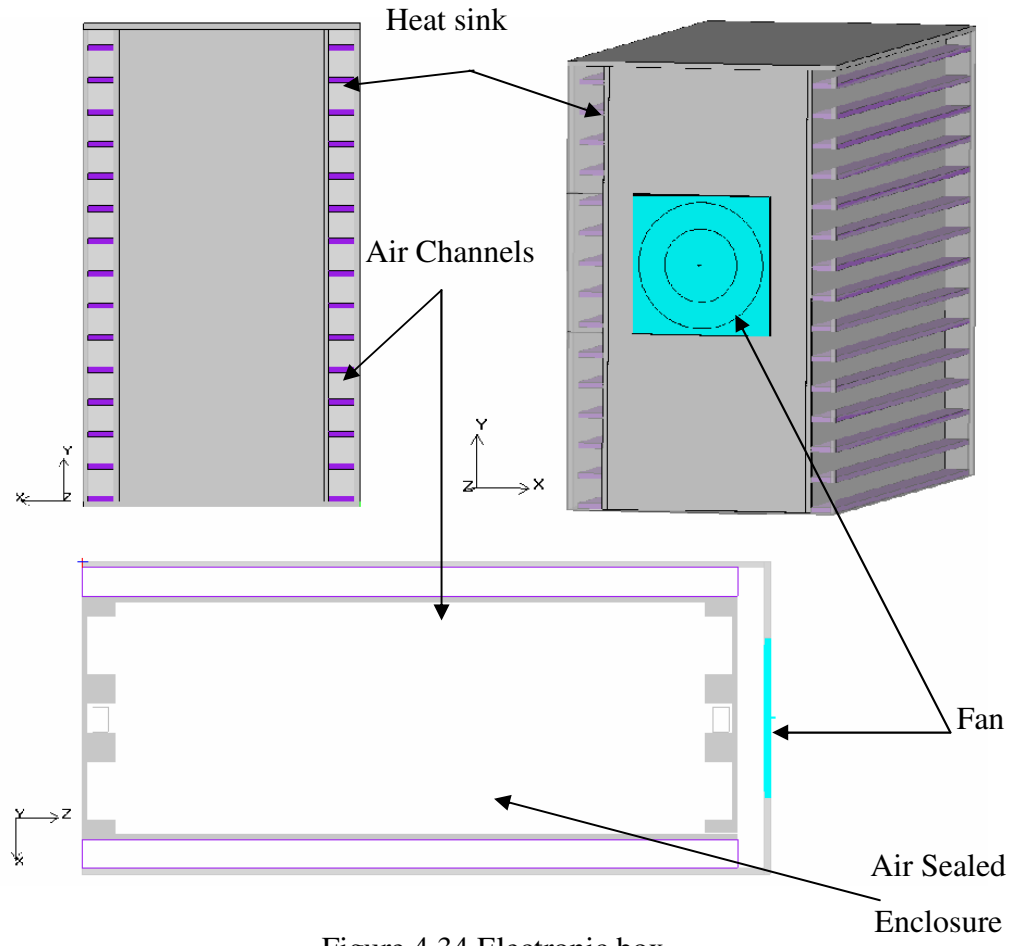

Figure 4.34 Electronic box

Fan

The fan is selected to be the same as the one used in the previous forced convection problem. It is used to suck air through the air channels located outside the electronic box.

Plastic Quad Flat Package (PQFP)

Thermal model of PQFP electronic component shown in Figure 4.35 is taken to be the same as the one developed by Rosten et. al [16], which was summarized in Chapter 2. Not only DC/DC converters but these components also dissipate heat (1W each). Four of these PQFPs are located on the PCB.

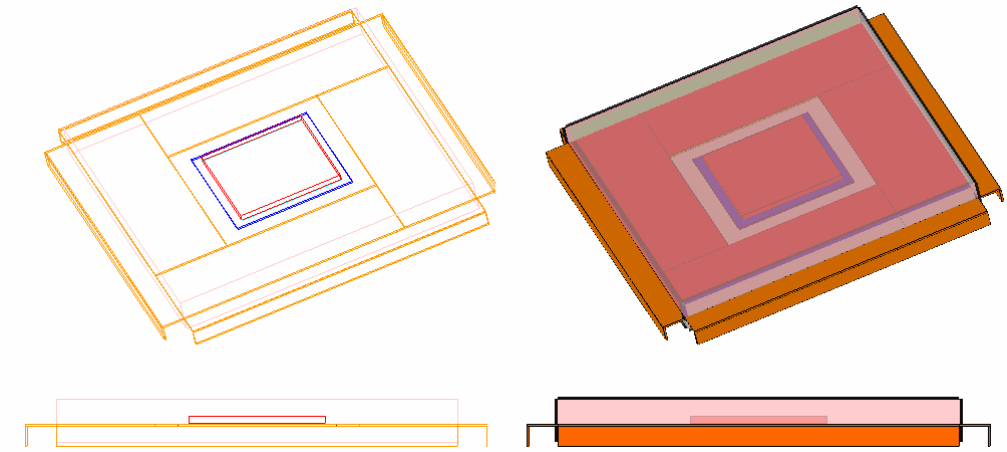

Figure 4.35 Thermal model of the PQFP [16]

Printed Circuit Board Assembly of the Third Case

A PCB model is created based on standard dimensions of 6U VME boards [54]. which has dimensions of 233.35 x 160 x 1.6 mm. These VME boards are commonly used PCBs of avionics electronic systems and their external dimensions has been standardized by committees like IEEE SA Standard Boards. Orthotropic material

properties, which were previously computed for the first problem are used for the PCB of this problem too.

8 TPS54610 DC/DC converter and 4 PQFP thermal models are placed on the PCB as shown in Figure 4.36. Total heat dissipation of the PCB assembly is 8x0.42 + 4x1 = 7.36 W. Location of PCB inside the air-sealed region can be seen in Figure 4.37.

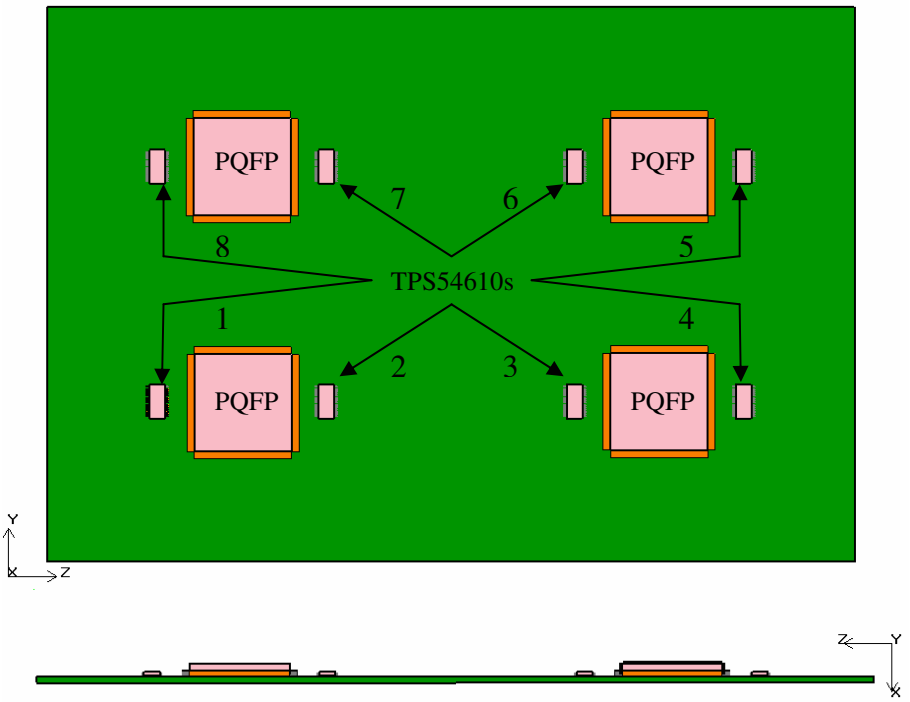

Figure 4.36 PCB with 8 DC/DC converters and 4 PQFPs

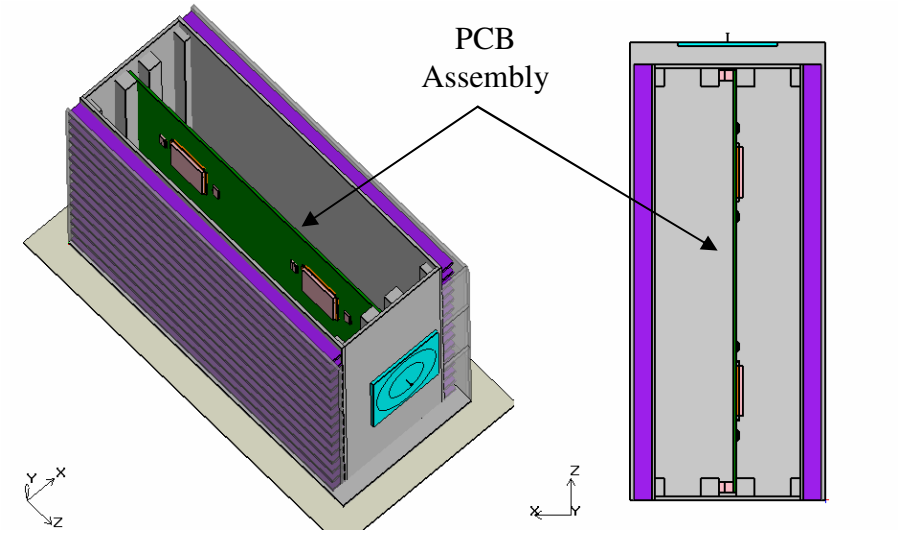

Figure 4.37 Placement of PCB in the air sealed region

4.3.1 Boundary Conditions and Solver Settings

Similar to the previous problems ICEPAK creates a cabinet around the electronic box to create the computational domain shown in Figure 4.38. This time cabinet dimensions are 148 x 200 x 292 mm. Cabinet faces, except the bottom one, are all open to mass and heat transfer. Bottom face is taken to be adiabatic at the ambient temperature of 20 °C. No slip boundary condition is applied at all solid surfaces.

3D Rectangular Cabinet

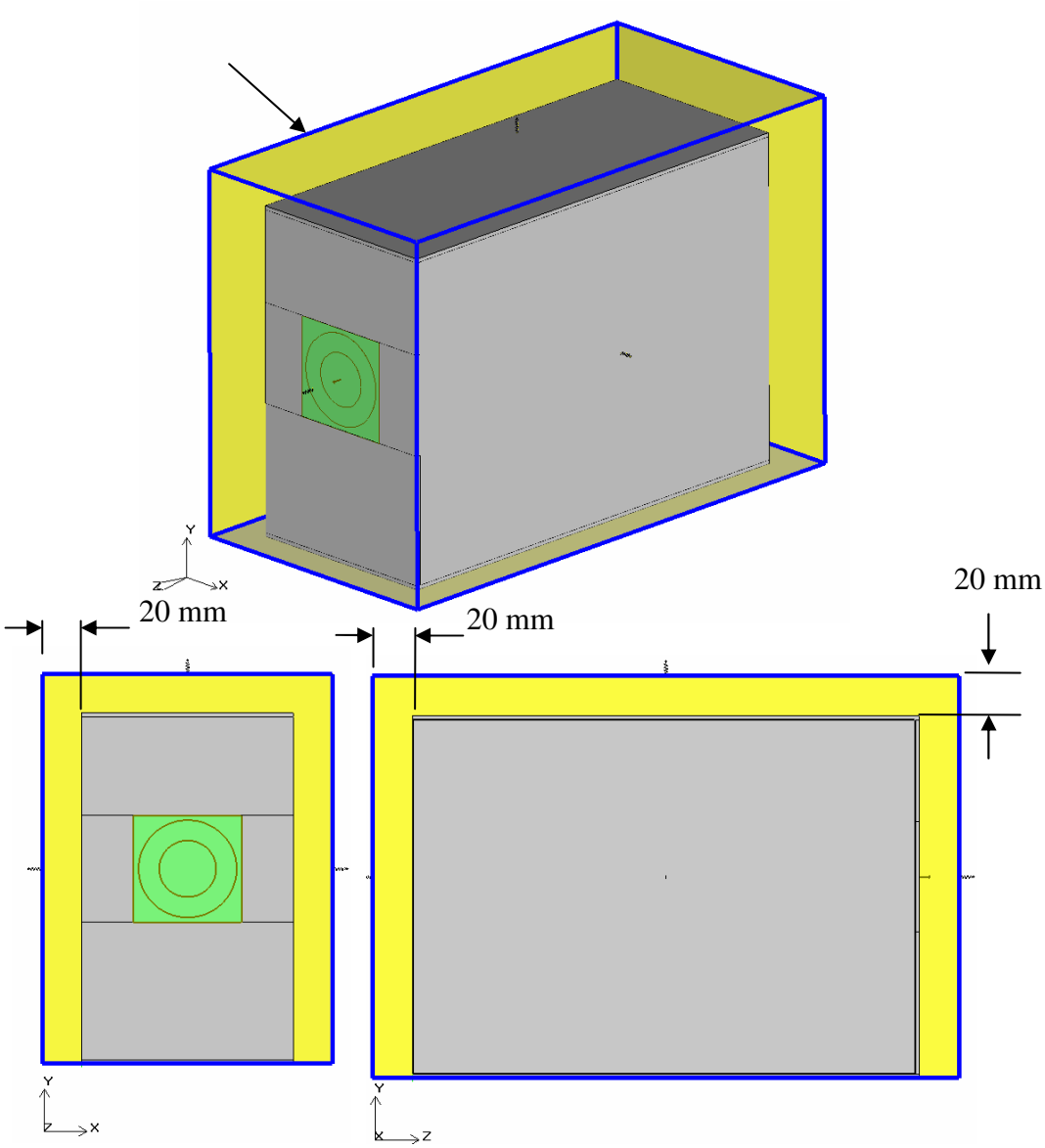

Figure 4.38 Computational domain of the third problem

Although velocities inside the air channel have velocities in the order of 7 m/s and the flow inside the air sealed region is driven purely by buoyancy effects, flow regime is taken to be turbulent considering the irregularities and the swirl motion introduced by the fan. Radiative heat transfer is not neglected and discrete ordinate radiation model is used in analyses. Other solver settings were the same as the ones used in previous problems with the limitation that only 1st order discretization is tried for this problem.

4.3.2 Grid Generation on Numerical Models of the Third Case

Similar to first and second problems, hexa-unstructured mesh generation technique is used in the third case, which results in meshes as the one shown in Figure 4.39. A non-conformal mesh strategy is also applied for efficient grid refinement around small electronic package regions (Figure 4.40). Different CCMs used for the DC/DC converter resulted in the mesh counts given in Table 4.22. The mesh count of NM 15, approximately 5 billion, is the highest mesh count that could be created and solved by the author's current computational resources.

To keep y-plus values for the air channels under 1 so that the use of standard wall functions can be justified, based on preliminary simulations initial wall height in these regions is selected to be 0.1 mm.

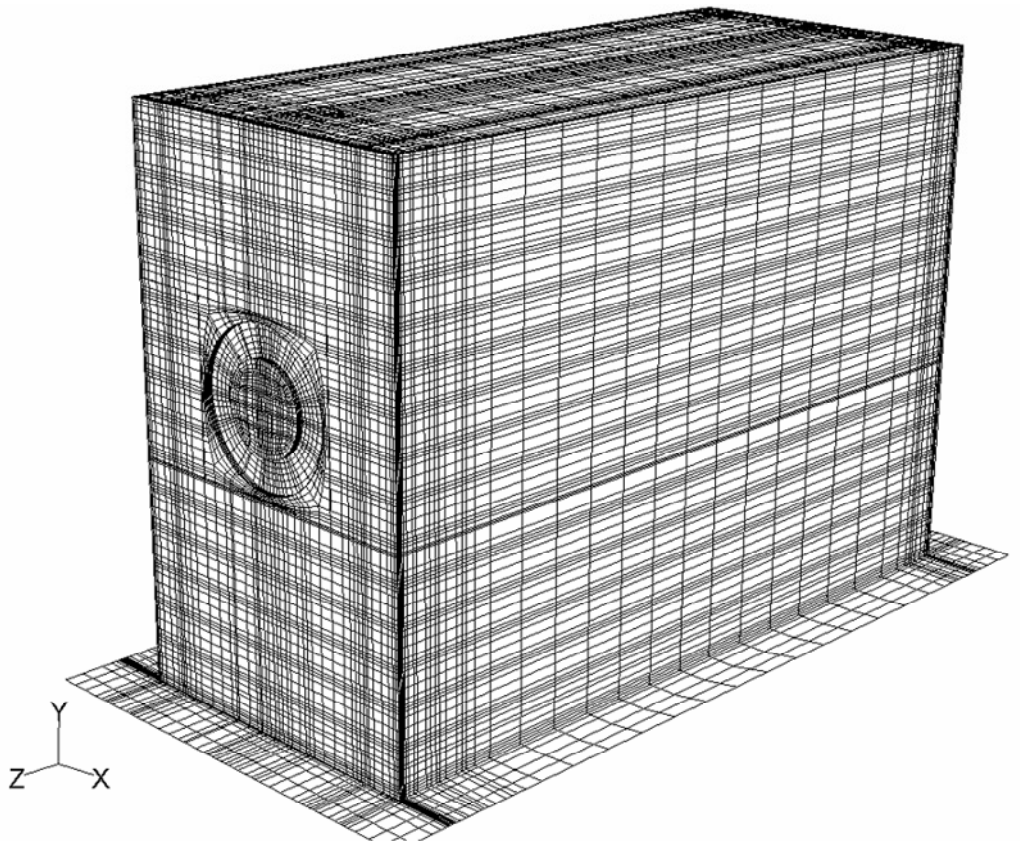

Figure 4.39 Asample hexa-unstructured mesh generated for the third problem

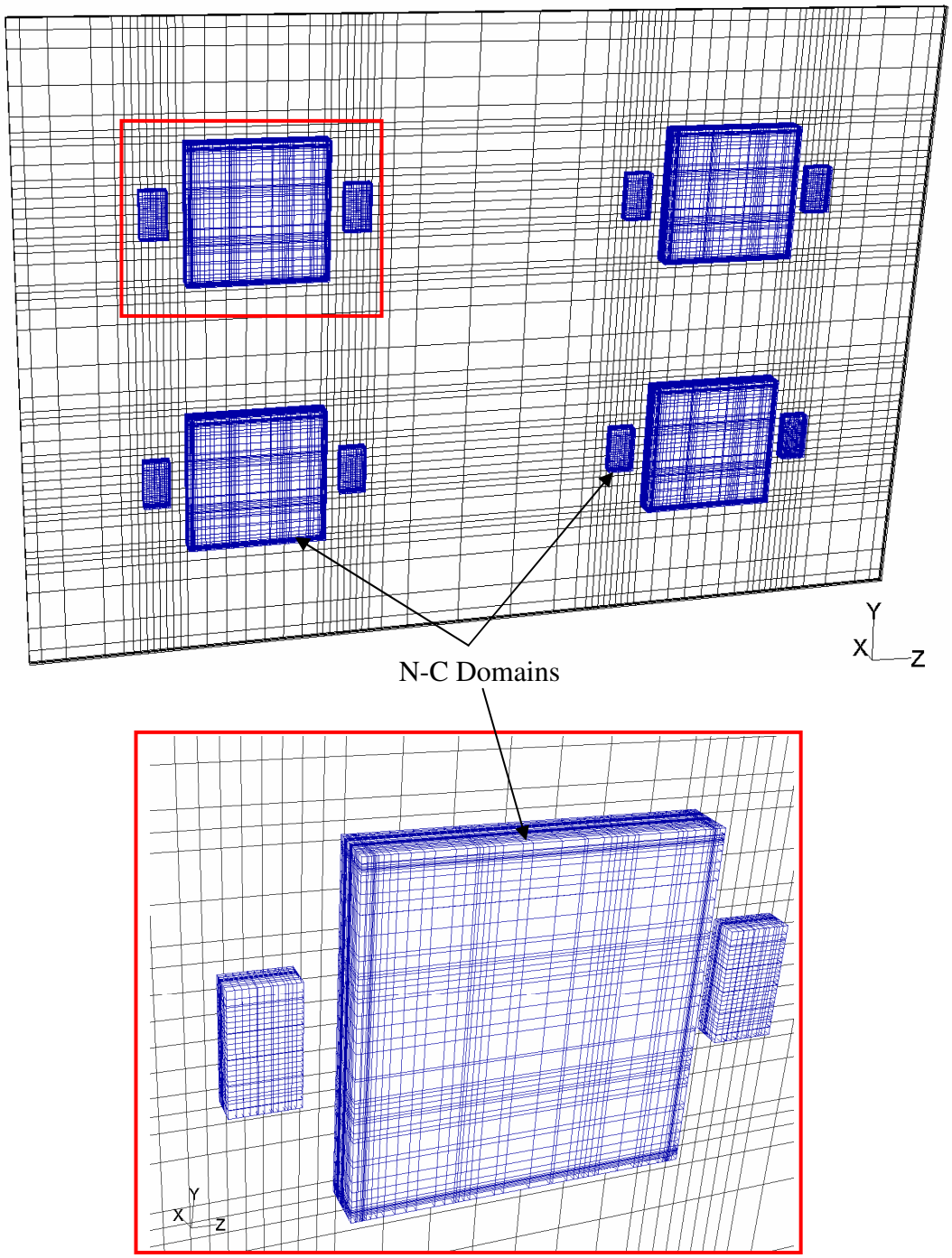

Figure 4.40 Non-conformal domain details used in the third problem

Table 4.22 Grid counts for different CCM models

# of numerical model	Thermal model of TPS54610 DC/DC converter	Total mesh count on the computational domain	Total mesh count inside the non-conformal domain of TPS54610
NM-15	DTM	4567540	256523
NM-16	CCM 3	2857247	22550
NM-17	CCM 4	2634846	2380
NM-18	CCM 5	2623742	2030

4.3.3 Numerical Simulation

As shown in Table 4.23, were carried out. a total of six simulations are performed. First NM 15 is simulated using both k-ε and realizable k-ε turbulence models to obtain a base solution. Alternatively NM 15 is solved with zero equation turbulence model to reduce solution time. After seeing the success of zero equation modelling, remaining simulations, which compares different CCMs, are also run with zero equation modelling.

Table 4.23 Summary of performed analysis of the third problem

Analysis Number (AN)	Used Numerical model	Turbulence Model
26	NM-15	Realizable k-ε
27	NM-15	k-ε
28	NM-15	Zero equation
29	NM-16	Zero equation
30	NM-17	Zero equation
31	NM-18	Zero equation

4.3.4 Comparison of Numerical Results and Discussion

In all simulations temperature data is gathered at five points shown in Figure 4.41. Points 1 and 3 are placed on top surfaces of two different DC/DC converters. Points 2 and 4 are selected to be on the PCB and as close as possible to the external leads of two converters. Finally point 5 is located on the top surface of a PQFP.

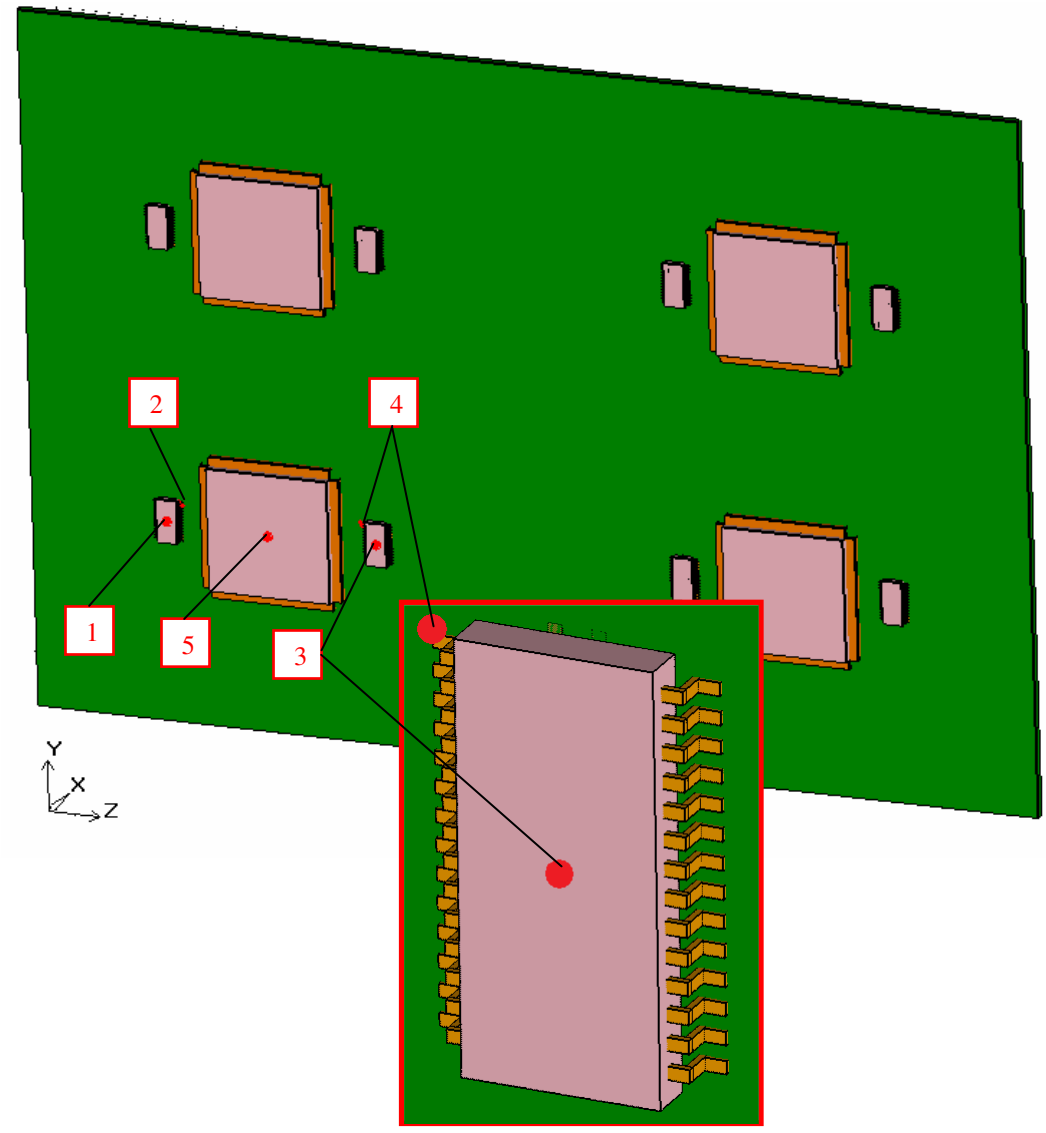

Figure 4.41 Locations of the temperature points used in the third problem

Simulation results are summarized in Table 4.24. Except for the first two simulations, percent deviations are calculated with respect to the base simulation 26.

Table 4.24 Simulation results of the third problem

T (ºC) : Temperature %: Percent deviations with respect to simulation 26

Simulation Number		**Thermocouple No**				
		1	**2**	**3**	**4**	**5**
26	T ºC	32.1	29.5	34.8	32.0	51.3
	%					
27	T ºC	32.0	29.4	34.7	31.9	51.4
	%					
28	T ºC	32.0	29.4	34.7	31.8	51.4
	%	-0.3	-0.3	-0.3	-0.6	0.2
29	T ºC	31.3	29.5	33.8	31.8	51.4
	%	-2.5	0	-2.9	-0.6	0.2
30	T ºC	33.6	30.0	36.7	32.6	51.7
	%	4.8	1.5	5.5	1.9	0.7
31	T ºC	33.7	29.8	36.7	32.4	51.4
	%	4.9	1.0	5.3	1.4	0.2

Unlike the first and second problems, there is no experimental study performed for this third problem. Hence CCM performance evaluations are made with respect to simulations that make use of a detailed thermal model of DC/DC converters. Base simulations 26 and 27 make use of k-ε turbulence model, whereas base simulation 28 makes use of zero equation turbulence modelling. To support point temperature comparison provided by Table 4.24, streamlines for the flow inside air channels and electronic box surface temperature contours are presented in Figure 4.42 and 4.43.

Compared to simulation 26, simulations 26 and 27 result in higher speeds inside air channels (Note that air is sucked from air channels by the fan). As a result of this for simulation 28 electronic box and the heat sink around it are slightly warmer compared to simulations 26 and 27, but differences are not remarkable.

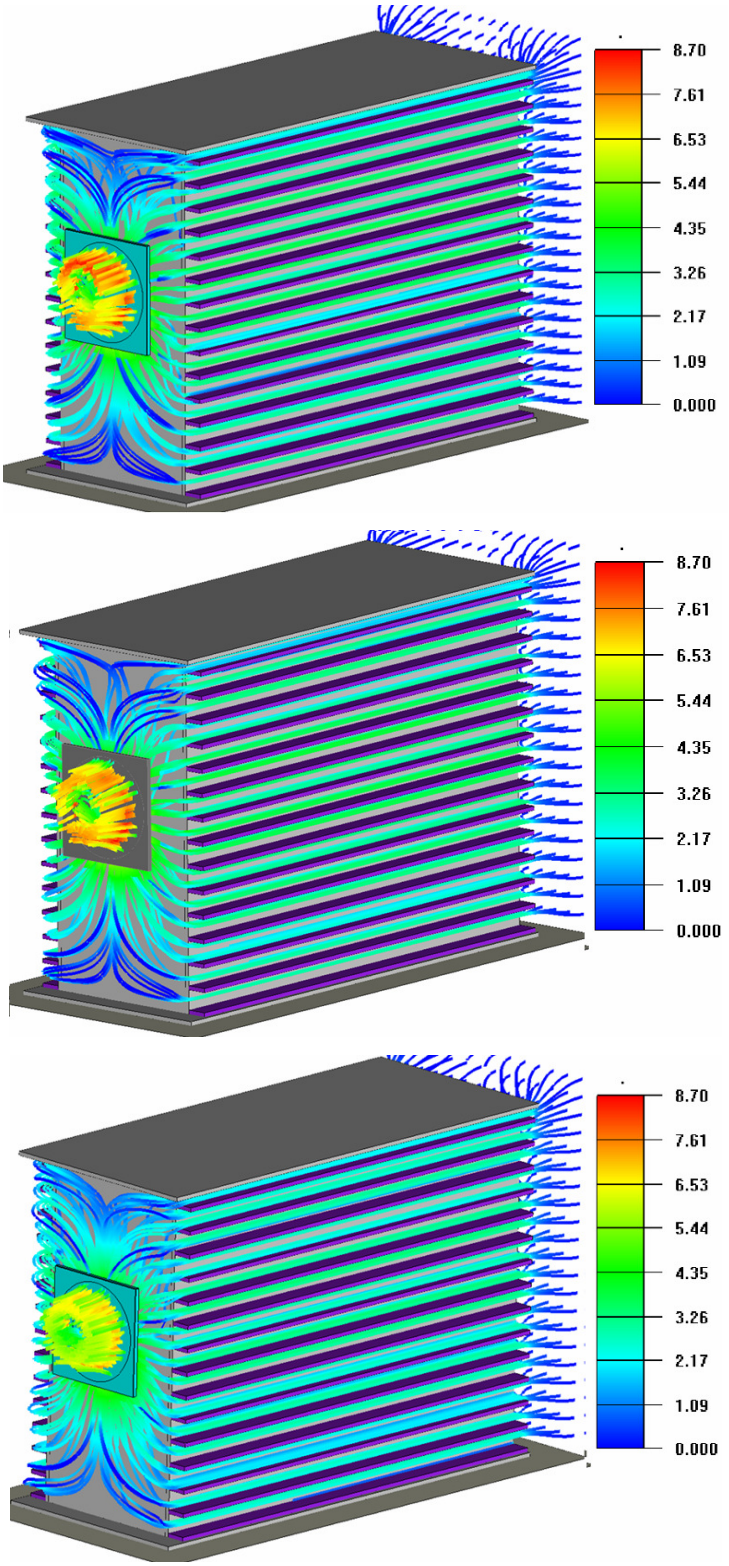

Figure 4.42 Speed (m/s) colored streamlines for air flow inside air channels obtained by simulations 26 (top), 27 (middle) and 28 (bottom)

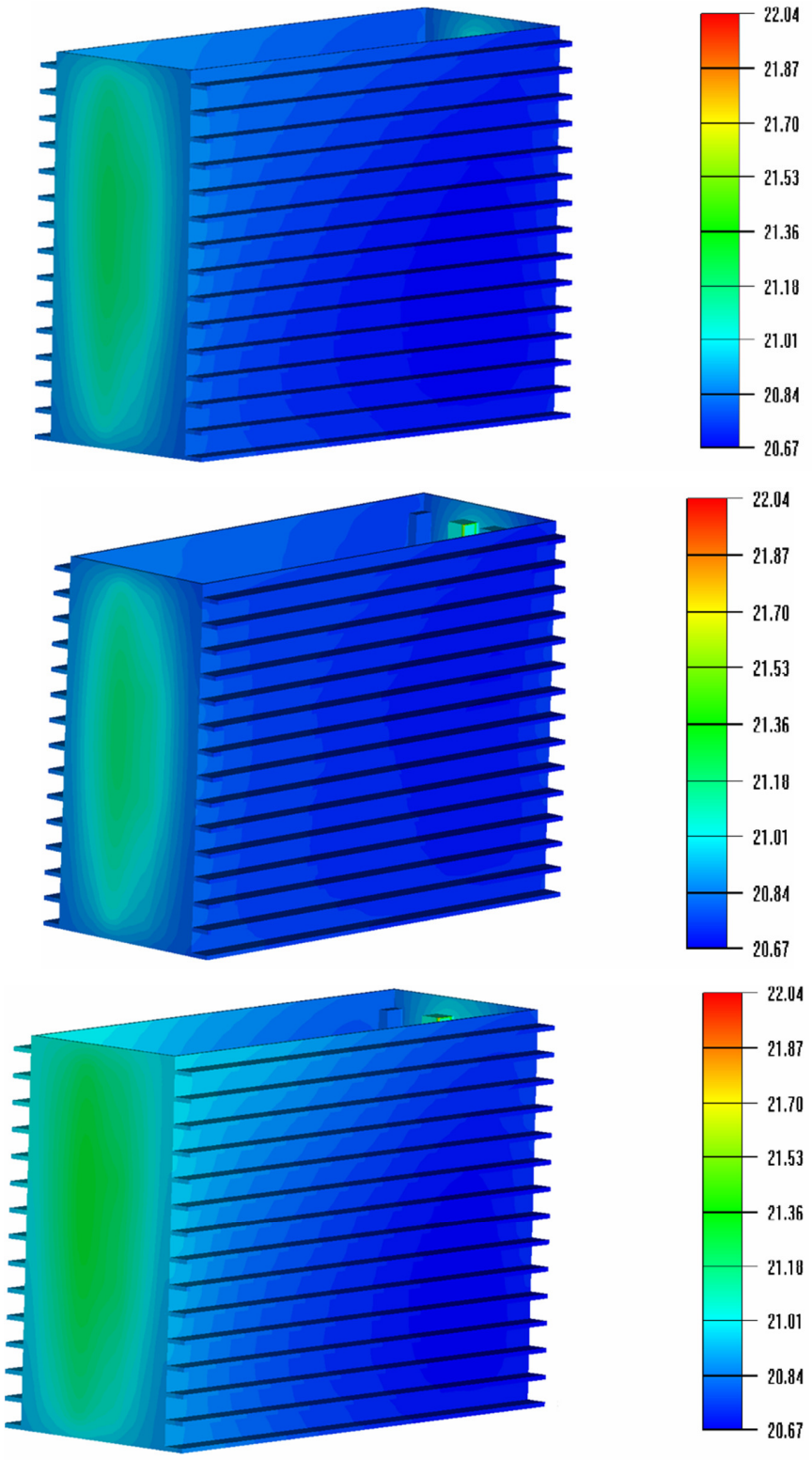

Figure 4.43 Electronic box surface temperature (^{o}C) contours obtained by simulations 26 (top), 27 (middle) and 28 (bottom)

Fluid flow details inside the air sealed region are given in Figure 4.44 in terms of vertical velocity components. It can be said that air flow inside the air-sealed region are very similar for all three base simulations.

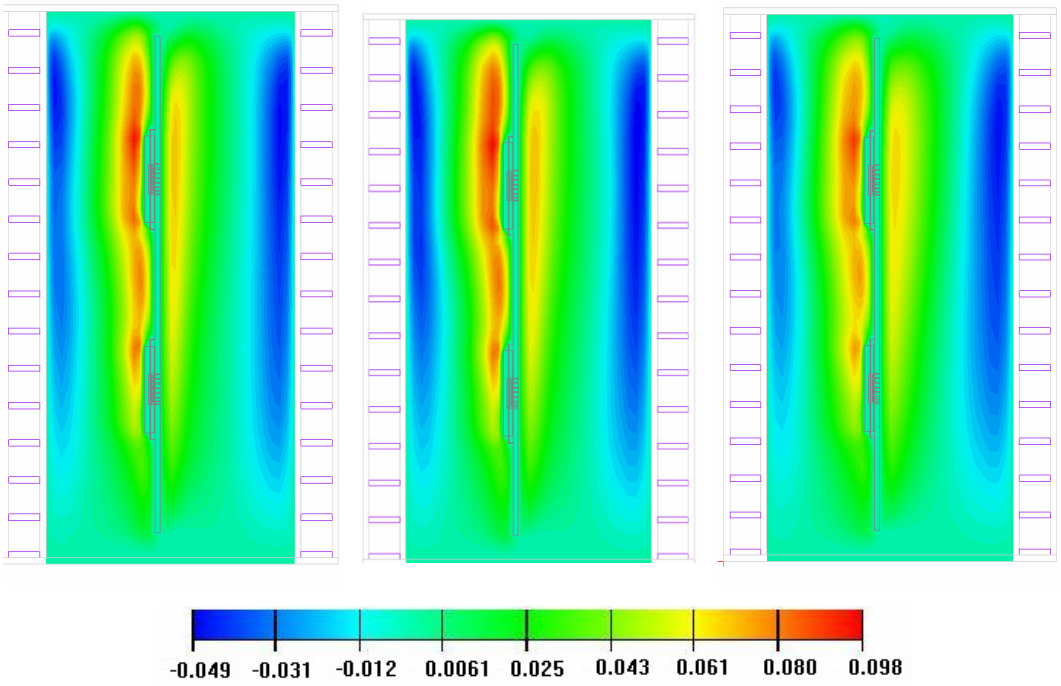

Figure 4.44 z-axis section view of vertical velocity component (m/s) obtained for simulations 26 (left), 27 (middle) and 28 (right)

Temperature contours on the PCB surface are given in Figure 4.45. Again, all three base models provide comparable results. On the other hand it was seen that how this VME board is cooling by the ATR chassis. As expected edges of the PCB are cold, since the heat is transferred outside the electronic box through these edges. Based on these results it is concluded that zero equation turbulence model is adequate for this problem and this model is also used for the remaining CCM based simulations.

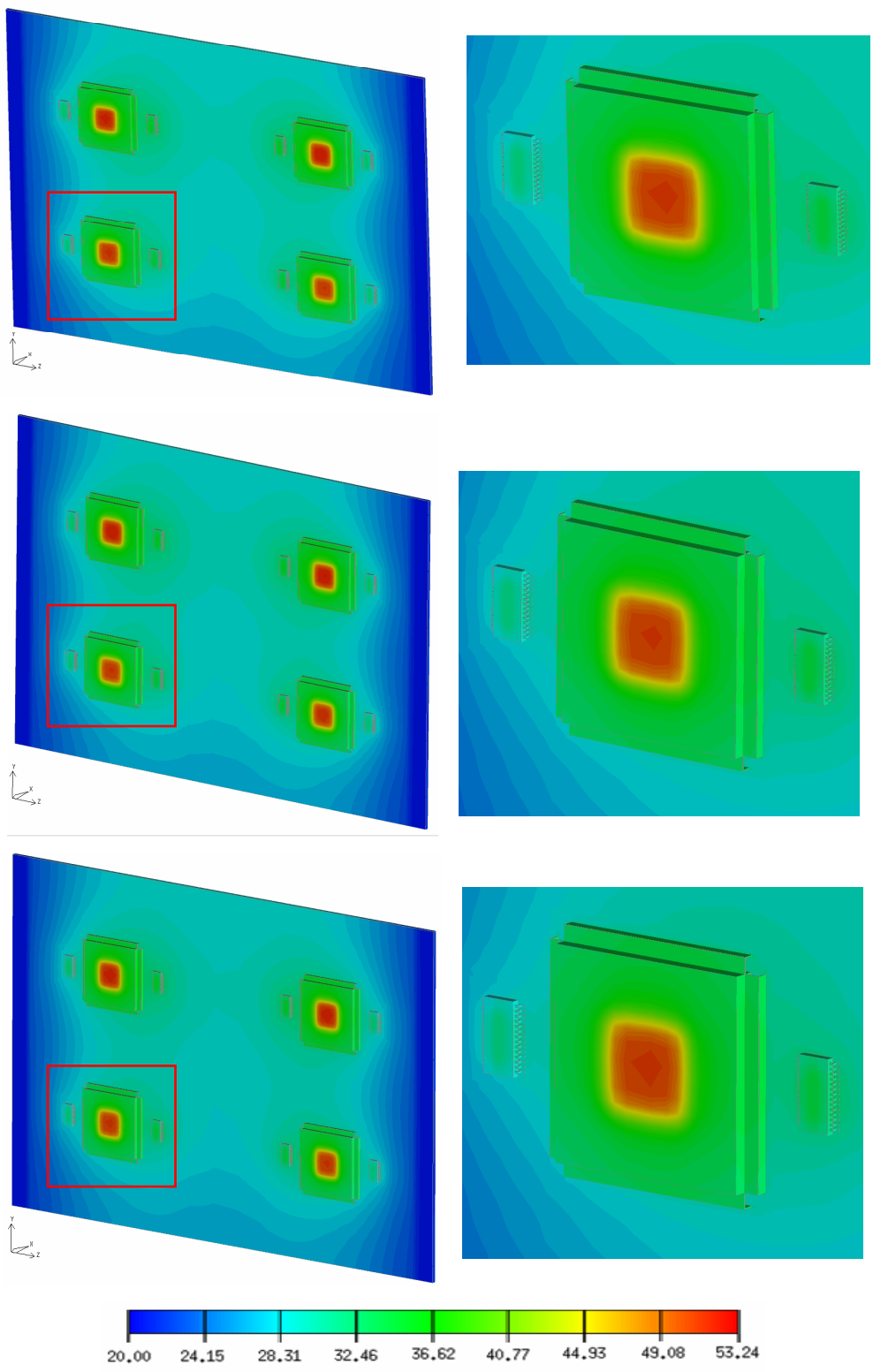

Figure 4.45 Surface temperature (ºC) distribution of PCB obtained by simulations 26 (top), 27 (middle) and 28 (bottom)

Temperature contours on the PCB surface obtained by different CCMs are given in Figure 4.46. For a better comparison Figure 4.47 presents a zoomed view of one of the DC/DC converters (7^{th} one). DTM of simulation 28 is also included in this figure for comparison purposes. It can be said that CCM 3 results are very close to that of DTM, whereas CCMs 4 and 5 provides over predicted surface temperatures. This goes parallel to the previous observation made for the first problem.

Figure 4.48 shows the grid count reduction obtained by the use of CCMs. Even for CCM 3 total grid count in the computational domain is reduced by 37,5 %.

Finally in addition to the simulations discussed here, extra runs with 2^{nd} order discretization schemes are also conducted with results similar to the ones presented here.

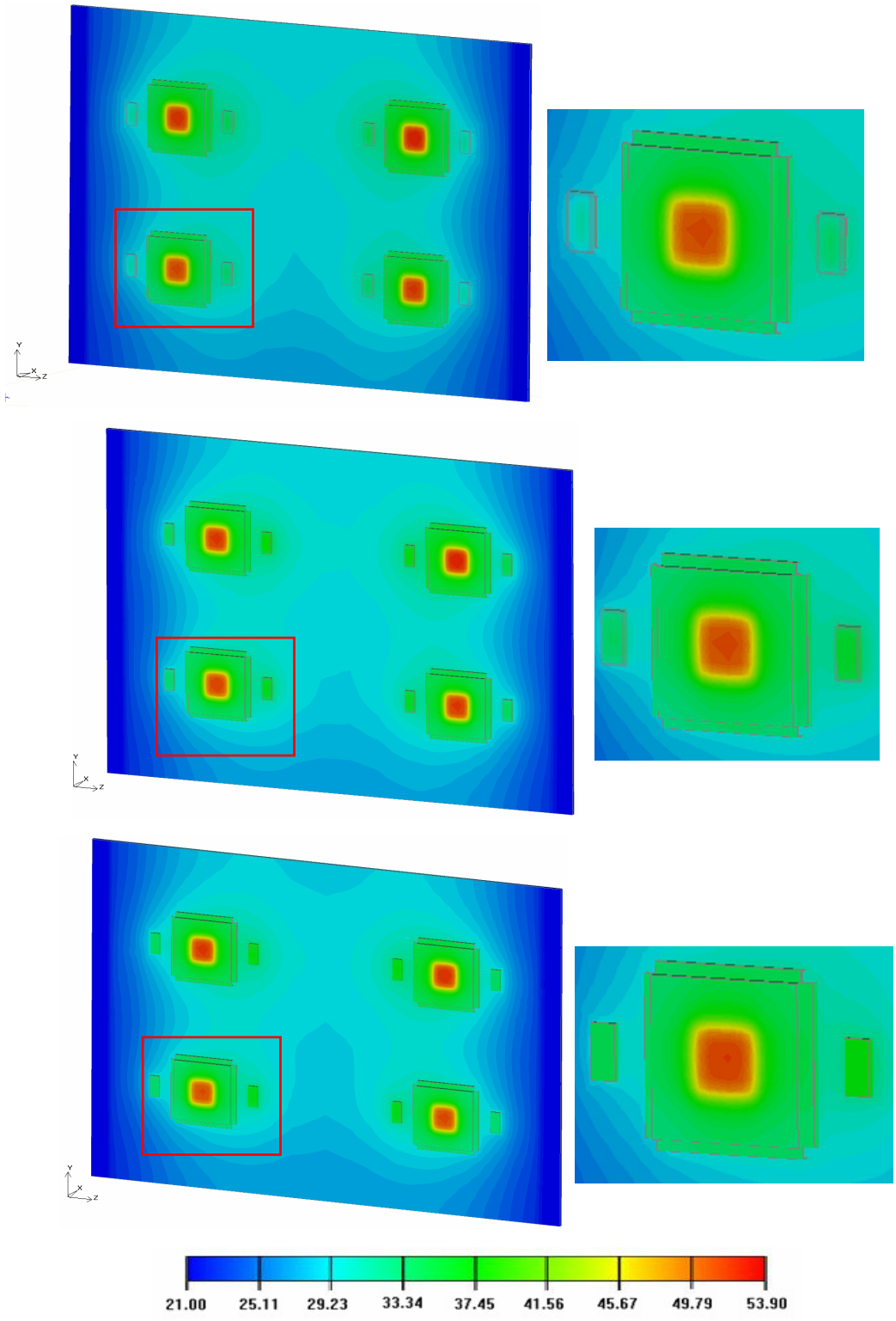

Figure 4.46 Surface temperature (ºC) distribution of PCB obtained by simulations 29 (top), 30 (middle) and 31 (bottom)

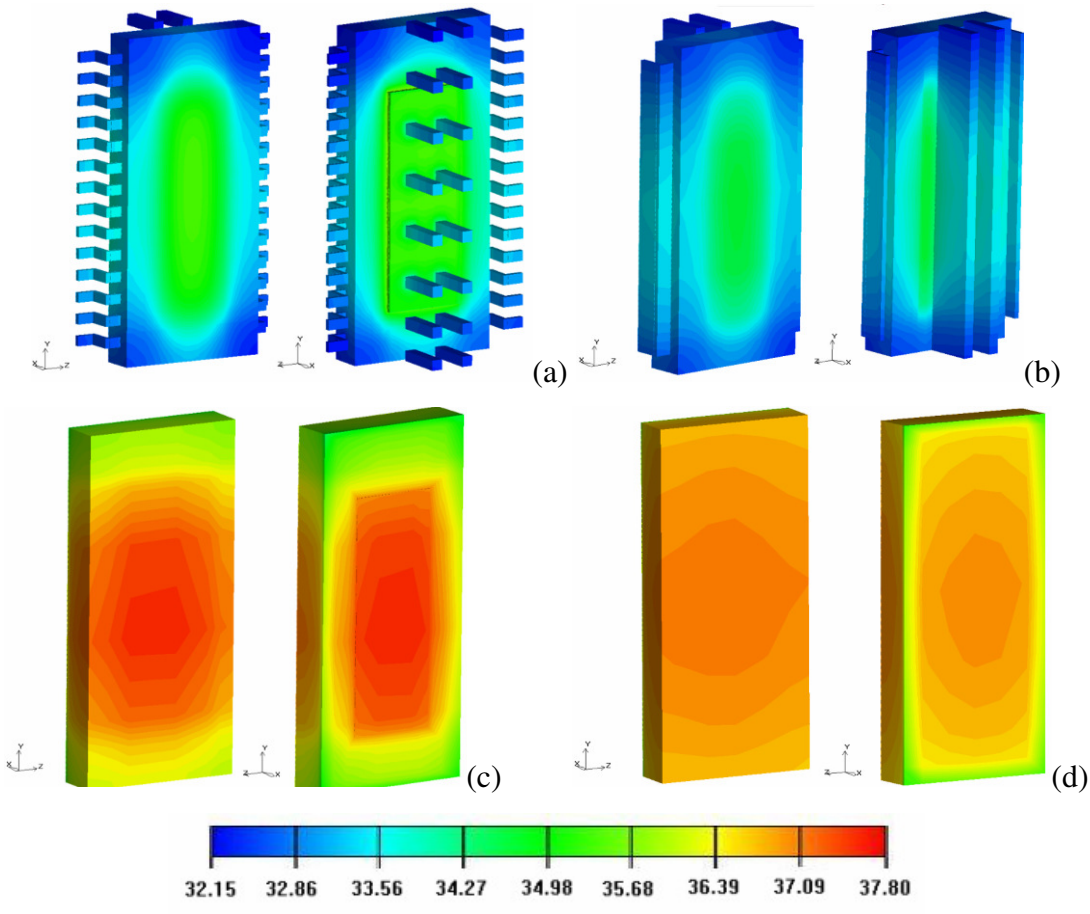

Figure 4.47 Surface temperature (ºC) distribution of a DC/DC converter obtained by simulations a) 28, b) 29, c) 30 and d) 31

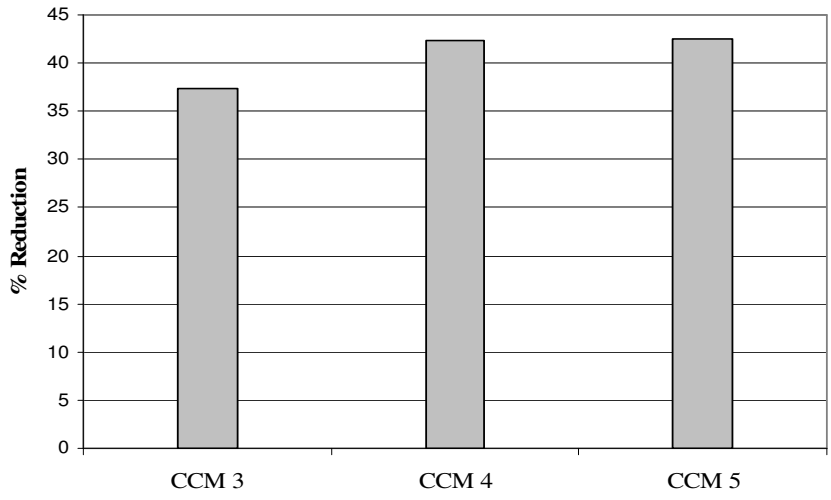

Figure 4.48 Percent reduction on the total grid count by the use of CCMs

CHAPTER 5

CONCLUSIONS

In this research, numerical and experimental studies are performed to understand thermal behaviours of DC/DC converters in component, board and system level simulations. Simplified thermal models of these electronic packages are also investigated to obtain thermally satisfactory and numerically efficient compact alternatives.

5.1 Conclusions for the First Problem

It can be concluded from the surface contour and temperature point results that the detailed thermal modelling approach predicts the thermal behaviour of the TPS54610 DC/DC converter with an error margin 5 %. Although detailed thermal modelling (DTM) is feasible for component level simulations, it has great disadvantages for board or system level analyses, because of computational limitations.

All conduction based compact thermal models are appraised as useful both for solution and modelling time. In spite of simplifications applied on CCMs 1, 2 and 3, they still showed similar thermal behaviours with DTM. Therefore it is concluded that lumping of internal leads, external leads, vias and using a 2D, zero thickness entity instead of the air gap under the package do not influence the results drastically.

Also grid count has reduced approximately 70 % by the use of these compact models instead of DTM. But using tens of these CCM 3 in a system level simulation can still be impractical considering computational resources. In CCMs 4 and 5 physical parts such as internal leads, external leads and vias are totally excluded. This brings considerable simplification to the thermal modelling of system level analysis. Also grid reduction reaches up to 90%, compared with DTM. Although these CCMs provide temperature point results with an acceptable error margin of 10 %, surface temperature distributions show great discrepancies with DTM results. Reduction of heat transfer paths by the elimination of leads and vias are identified as the main causes of discrepancies. In addition to this, presence of heat dissipation on the whole mold homogeneously (in CCM 5) is a factor for discrepancies too. Elimination of vias also changes the temperature distribution on the PCB. Therefore it is concluded that CCMs 4 and 5 should not be used as thermal models for electronic packages which have no additional heat transfer path (such as powerPAD) other than leads between PCB and mold. But these CCMs can still be used as thermal models for thermally enhanced electronic packages such as TPS54610, which is directly soldered to a PCB with its powerPAD. They can also be used for less critical electronic components of the PCB such as inductors, resistors, capacitors, etc. As known, accurate prediction of surface temperature distributions of such components is not so important.

5.2 Conclusions for the Second Problem

In the second problem, three different compact thermal models of module type DC/DC converters are developed and placed on a PCB to create a forced convection cooling ambient. Complicated internal structure of module type converters used in this problem are totally different than generic BGA or QFP type electronic packages. This time a detailed compact thermal model is not used for creation of conduction based compact thermal model alternatives. Instead, compact models are created with the help of vendor data sheets and past studies.

Effects of different grid structures and turbulence models on the numerical solutions are investigated in this board level analysis. It is shown that upper temperatures of various locations (TC point 1,4 and 6) can be obtained numerically with deviations of less than 10 % (for all CCM alternatives) compared to the experimental measurements. A valuable outcome of the study is the insensitivity of the surface temperature of a heating DC/DC converter to the complexity of the CCM as well as to the conductivity values used in its modelling. Besides the importance of convenient modelling of inner details of a heating component, the accuracy of the external flow field that eventually takes the heat away is important for the accurate prediction of the surface temperatures. And the proper computation of the flow field is affected by the grid resolution together with the proper modelling of the turbulent flow around the heating component. Hence better temperature point and temperature contour plot results are obtained with fine grid resolution (where default max size ratio is set to 1.35) for all CCM alternatives.

5.3 Conclusions for the Third Problem

This last problem gave a chance to evaluate the performance of previously developed CCMs in a system level analysis. Computational effectiveness of using CCMs are seen clearly in such complex systems. CCMs 3, 4 and 5 created for the first problem are also utilized for this one.

As expected both solution and modelling times decreased remarkably with the use of compact thermal models. But numerical errors increase with the increasing simplicity of CCMs, similar to the results of the first study. It is worth to mention that deviations for temperature points are computed according to DTM results, different than the first case where experimental results are used. CCM 3 and its simplifications do not change temperature results and temperature contour representations significantly; however the total grid count inside the computational domain is reduced by approximately 37,5 %. As a result it is concluded that CCM 3 can be used as a useful thermal model.

Although % deviations are seen satisfactory for CCMs 4 and 5, temperature contour representations revealed that their surface temperature contour results are considerably different than the DTM results. Another point is that grid reductions (with the use of CCM 4 or 5) are not so different than those of CCM 3 which is a clear difference between component and system level analyses. On the other hand it is still recommended that CCMs 4 and 5 can be used as thermal models for thermally enhanced electronic packages and for less critical electronic components of a PCB.

Another significant outcome of the system level analyses is the importance of radiation heat transfer mode. Compared to the results obtained from preliminary analysis where radiation heat transfer is neglected, it is realized that the temperatures on the PCB assembly increases about 4-5 °C. And it is concluded that the temperature distribution inside the air sealed region is considerably affected by the radiative heat transfer. Buoyancy force induced convective and radiative heat transfer are seen as primary mechanisms of the heat transfer inside the air sealed region.

REFERENCES

[1] Intel Corporation, http://www.intel.com/technology/mooreslaw/, Last visited on January 2010.

[2] Moore's law From Wikipedia, the free encyclopedia, http://en.wikipedia.org/wiki/Moore%27s_law#cite_note-0, Last visited on January 2010.

[3] Intel Corporation, Intel Pentium 4 Processor in the 478-Pin Package Thermal Design Guidelines, May 2002.

[4] The Uptime Institute Inc., 2005-2010 Heat Density Trends in Data Processing, Computer Systems and Telecommunications Equipment white paper, 2006.

[5] ARINC 404A, "Air Transport Equipment Cases and Racking", March 1974.

[6] Startco Engineering, Thermal Modeling, Techincal Informaiton 4.13 White paper, http://www.startco.ca/library/techinfo/section4/4.13.pdf , Last visited, January 2010.

[7] Shidore S., "Compact Thermal Modeling in Electronics Design", Electronics-Cooling Magazine, Vol. 13 no.2, http://electronics-cooling.com/articles/2007/may/a2/ , Last visited January 2010

[8] JESD15, "Thermal Modeling Overview", October 2008.

[9] JESD15-1, "Compact Thermal Model Overview", October 2008.

[10] Siegel B. S., "Measuring thermal resistance is the key to a cool semiconductor", Electronics, 51, 121–126, (1978).

[11] JESD15-4, "DELPHI Compact Thermal Model Guideline", October 2008.

[12] Dutta V. B., "Junction-to-Case Thermal Resistance - Still a Myth?", Fourth IEEE SEMITHERM Symposium, Feb. 10-12, (1988), San Diego, California.

[13] Joiner B. and Adams V., "Measurement and Simulation of Junction to Board Thermal Resistance and Its Application in Thermal Modeling", Proc. of SEMITHERM, 212-220, (1999), San Diego.

[14] Karimanal K. and Nair R., "Use of Zero Thickness Conducting Plate Object in Electronics Cooling Applications of CFD", Inter Society Conf. on Thermal Phenomena, 308-313, (2000).

[15] Cooley W. T. and Razani A., "Thermal Analysis of Surface Mounted Leadless Chip Carriers", Journal of Electronic Packaging of ASME, 13, 156-163, (1991).

[16] Rosten H. I., Parry J. D., Addison J. S., Viswanath R., Davies M. and Fitzgerald E., "Development, Validation and Application of a Thermal Model of a Plastic Quad Flat Pack", Proc. 45th Electron. Comp. Technol. Conf., 1140-1151, (1995), Las Vegas.

[17] Karimanal K. and Ahmed G. R., "Validation of Compact Conduction Models of BGA Under An Expanded Boundary Condition Set",ITHERM 2002, 99-105 , (2002).

[18] Guenin B. M., Lall B. S., Molnar R. J., and Marrs R. C., "A Study of the Thermal Performance of BGA Packages", '95 Flip Chip, BGA, TAB & AP Symposium, 37-46, (1995).

[19] Parry J., Rosten H., and Kromann G. B., "The Development of Component-Level Thermal Compact Models of A C4/CBGA Interconnect technology: The Motorola PowerPC 603 and PowerPC 604 RISC Microproceesors", Components, Packaging, and Manufacturing Technology–Part A, IEEE Transactions on, 21(1), 104–112, (1998).

[20] Tom Lee T. and Mahalingam M., "Thermal Limits of Flip Chip Package Experimentally Validated CFD Supported Case Studies", Components, Packaging, and Manufacturing Technology–Part B, IEEE Transactions on, 20(1), 94-103, (1997).

[21] Zahn B. A., "Evaluating Thermal Characterization Accuracy Using CFD Codes - A Package Level Benchmark Study of IcePaK and Flotherm", Proc., Sixth Intersociety Conference on Thermal and Thermomechanical Phenomena in Electronic Systems, 322–329, (1998).

[22] Rodgers P., Eveloy V., Lohan J., Fager C. M., and Rantala J., "Experimental Validation of Numerical Heat Transfer Predictions for Single- and Multi-Component Printed Circuit Boards in a Forced Convection Environment: Part I -Experimental and Numerical Modelling", Fifteenth IEEE SEMI-THERM Symposium, 54-64, (1999).

[23] Adams V. H., Blackburn D. L. and Joshi J., "Package Geometry Considerations in Thermal Compact Modelling Strategies", Proceedings of EUROTHERM Seminar 58: Thermal Management of Electronic Systems 111, 122-130, (1997).

[24] Aranyosi A., Ortega A. and Evans J., "Development of Compact Thermal Models for Advanced Electronic CPGA Package Packing: Methodology and Experimental Validation for A Single-chip CPGA Package", ITHERM 2000 17th Intersociety Conference, 1, 225-232, (2000).

[25] Ying T. M. and Toh K. C., "A Heat Spreading Resistance Model For Anisotropic Thermal conductivity Materials in Electronic Packaging", ITHERM 2000 17th Intersociety Conference, 1, 314-321, (2000).

[26] Lasance C. J. M., "Two Benchmarks to Facilitate the Study of Compact Thermal Modeling Phenomena", Comp. and Pack. Tech., IEEE Transactions on, 24, 559-565, (2001).

[27] Eveloy V., Rodgers P. and Lohan J., "Comparison of Numerical Predictions and Experimental Measurements for the Transient Thermal Behavior of a Board-Mounted Electronic Component," Proc of 8th Intersociety Conf on Thermal and Thermomechanical Phenomena in Electronics Systems (ITHERM'02), 36-45, (2002).

[28] Mohammadi F. and Marami M., "Creation and Verification of Dynamic Compact Thermal Model of A BGA Package", Microelectronics International, 25/3, 3–13, (2008).

[29] Garcia A. E. and Chiu C.-P. , "Compact Modeling Approaches to Multiple Die Stacked Chip Scale Packages", 19th IEEE SEMITHERM Symposium, 160-167, (2003).

[30] JESD51-2a, "Integrated Circuits Thermal Test Method Environmental Conditions - Natural Convection (Still Air)", January 2008.

[31] JESD51-8, "Integrated Circuits Thermal Test Method Environmental Conditions - Junction-to-Board", October 1999.

[32] Dhinsa K. K., Bailey C.J., and Pericleous K.A., "Turbulence Modeling and Its Impact on CFD Predictions for Cooling of Electronic Components," Proc. Ninth Intersoc. Conf. Thermal and Thermomechanical Phenomena in Electronic Systems, 487-494, (2004).

[33] Pang Y. F., "Assessment of Thermal Behaviour and Development of Thermal Design Guidelines for Integrated Power Electronics Modules", PhD thesis, Virginia Polytechnic Institute and State University, (2005).

[34] Vellvehi M., Jorda X., Godignon P., Ferrer C. and Millan J., "Coupled Electro-thermal Simulation of A DC/DC Converter", Microelectronics Reliability, 47, 2114–2121, (2007).

[35] ANSYS ICEPAK 12.0 User's Guide, Fluent Inc., 2009.

[36] ANSYS FLUENT 12.0 Theory Guide, Fluent Inc., 2009.

[37] Wendt J. F., "Computational Fluid Dynamics an Introduction", 3rd Edition, Springer, (2009).

[38] Modest M. F., "Radiative Heat Transfer", 2nd Edition, Academic Press, (2003).

[39] Wilcox D. V., "Turbulence Modelling for CFD", 2nd Edition, DCW Industries Inc., (1994).

[40] Texas Instruments, "TPS54610EVM 6-amp Externally Compensated SWIFT Regulator Evaluation Module Users Guide", August 2001.

[41] Texas Instruments, "3V to 6V Input, 6A Output Synchronous Buck PWM Switcher With Integrated Fets (SWIFT™)-TPS54610 Data Sheet", April 2007.

[42] Omega Engineering, "SA1XL Series Surface Thermocouples Specs", http://www.omega.co.uk/Temperature/pdf/SA1XL.pdf , Last visited on January 2010.

[43] Omega Engineering, "5TC Series Insulated Wire Thermocouples with Stripped Ends Specs", http://www.omega.co.uk/ppt/pptsc.asp?ref=5TC&flag=1 , Last visited January 2010.

[44] Omega Engineering, "ANSI and IEC Colour Codes for Thermocouples, Wire and Connectors Hand Book", http://www.omega.com/Temperature/pdf/TC_GEN_SPECS_REF.pdf , Last visited on January2010.

[45] Vishay Intertechnology Inc., "Wirewound Resistors, Military, MIL-PRF 18546 Qualified, Type RE, Aluminium Housed, Chassis Mount Data Sheet", http://www.vishay.com/docs/30201/30201.pdf , Last Visited on January 2010.

[46] Cooper Bussmann Electronic Technologies, "UNI-PAC™ Surface Mount Power Inductors Data Sheet", www.cooperbussmann.com , Last visited January 2010.

[47] GAIA Converter Inc., "Hi-Rel DC/DC Converters MGDM-150 Series Data Sheets", www.gaia-converter.ca/content/datasheet/MGDM150.pdf , Last visited January 2010.

[48] Ametek Inc., "W487-14B ½ Aximax 2L 3162 SF 28V DC, Vane Axial Fan Data Sheets", www.ametekaerodefense.com, Last visited January 2010.

[49] Navos J. T., "Uncertainty Analysis of Thermocouple Measurements Used in Normal and Abnormal Thermal Environment Experiments at Sandia's Radiant Heat Facility and Lurance Canyon Burn Site", Sandia National Laboratories, SAND2004-1023, (2004).

[50] Texas Instruments, "PowerPAD ™ Thermally Enhanced Package Application Report", www.ti.com , October 2008.

[51] Shidore S. and Lee T.Y.T., "A Comparative Study Of The Performance Of Compact Model Topologies And Their Implementation In CFD For A Plastic Ball Grid Array Package", Pacific Rim/ASME International, Intersociety Electronic & Photonic Pack. Conf., (1999), Hawaii, USA.

[52] Kordyban T., "Estimating the Influence of PCB and Component Thermal Conductivity on Component Temperatures in Natural Convection", Flomerics, http://www.flomerics.com/files/casestudies/488/t71.pdf , Last visited July 2008.

[53] Kromann G. B. and Argento C. W., "CFD Modeling for Component-level and Board-level Thermal Analysis: A PBGA Interconnect Technology for Low-Velocity Air-Cooling", Flomerics, http://www.flomerics.com/files/casestudies/526/t153.pdf , Last visited July 2008.

[54] IEEE Std 1101.1, "IEEE Standard for Mechanical Core Specifications for Microcomputers Using IEC 60603-2 Connectors", September 1998.

APPENDIX A

EXTERNAL DIMENSIONS

Some important detailed external dimensions of numerical entities are given below. In Figure A.1 external dimensions of the TPS54610 PCB and location of the TPS54610 DC\DC converter are given. In Figure A.2, external dimensions of PCB Assembly of the third case and locations of the used TPS54610 DC\DC converters and PQFPs are given. In Figure A.3 external dimensions of the ½ ATR chassis are given. In Figure A.4 external dimensions of AMETEK ROTRON ½ Aximax 28VDC fan are given and also fan curve is added in Figure A.5.

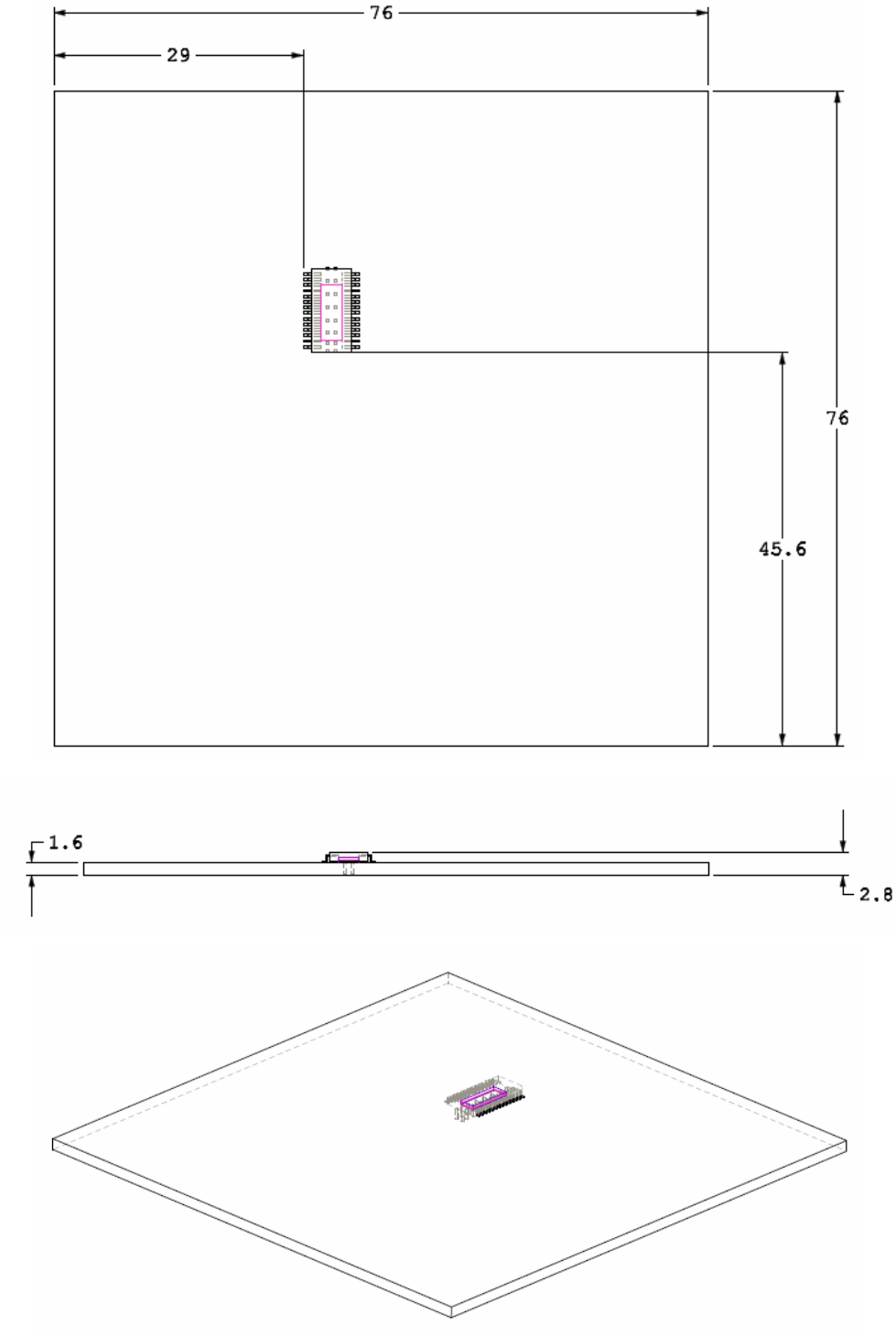

Figure A.1 External dimensions of the TPS54610 PCB and location of the TPS54610 DC\DC converter on PCB

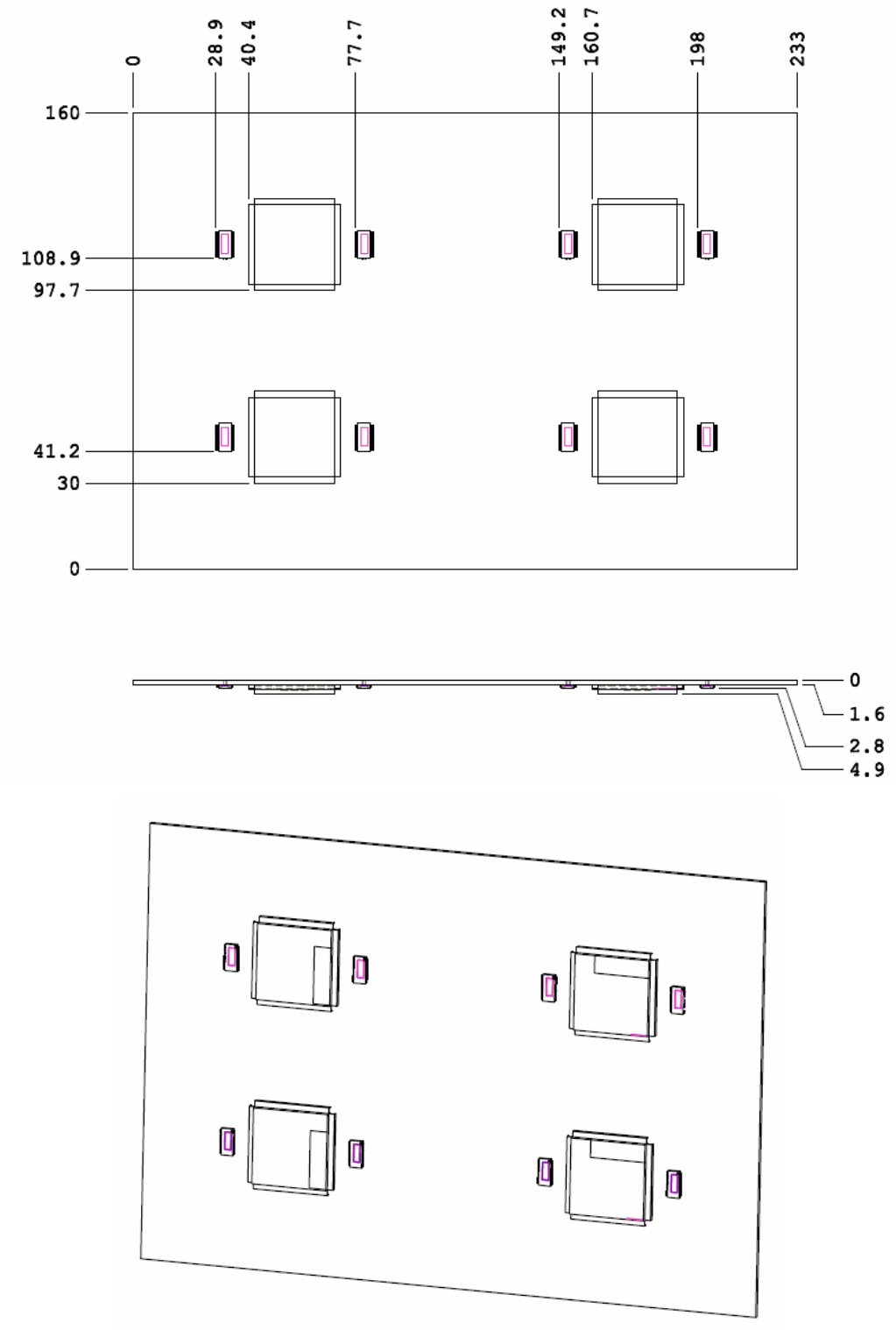

Figure A.2 External dimensions of the PCB Assembly of the third case and location of the TPS54610 DC\DC converters and PQFPs on that PCB

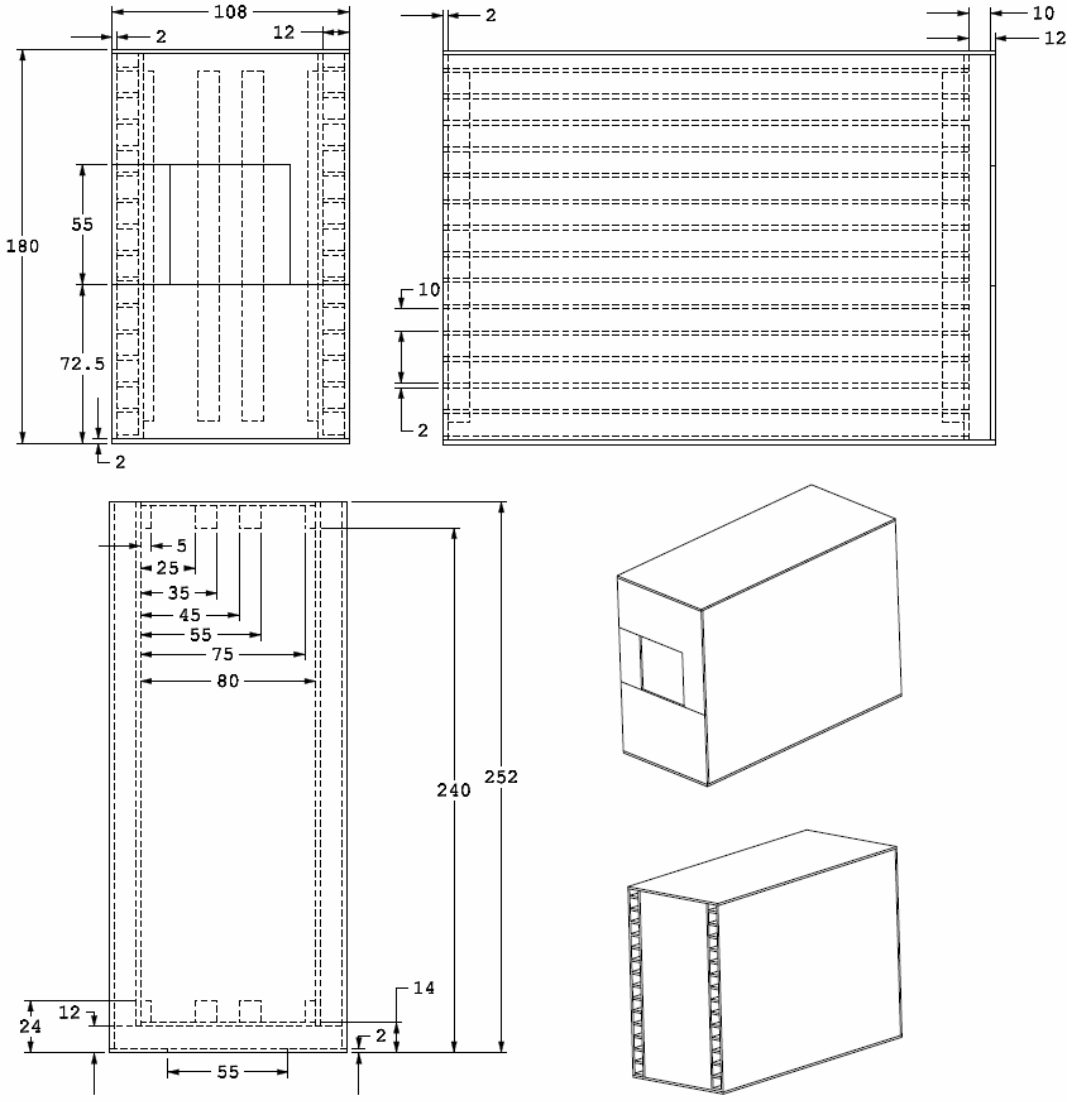

Figure A.3 External dimensions of ½ ATR Chassis of the third case

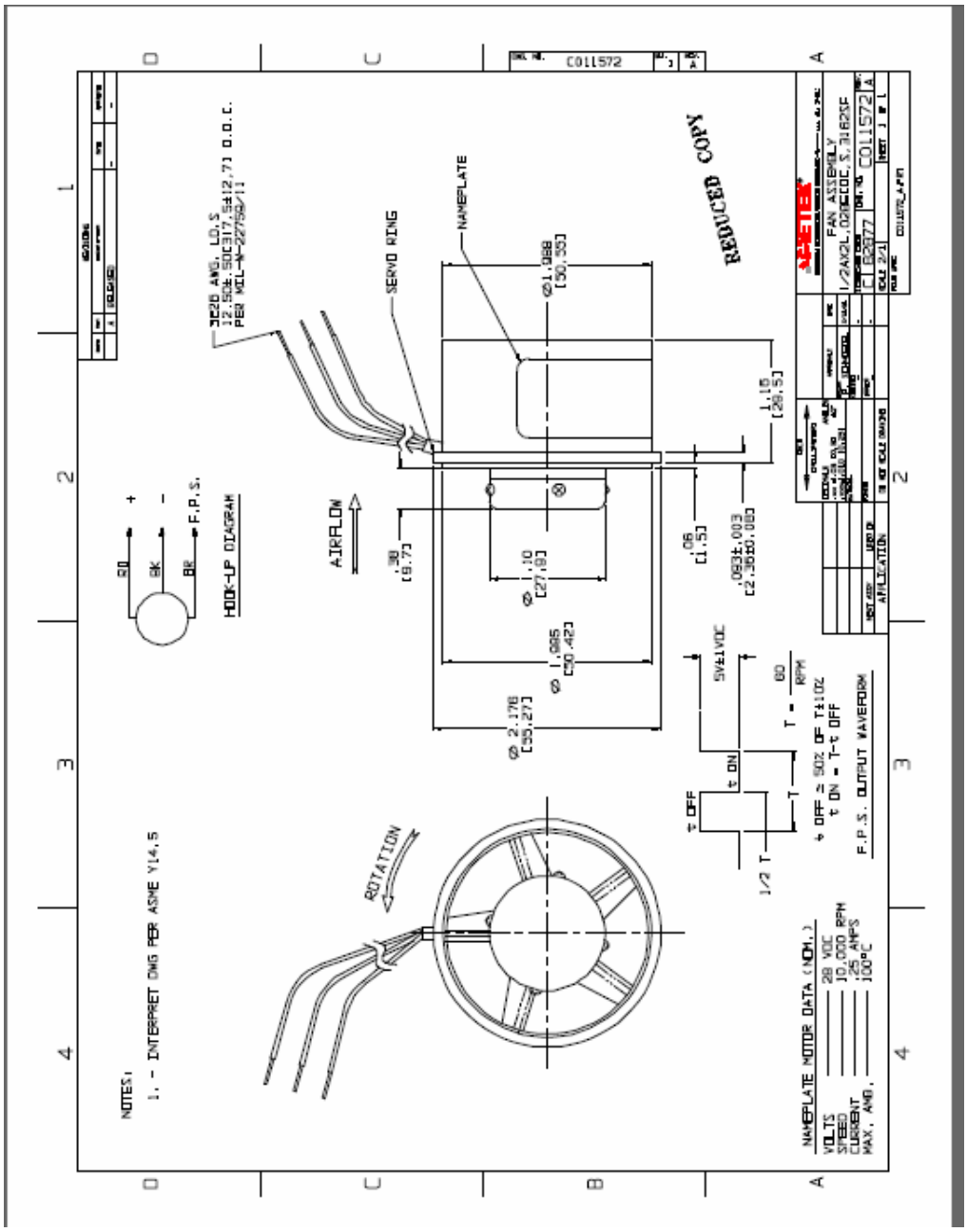

Figure A.4 External dimensions of Ametek Rotron ½ Aximax 28VDC Fan [48]

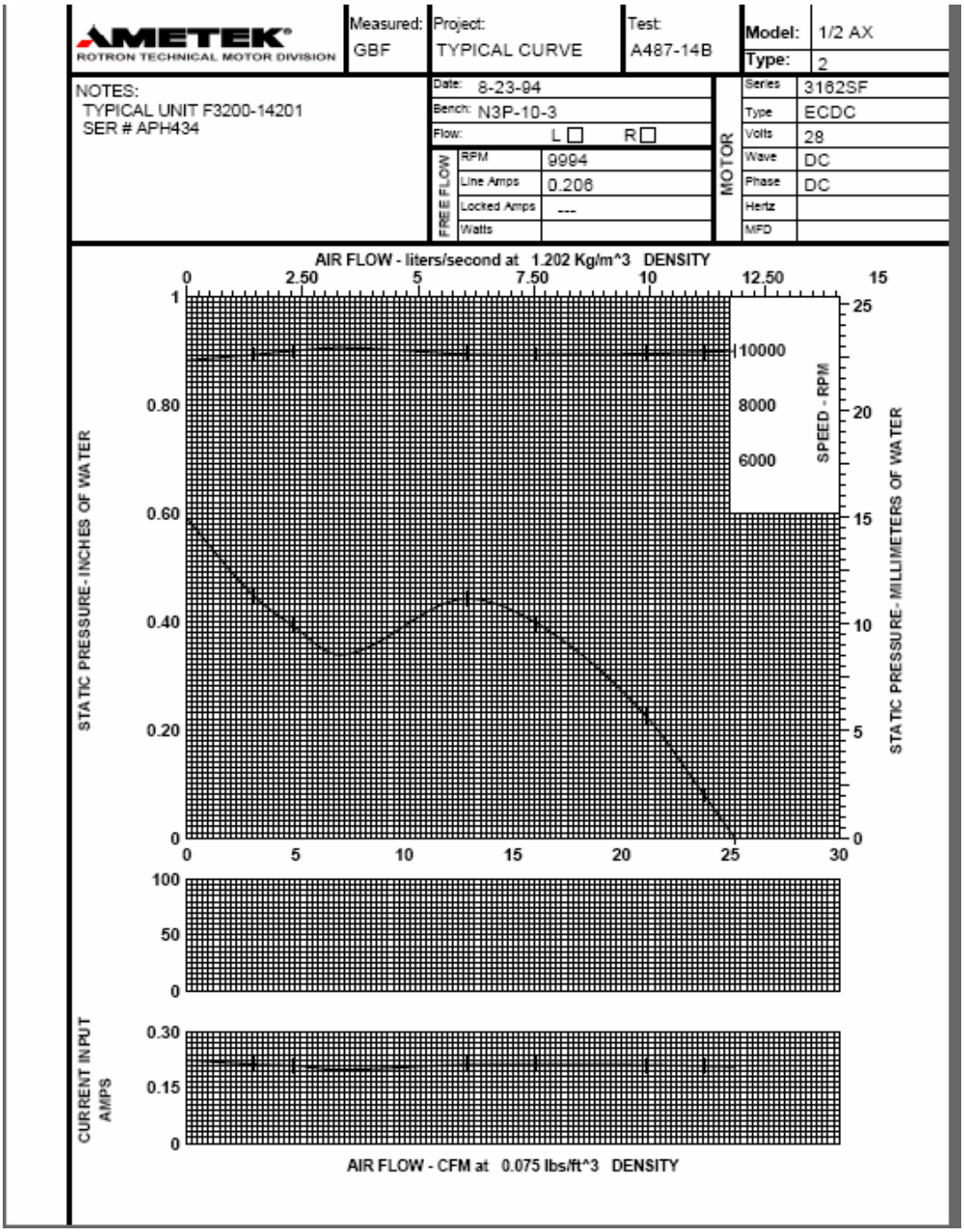

Figure A.5 Typical fan curve of Ametek Rotron ½ Aximax 28VDC Fan [48]

APPENDIX B

CONVERGENCE PLOTS

Sample convergence plots of governing equations are given below for case studies as seen in Figure B. 1-3.

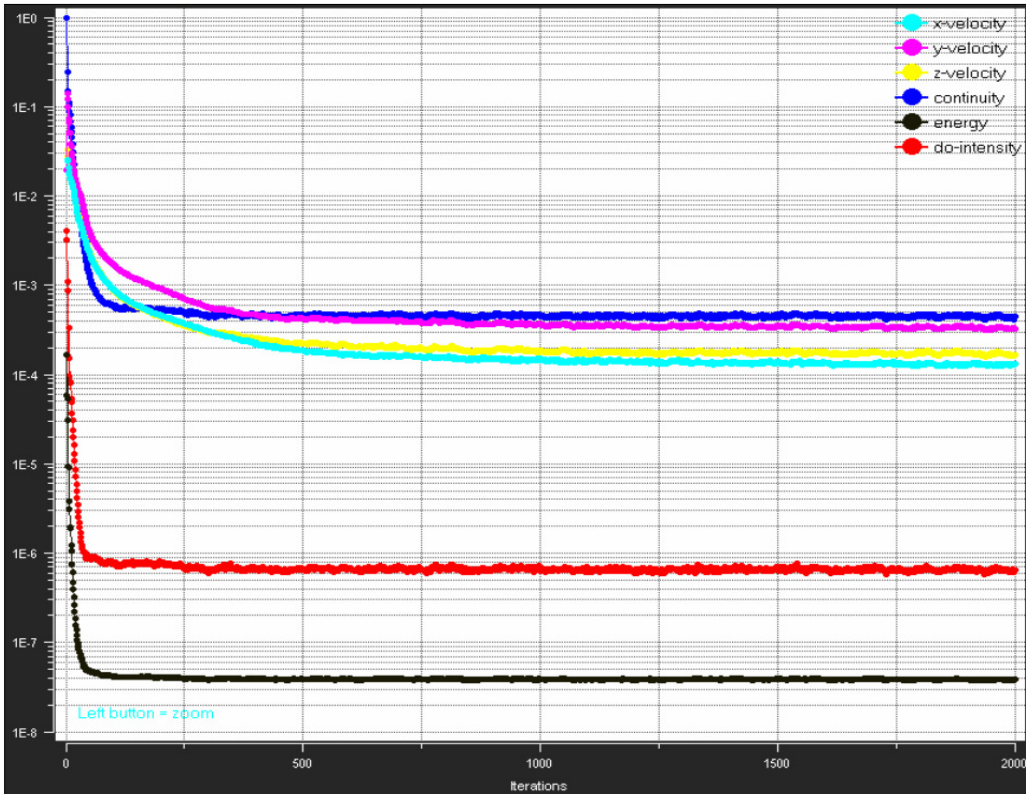

Figure B. 1 Convergence plot of for the 2nd simulation of the first problem

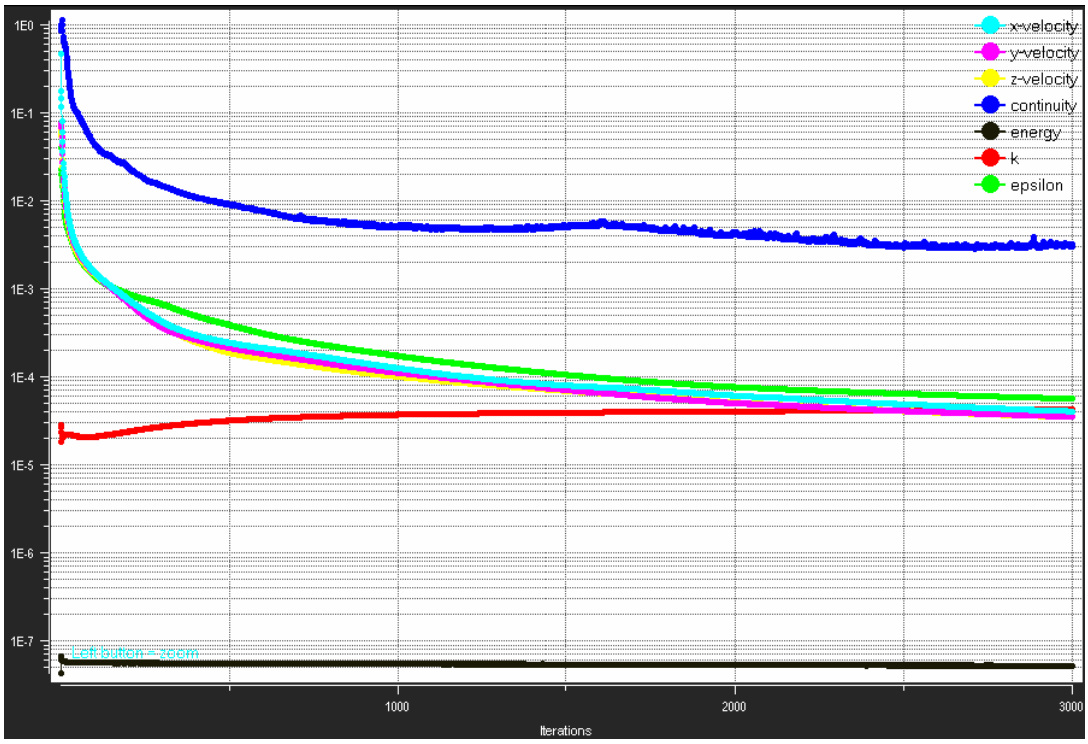

Figure B. 2 Convergence plot of for the 19th simulation of the second problem

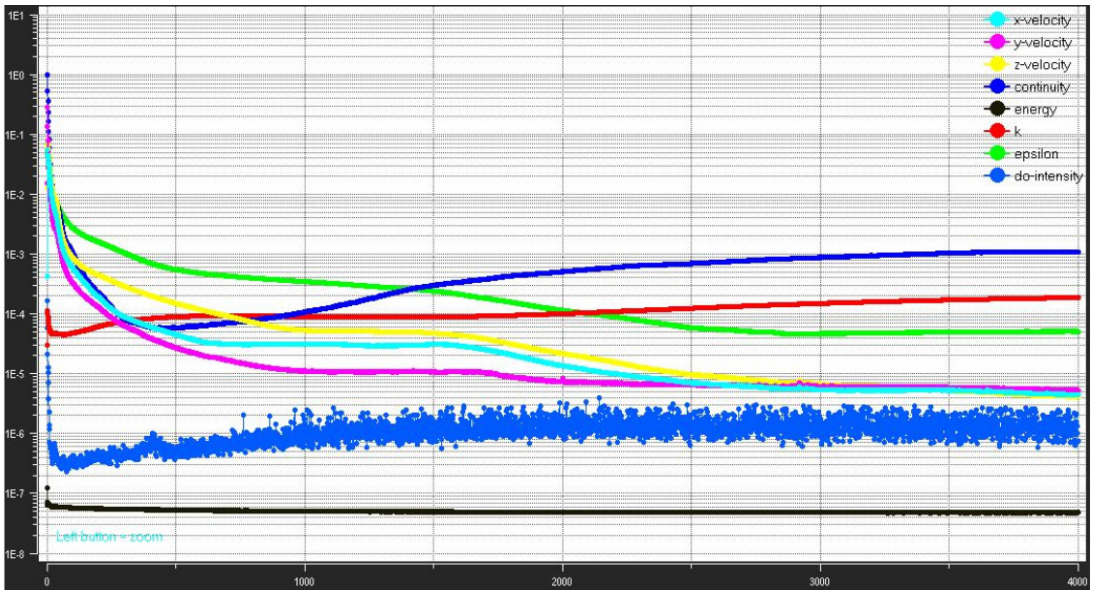

Figure B. 3 Convergence plot of for the 26th simulation of the third problem